

This dissertation has been
microfilmed exactly as received 67-6936

LEE, Thomas Alan, 1939-
INTERSTELLAR EXTINCTION IN THE ORION
ASSOCIATION.

University of Arizona, Ph.D., 1967
Astronomy

University Microfilms, Inc., Ann Arbor, Michigan

INTERSTELLAR EXTINCTION IN THE
ORION ASSOCIATION

by

Thomas Alan Lee

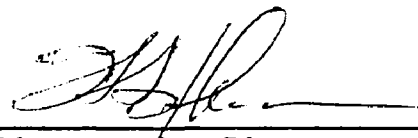
A Dissertation Submitted to the Faculty of the
DEPARTMENT OF ASTRONOMY
In Partial Fulfillment of the Requirements
For the Degree of
DOCTOR OF PHILOSOPHY
In the Graduate College
THE UNIVERSITY OF ARIZONA

1 9 6 7

THE UNIVERSITY OF ARIZONA

GRADUATE COLLEGE

I hereby recommend that this dissertation prepared under my
direction by Thomas A. Lee
entitled Interstellar Extinction in the
Orion Association
be accepted as fulfilling the dissertation requirement of the
degree of Doctor of Philosophy


Dissertation Director

Nov. 30, 1966
Date

After inspection of the dissertation, the following members
of the Final Examination Committee concur in its approval and
recommend its acceptance:*

<u>Barry Bole</u>	<u>Nov. 30 '66</u>
<u>Ray Weyman</u>	<u>Nov. 30 '66</u>
<u>Walter Stitch</u>	<u>30 Nov '66</u>
<u>Beverly J. Lynd</u>	<u>30 Nov 66</u>

*This approval and acceptance is contingent on the candidate's
adequate performance and defense of this dissertation at the
final oral examination. The inclusion of this sheet bound into
the library copy of the dissertation is evidence of satisfactory
performance at the final examination.

STATEMENT BY AUTHOR

This dissertation has been submitted in partial fulfillment of the requirements for an advanced degree at The University of Arizona and is deposited in the University Library to be made available to borrowers under rules of the Library.

Brief quotations from this dissertation are allowable without special permission, provided that accurate acknowledgment of the source is made. Requests for permission for extended quotation from or reproduction of this manuscript in whole or in part may be granted by the head of the major department or the Dean of the Graduate College when in his judgment the proposed use of the material is in the interests of scholarship. In all other instances, however, permission must be obtained from the author.

SIGNED: _____

Thomas A. G. Lee

ACKNOWLEDGMENTS

It is a pleasure to thank the many people who aided me in the various phases of this work. Assistance from the following individuals is hereby gratefully acknowledged:

Mrs. Kathryn Sheffer for managing the data processing and being helpful in many, many ways;

Mr. Richard Mitchell for helpful discussions concerning photometric systems and data analysis;

Mr. Braulio Iriarte and Dr. Manuel Mendez for courtesies extended to me during a pleasant and rewarding visit to Mexico;

Dr. Guillermo Haro for allowing me to take several of his infrared plates to Tucson for copying and detailed study;

Dr. Bart Bok for his interest, encouragement, and helpful suggestions;

Drs. Manuel Mendez and Robert Williams for interesting and valuable discussions;

Mr. Ed Howell for his help with photographic problems;

Mrs. Helena Davis and Miss Judy Ackerman for assisting in the preparation of the final draft;

Mrs. Dorothy Conniff for typing the final draft;
and all the personnel of the Lunar and Planetary
Laboratory who helped make this project so enjoyable.

I am greatly indebted to Dr. Harold L. Johnson, who directed this research and made the photometric equipment of the Lunar and Planetary Laboratory available for this investigation. He has given freely of his time and energy in providing continued guidance and encouragement. The consideration and interest he has shown are deeply appreciated.

This project was supported by the National Science Foundation under grants GP 3414 and GP 5129.

TABLE OF CONTENTS

	Page
LIST OF FIGURES	vii
LIST OF TABLES	ix
ABSTRACT	x
 I. Introduction	 1
A. Observational Work	1
B. Theoretical Results	10
C. The Orion Region	19
1. General	19
2. Extinction in the Orion Nebula	19
II. Observational Data	25
A. Selection of Stars	25
B. Equipment and Techniques	25
C. The Data	30
III. Intrinsic Colors of Early-Type Stars	43
A. Unreddened Early-Type Stars	43
B. The U-B and B-V Color Indices	43
C. The Infrared Color Indices	46
D. The V-L Index	51
IV. Extinction Curve Calculations	54
A. Method	54
1. Color Excesses	54

	vi
2. Normalization and Scaling	54
B. The E_{U-V}/E_{B-V} Ratio	55
V. Regional Mean Extinction Laws	59
A. Probable Errors and Weights	59
B. Properties of the Regional Laws	69
VI. Related Phenomena Modifying the Extinction Interpretation	80
A. The 'Belt' Region	80
B. The 'Sword' Region	83
1. Anomalous Energy Distributions	83
2. Nebular Radiation	86
3. Faint Red Stars in the Orion Nebula	95
VII. Regional Monochromatic Extinction Laws	102
A. Method	102
B. General Properties of Wideband Extinction Laws	105
C. Regional Monochromatic Curves	111
D. Properties of the Monochromatic Laws	121
VIII. Discussion	126
A. Regions of 'Normal' Extinction	126
B. Regions of 'Anomalous' Extinction	127
C. Extinction and Nebulosity	131
D. Monochromatic Extinction Laws	136
IX. Conclusions	143
APPENDIX A	145
APPENDIX B	147
REFERENCES	164

LIST OF FIGURES

	Page
1. Schematic Extinction Curve	4
2. Normalized Extinction Curves for the Cepheus and Scorpius Regions (Johnson, 1966a)	8
3. Theoretical Extinction Curves (van de Hulst, 1949)	13
4. Normalized Filter-Cell Response Functions	28
5. V-R versus B-V for O and B O Stars	48
6. V-I versus B-V for O and B O Stars	49
7. V-K versus B-V for O and B O Stars	50
8. K-L versus I-K for B 1 and Earlier-Type Stars	53
9. Normalized Extinction Laws for the Orion East 'Belt' and NGC 2024 No. 1	71
10. Normalized Extinction Laws for M 78 A, B and the Northwestern Region	72
11. Normalized Extinction Laws for the Outer 'Sword,' HD 37061, and the Trapezium Region	73
12. Schematic Map of Extinction Regions in the I Orion Association	74
13. Orion 'Belt' Color-Magnitude Diagram--Corrected for Extinction	82
14. East-West Division of the 'Belt' Region	82
15. Infrared Photograph of the Orion 'Sword'	89
16. Infrared Photograph of the Orion Nebula	90
17. θ^1 Orionis	91
18. Mean Normalized Emission Spectrum Required for 'Normal' Extinction in the Orion Trapezium	94

19.	Map of the Orion Trapezium Region (Parenago, 1954)	99
20.	E_{V-R} versus E_{B-V} for O-type Stars in Cygnus	108
21.	E_{V-I} versus E_{B-V} for O-type Stars in Cygnus	109
22.	Normalized Extinction Curves for Two Stars whose Color Temperatures are 3,500 and 30,000 Degrees	110
23.	Normalized Monochromatic Extinction Law for the East 'Belt' Region	113
24.	Normalized Monochromatic Extinction Law for NGC 2024 No. 1	114
25.	Normalized Monochromatic Extinction Law for the Northwestern Region	115
26.	Normalized Monochromatic Extinction Law for M 78 A, B	116
27.	Normalized Monochromatic Extinction Law for the Outer 'Sword' Region	117
28.	Normalized Monochromatic Extinction Law for HD 37061	118
29.	Normalized Monochromatic Extinction Law for the Trapezium Region (exact fit)	119
30.	Normalized Monochromatic Extinction Law for the Trapezium Region (smoothed)	120
31.	E_{V-I}/E_{B-V} versus Distance from θ^1 Orionis	129
32a.	Extinction from Combined Distributions of Particle Sizes	139
32b.	Extinction from Combined Distributions of Particle Sizes	140

LIST OF TABLES

	Page
1. Effective Wavelengths and Reciprocal Effective Wavelengths for the Photometric Filters	26
2. UBVRI Observations	32
3. UBVRIJKL Observations	41
4. Unreddened Early-Type Stars	44
5. Intrinsic Color Indices of Early-Type Main Sequence Stars	45
6. Intrinsic Color Indices of Early-Type Supergiants	45
7. The E_{U-V}/E_{B-V} Ratio in Orion	57
8. Color Excess Ratios	60
9. Observational Errors	65
10. Errors of Intrinsic Colors of O and B Stars	65
11. Probable Errors of Color Excesses for N Observations	68
12. Regional Extinction Data	70
13. Extinction Laws for θ^1 Orionis if Unseen Companions are Present	85
14. Normalized Monochromatic Extinction Data	112
15. Observed and Monochromatic Color Excess Ratios	122

ABSTRACT

Photoelectric photometry, covering a spectral region from $\lambda = .36 \mu$ to 3.4μ , is obtained for a large sample of early-type stars in the I Orion association with the photometric telescopes of the Lunar and Planetary Laboratory of the University of Arizona. The observations are interpreted in terms of the interstellar extinction phenomenon. The color excesses of the stars are calculated from the observed (reddened) and intrinsic (unreddened) color indices. Normalized curves revealing the wavelength dependence of the extinction are then computed. Because of the low reddening in many parts of the association, the errors of the extinction curves are often large. For this reason, regional mean extinction laws are determined from the data of individual stars in localized areas. A method that eliminates the use of filter effective wavelengths is then employed to obtain the corresponding monochromatic extinction laws.

The extinction in a large fraction of the association is essentially 'normal.' However, two regions, one in the east 'Belt' near ζ Orionis and the other in the center of the Orion Nebula (NGC 1976), exhibit distinctly 'non-normal' extinction characteristics. The anomalies found in these regions are a steeper extinction gradient in the infrared

and a high ratio of total to selective absorption. The Orion Nebula region is studied in considerable detail. The anomaly seen here, first noted some thirty years ago, is found only in the very center of the nebula--within 15' of θ^1 Orionis--and is not characteristic of the whole nebular region. Several factors which tend to complicate the interpretation--anomalous energy distributions for the stars, nebular radiation, and emission from faint red stars in this region--can account for only a small fraction of the strong infrared radiation from the early-type stars in this area. The additional observational data obtained in this study strengthen the conclusion that the extinction here is truly 'non-normal'; a lower limit of 5.0 for the ratio of total to selective absorption is indicated.

All of the stars in the Orion region that exhibit highly 'non-normal' extinction characteristics are of the earliest spectral types and are visibly associated with emission nebulae. These correlations favor the suggestion that the size distribution of interstellar grains near hot young stars is modified by radiation pressure. The observed variation in the wavelength dependence of interstellar polarization is also in agreement with this hypothesis. Moreover, the 'non-normal' features seen in some of the monochromatic extinction laws for the Orion region can arise from bimodal particle size distributions; the relative number of large size particles is very small.

I

INTRODUCTION

A. Observational Work

From a casual observation of the night sky, the untrained astronomer is often impressed with the apparent emptiness of space. Stars, which seem to be the only celestial ingredient, are the exception rather than the rule as far as the projected area of the sky is concerned. Modern-day astronomers, however, realize that this appearance is illusory. Not only does space contain millions of stars that are too faint to be seen with the naked eye, but the presence of another constituent, consisting of tenuous clouds of gas and dust particles and called interstellar material, is now universally accepted.

The first conclusive evidence that interstellar space is not completely transparent to star light came from the classic work of R. J. Trumpler (1930). Trumpler made an extensive statistical study of galactic star clusters. From photographic plates of these objects he was able to group the clusters into several classes according to their physical appearance (number of visible stars and the degree of central condensation), and then studied the members of each class

separately. He computed the relative distances to the clusters and noted that the distance resulting from a comparison of their apparent sizes was always smaller than that found from their relative brightnesses. In this manner Trumpler concluded that the perfect transparency of space, which was a tacit assumption in his calculation of the photometric distances, did not exist. Not only did he thereby determine the existence of an interstellar obscuring medium, but by observing that the fainter clusters were also the reddest, he showed that this extinction is wavelength dependent--blue light being more strongly attenuated than red light. Trumpler found that the average visual extinction was 0.79^m per kiloparsec and the average differential extinction or reddening (pg. - vis.) was 0.31^m per kiloparsec.

Subsequent investigations were concerned with the exact functional dependence of interstellar extinction on wavelength. Hall (1937) photoelectrically studied the pair of stars, ζ and ϵ Persei, and found that the extinction varied approximately as $1/\lambda$. Stebbins, Huffer, and Whitford (1939) observed a group of B-type stars and found the $1/\lambda$ relation as well as a correlation between the color excess and the strength of interstellar spectral lines. However, these authors noted that the obscuring matter is not uniformly distributed, as Trumpler thought, but is located in discrete clouds, which are now known to lie predominately in the plane of the galaxy. Stebbins and Whitford (1943) made

photometric observations of stars in the 3,500 Å to 10,000 Å spectral range. They examined the deviations from the $1/\lambda$ law and concluded that the extinction law is essentially the same in all parts of the sky. Later, Whitford (1948) used an infrared cell and observed a limited number of stars out to $\lambda = 2.2 \mu$, thereby extending the extinction curve farther into the infrared. This work indicated a definite leveling off of the extinction in the infrared and, to a lesser degree, in the ultraviolet--making the extinction curve somewhat S-shaped.

A schematic extinction curve of this type is shown in Figure 1 where the absorption is plotted as a function of $1/\lambda$. Figure 1 shows that the differential extinction between the B and V filters, E_{B-V} , is simply:

$$(1) \quad E_{B-V} = A_B - A_V = (B-V) - (B-V)_0$$

where $(B-V)$ is the observed B-V color, $(B-V)_0$ is the intrinsic or unreddened B-V color, and A is the total extinction. The ratio of total to selective absorption is then:

$$(2) \quad R = A_V / (A_B - A_V) = A_V / E_{B-V}.$$

The total visual extinction of the light from a given star follows from knowing R and the color excess of the star.

Whether the shape of the curve shown in Figure 1 is unique has been a question of considerable interest and

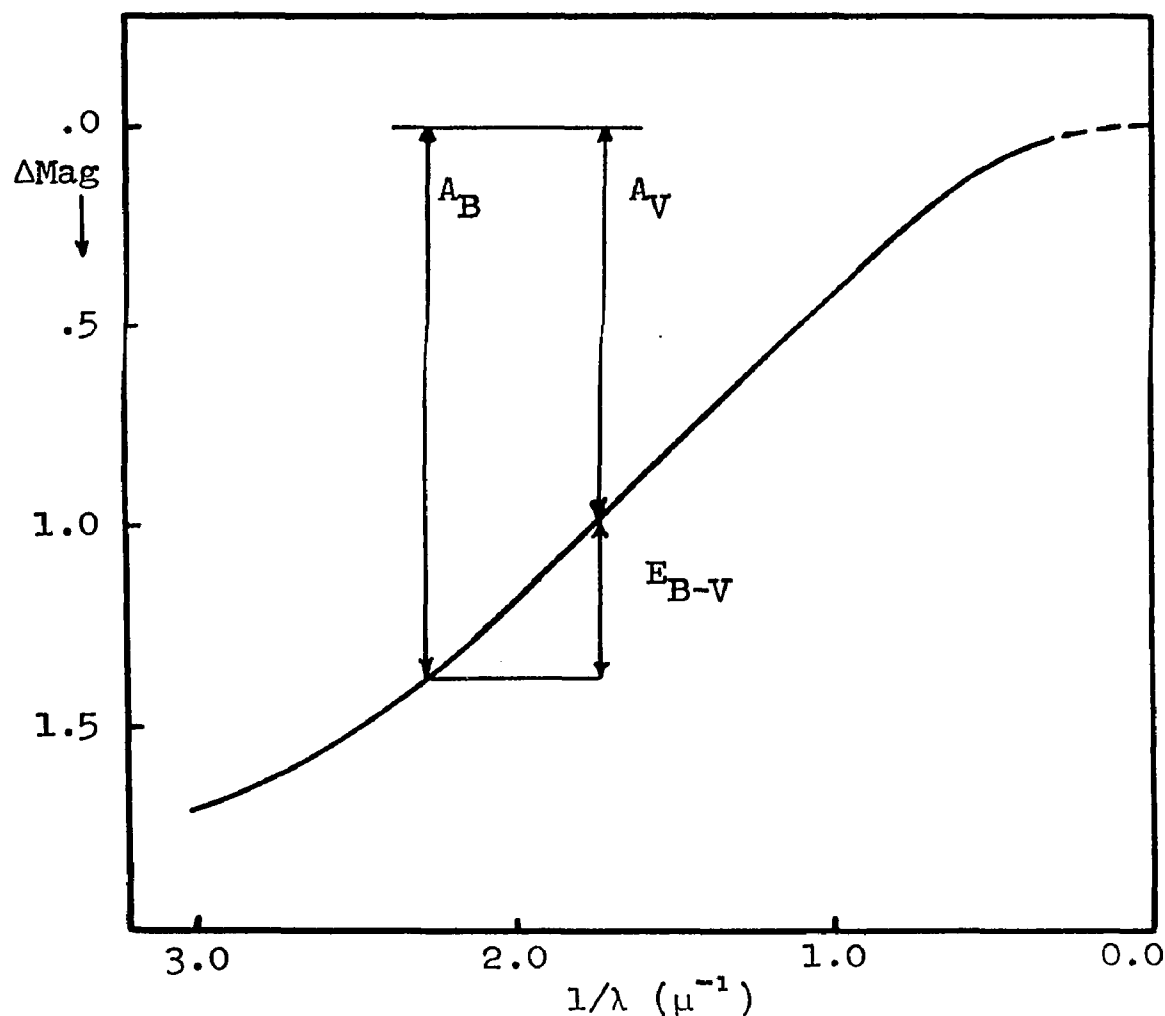


FIGURE 1

Schematic Extinction Curve

The total extinction in magnitudes is plotted against $1/\lambda$ in reciprocal microns. The differential extinction or reddening (E_{B-V}) is shown, as well as the total extinction in the B and V filters.

importance. Clearly the problem of determining true photometric distances is greatly simplified if we can assume that a single value of R is applicable for all parts of the galaxy. Evidence against such a uniform extinction law was first found in the Orion Nebula by Baade and Minkowski (1937b), who noted that considerably more red and infrared light seemed to be absorbed here than in other regions. This was also the conclusion of Stebbins and Whitford (1945), who observed the Trapezium photometrically. Using wide-band photometry, Johnson and Morgan (1955) and Hiltner and Johnson (1956) investigated the deviations in the positions of O-type stars in a two-color diagram. They found that the slope of the reddening line, E_{U-B}/E_{B-V} , is slightly higher in the Cygnus Rift (0.81) than in other regions where it appeared very uniform (0.72). In this same context, Divan's (1954) detailed spectrophotometric study of reddened stars in all regions of the sky showed that in the 3,130 Å to 6,100 Å range, the reddening law is everywhere the same--including the Orion Nebula. Hallam (1959), using seven-color photometry in the 2,950 Å to 11,000 Å spectral region, again confirmed the earlier results for the Orion Trapezium and found that stars associated with nebulosity often show the most significant deviations from a $1/\lambda$ dependence.

Although some variations in the wavelength dependence of interstellar extinction were indicated by these

early investigations, many astronomers assume that the so-called 'normal' relation shown in Figure 1 adequately represents the extinction law in most regions. The value of $R = 3.0$ has been used for all parts of the galaxy (excluding Orion) even though direct evidence has not always been conclusive or even available.

During the last few years, infrared photometry has contributed considerably to our knowledge of the nature of interstellar extinction. The development of refined techniques and special detectors of high sensitivities (Johnson, 1962; Low and Johnson, 1964) has made it possible to observe fainter, more highly reddened stars in the $1-5 \mu$ spectral range. Observations at these wavelengths are very valuable since the extrapolation to $1/\lambda = 0$ --the dashed portion of the curve in Figure 1--is obviously more precise when the last determined point is as far into the infrared as possible. Johnson (1965, 1966a) obtained infrared observations and used the so-called color difference method, which involves the calculation of a series of color excesses from the observed and intrinsic colors of the stars, to derive normalized extinction curves. The only assumption implicit in this method is that stars of the same spectral type will have approximately the same intrinsic colors, and if the precepts of stellar classification are meaningful, then this assumption seems entirely justified. Johnson's results do

indicate that different parts of our galaxy exhibit strikingly different extinction laws. Figure 2 shows the normalized mean extinction curves (see Section IV) for two regions, Cepheus and Scorpius (Johnson, 1966a). The largest deviations from the 'normal' law exhibited by Cepheus and Scorpius curves are found at large wavelengths, beyond 1μ , which again emphasizes the importance of the infrared data. Johnson (1966a) also found that for clusters or groups of stars, the values of R determined by extrapolating the observed portion of the extinction curve to $1/\lambda = 0$ are in good agreement with those values determined from the slope of a distance modulus versus color excess plot. This latter method, the variable extinction method, requires knowledge of the absolute magnitudes of stars of various spectral types and assumes that all stars are at the same distance. Also, the value of R thus obtained pertains only to that component of the interstellar extinction which is variable across the cluster. Nevertheless, agreement between the values of R determined by different methods gives us some assurance that the basic assumptions made in each method are valid.

In addition to simply attenuating star light, aligned, asymmetrical interstellar particles produce another phenomenon, namely interstellar polarization. That is, radiation with its electric vector in a given plane is more

Figure 2. Normalized Extinction Curves for the Cepheus and Scorpius Regions (Johnson, 1966a)

The normalization produces one magnitude of differential extinction between the B and V filters. The Cepheus curve shows greater extinction in the far-infrared and a higher ratio of total to selective absorption. The 'normal' curve is shown for comparison.

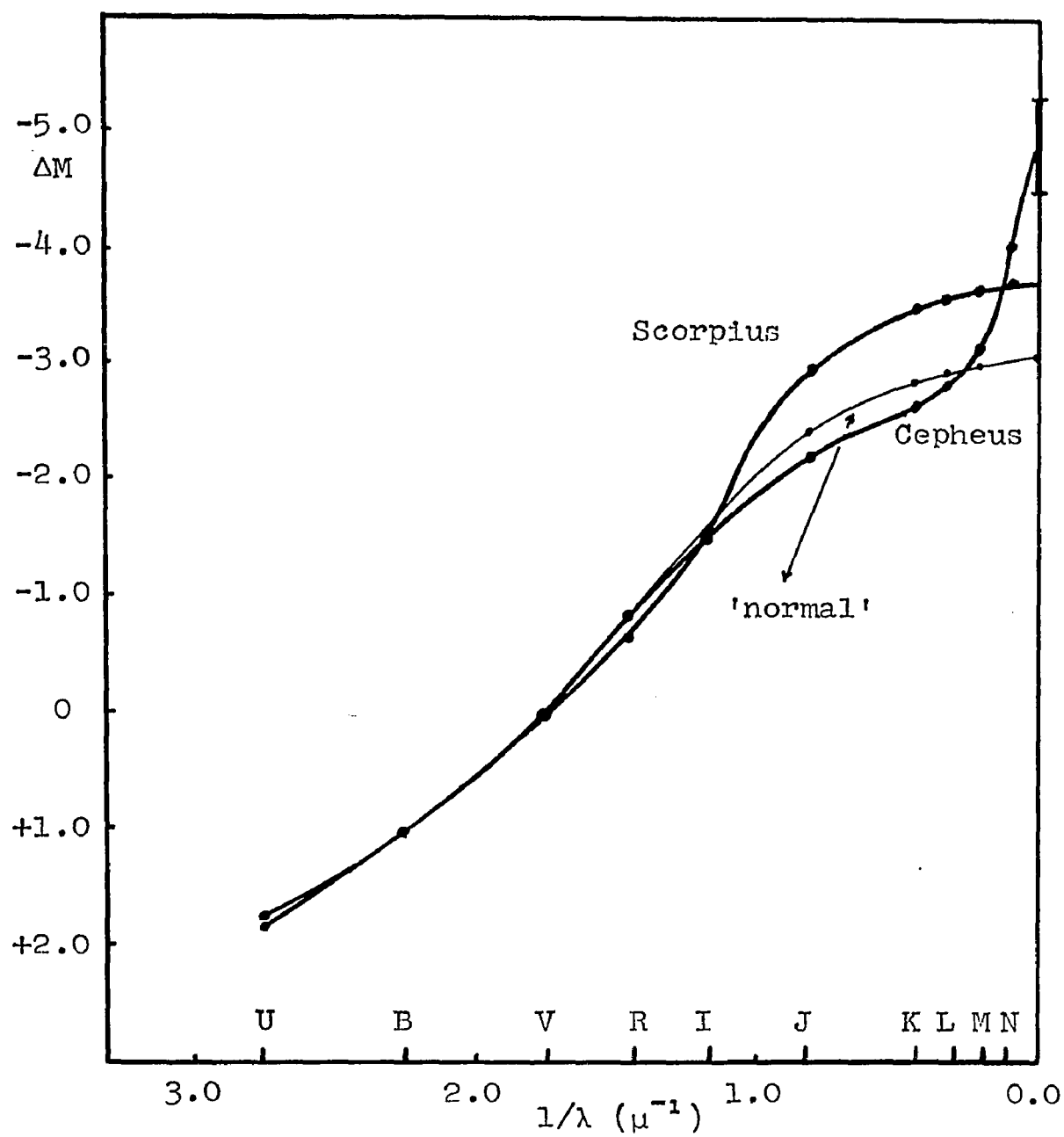


FIGURE 2

Normalized Extinction Curves for the Cepheus and Scorpius Regions (Johnson, 1966a)

strongly scattered by these grains, thereby making the transmitted light partially polarized. The relation between extinction and polarization was shown by Hiltner (1954), whose observations in M 29 clearly reveal that the amount of polarization depends on color excess. However, several stars, including μ Cephei and β Lyrae, are also known to be intrinsically polarized (Coyne and Gehrels, 1966; Shakhovskoi, 1965). The correlation between reddening and interstellar polarization appears to be definite, yet it is not a one-to-one relation. Nearly all highly polarized stars are considerably reddened, but other highly reddened stars exhibit very little polarization. Hall (1958) noted that the amount and plane of the polarization are often related. In regions where the polarization is large it is also very uniform and in the plane of the galaxy, while in areas where the polarization is small it is usually much more randomly oriented.

The wavelength dependence of polarization has been studied by Gehrels (1960), Coyne and Gehrels (1966), and in the southern sky, Visvanathan (1966). These investigations show that the maximum percentage polarization is usually near $\lambda = 6,500 \text{ \AA}$, with a rapid decrease toward the infrared and a more gentle drop toward the ultra-violet. Visvanathan's (1966) results show that the wavelength dependence of polarization in the $\lambda = 3,500 \text{ \AA}$ to $6,500 \text{ \AA}$ range is reasonably constant over the sky, but in the infrared near $\lambda = 9,000 \text{ \AA}$,

this dependence varies considerably from region to region. A recent high-altitude balloon observation of the polarization of ζ Ophiuchi in the ultraviolet at $\lambda = 2,250 \text{ \AA}$ indicates some preference for dielectric particles (Gehrels, 1966).

The evidence for significant variations in the law of interstellar extinction in the regions of Cepheus, Scorpius, Orion, NGC 2244, and recently NGC 6530 (Johnson, 1966c), as well as the variations in the wavelength dependence of interstellar polarization, may indicate that the concept of a 'normal' extinction law is no longer meaningful. The 'normal' ratio of the total to selective absorption of 3.0, which has somehow acquired a strange and perhaps unwarranted degree of sanctity, may now be little more than a lower limit for this parameter. The importance of these variations in such a field as galactic structure is difficult to overemphasize.

B. Theoretical Results

The physical nature of the matter that causes interstellar extinction has been the subject of numerous studies. The problem transcends the extinction phenomenon and involves such related subjects as cosmic abundances, low-temperature chemistry, heating and cooling of the interstellar medium, star formation, and even galactic dynamics. The pioneering

work in the field of the formation and growth of interstellar particles was done by Oort and van de Hulst (1946) and van de Hulst (1949). These authors studied the formation of condensations of atoms or molecules that could then become the nuclei for larger particles. The growth and final composition of a particle depend on the accommodation coefficient or sticking probability of the various atoms and ions with which the particle collides. The destruction of the grains arises primarily from encounters between separate clouds of particles resulting in energetic collisions of individual grains and causing a loss or evaporation of some or all of the granular constituents.

Van de Hulst (1949) also treated the problem of the optics of small spherical particles and calculated theoretical extinction curves for various particle size distributions and indices of refraction. The solutions require solving the appropriate Maxwell equations for the components of the fields that are scattered by and transmitted through the particle. The index of refraction and the size of the particle are introduced through the specification of the boundary conditions. The final solutions are given in terms of the extinction efficiency factors which are defined as follows:

$$(3) \quad E(\lambda) = \frac{\text{Real Extinction Cross Section}}{\text{Geometrical Cross Section}}$$

In Figure 3, taken from van de Hulst (1949), E is plotted against X ($X = 2\pi r/\lambda$; r = radius of particle) for several indices of refraction and single size particles. The efficiency factors all start at zero for infinite wavelength, increase to a maximum, and then approach 2.0 for very large X . A λ^{-4} dependence is seen for particles that are small with respect to the wavelength (Rayleigh scattering) and a λ^0 relation results for particles much larger than λ (geometrical blocking). Since the observations indicate an extinction law that varies approximately as $1/\lambda$, the grains must be nearly the same size as the wavelength of light.

But spherical grains will not account for the polarization observations. Only aligned, elongated particles can produce polarized scattering. Therefore, not only the formation of elongated particles, but also some alignment mechanism must be explained. The question of the production of asymmetrical particles is by no means solved. Two possible mechanisms are:

- a) The fusion of two or more grains following a low-energy collision (van de Hulst, 1949).
- b) An ordered accretion in which the electric dipole moment of the water molecule causes a new H_2O molecule, formed on the surface of the grain, to align itself parallel to the other

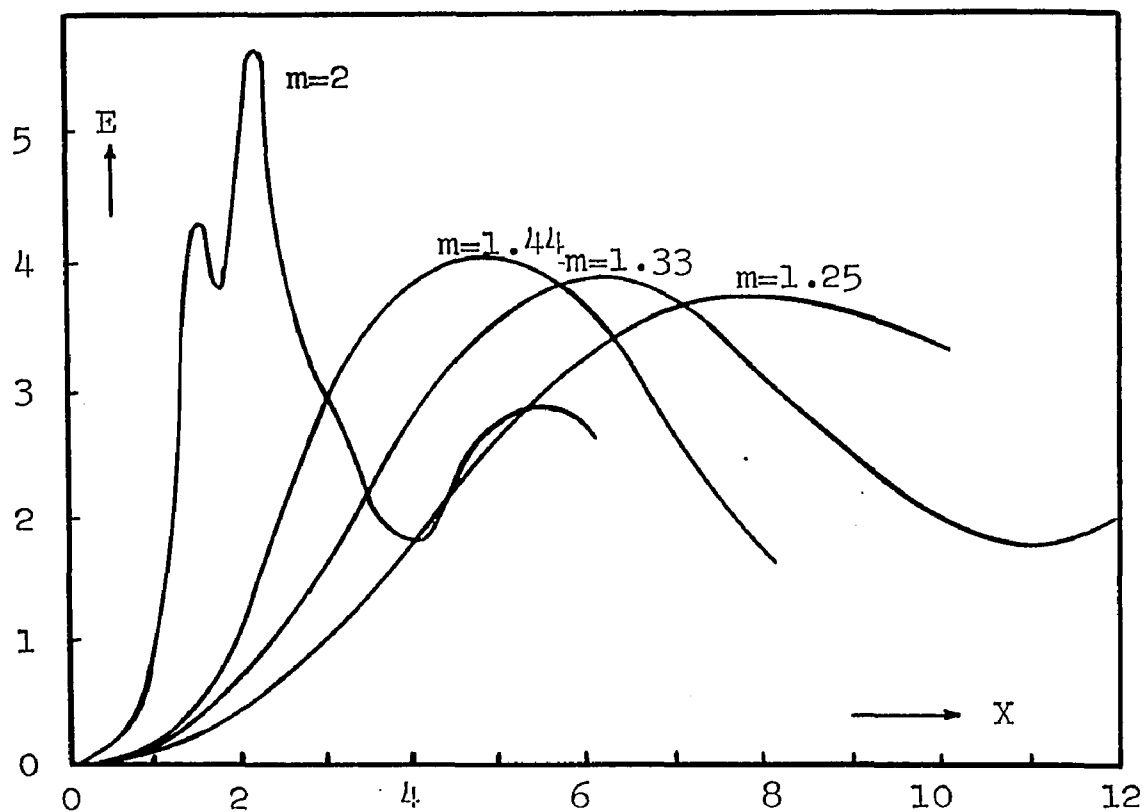


FIGURE 3

Theoretical Extinction Curves (van de Hulst, 1949)

The extinction efficiency, E , is plotted against X , where $X = 2\pi r/\lambda$; r = particle radius. The curves refer to single size particles with index of refraction m .

H₂O molecules in the particle--thereby
producing an elongation (Kahn, 1952).

The alignment mechanism seems to be better understood. Davis and Greenstein (1951) suggested that a spinning, elongated, paramagnetic particle that experiences a sinusoidally varying magnetic field will be subjected to a torque which will tend to orient the axis of rotation--the short axis--parallel to the external field. The spinning is produced by collisions among the grains. The paramagnetism presumably results from minute traces of iron in the 'dirty ice' composition. Collisions will also tend to disorient the rotational axes of the particles, and this effect sets a lower limit on the galactic magnetic field of $B \approx 2 \times 10^{-5}$ gauss if a sufficient degree of alignment is to be maintained.

Such a value for the mean strength of the galactic magnetic field is higher by one order of magnitude than that indicated by the Zeeman splitting of the 21-cm hydrogen line and the retarding effects of a magnetic field on star formation (Woltjer, 1965). On the other hand, observations of synchrotron radiation and the solar wind suggest a stronger field on the order of $B \sim 10^{-5}$ gauss. All of these determinations involve assumptions, some of which are highly uncertain. The differences in the strength of the mean galactic magnetic field are significant since a field of 10^{-5} gauss will strongly control the motions of the

interstellar gas and dust, whereas a field strength of 10^{-6} gauss will have a negligible effect. Certainly, localized variations in the galactic magnetic field cannot be ruled out at this juncture.

The observed wavelength dependence of polarization has been reasonably well reproduced by Greenberg, et al. (1963), who computed the scattering produced by infinitely long cylinders with an equilibrium radius distribution (van de Hulst, 1949) and an index of refraction of 1.3. Although an infinitely long cylinder is a rather improbable configuration, the extinction and polarization from such a particle qualitatively resembles that produced by finite elongated grains (Greenberg, 1966).

Other important comments and theories concerning the nature of interstellar grains have been put forth in recent years. The Oort-van de Hulst theory of grain formation has suffered some criticism (Donn, 1955) with regard to the chemical reactions that will take place on the surface of the grains at very low temperatures. Some experimental evidence indicates that the reaction producing H_2O from H_2 and O may be greatly retarded at very low temperatures, and hence, the H_2O content of the interstellar particles may be considerably less than that given by van de Hulst (1949). Additional evidence to this effect may be found in the results of Danielson, Woolf, and Gaustad (1965), who found,

from high altitude balloon observations, no trace of the 3.1μ absorption band due to ice in the infrared spectrum of the reddened supergiant, μ Cephei. This result indicated that no more than 25% of the extinction for this star can be due to ice crystals. Platt (1956) suggested that the interstellar grains may be just large molecules--radius = 1 \AA to 10 \AA --which have formed by accretion out of the gaseous medium. These particles would be neither chemically stable nor electrically neutral. The optical properties of these Platt particles depend on the arrangements of the electrons in their states, and since their exact extinction curve is unknown, no comparison can be made with the observations.

Another interesting and promising theory proposes that the interstellar grains are graphite particles. Hoyle and Wickramasinghe (1962) suggested that such graphite grains will condense in the atmospheres of carbon stars during a certain phase of their pulsation cycles. The particles are then blown away from the stars by radiation pressure. An estimate of the total amount of graphite lost by all the N-type stars in the galaxy in somewhat less than 10^{10} years is consistent with the present mean interstellar grain density of 10^{-27} g/cu cm . Wickramasinghe (1965) also showed that these carbon particles--mean radius = $3.6 \times 10^6 \text{ cm}$ --will tend to grow ice mantles. The processes of growth and destruction indicate that equilibrium will normally be

reached when the mantle has grown to two or three times the core radius. The optical properties of these composite particles have been investigated by Wickramasinghe, Dharmawardhana, and Wild (1966), who found no difficulty in obtaining extinction curves that agree reasonably well with the observations in the visible spectral regions. An analysis of some rocket observations of six stars at $\lambda = 2,200 \text{ \AA}$ indicated that the extinction in the ultraviolet is much greater than was previously expected (Boggess and Borgman, 1964). The composite graphite-ice particles appear to show greater promise of accounting for these observations than does the Oort - van de Hulst theory. The theoretical extinction curves of van de Hulst (1949), which approximate the 'normal' law from $\lambda = 3,500 \text{ \AA}$ to $10,000 \text{ \AA}$, show a leveling off in the ultraviolet.

Initially, the carbon-particle theory was thought to be in good harmony with the interstellar polarization phenomenon. These particles, due to their anisotropic electromagnetic properties, produce strong polarization and require only a small degree of alignment. A magnetic field of $B \sim 10^{-6}$ gauss is believed to be sufficient (Dieter and Goss, 1966). However, the polarization by small carbon grains determined theoretically (Greenberg, et al., 1963) increases monotonically from the infrared to the ultraviolet, and such a wavelength dependence is definitely contrary to that observed by Coyne and Gehrels (1966). On the other

hand, recently Wickramasinghe, et al. (1966) have found that the theoretical polarization resulting from larger carbon particles--radius = $0.08-0.11 \mu$ --and from composite graphite-ice grains is in reasonable agreement with the observations.

Finally, recent observations of the radio spectral lines of the hydroxyl radical suggest that OH is an important constituent of the interstellar medium. The 18-cm lines of OH have been detected in absorption in Cas A, Sgr A, and in several other radio sources (Robinson, 1965). These lines arise from electric dipole transitions of relatively high transition probabilities. In several cases however, the lines are not found in their proper intensity ratios, and in fact, some completely unknown excitation mechanism seems to be indicated. The 1665 Mc/sec line has been detected in the center of the Orion Nebula, but the 1667 Mc/sec line, which should be the stronger of the two, is not seen (Dieter and Goss, 1966). Since OH is probably formed by the dissociation of H_2O molecules that have evaporated from larger grains, microwave radiation from this radical should yield significant new information concerning grain formation, cosmic abundances, and the general conditions in the interstellar medium.

C. The Orion Region

1. General

The I Orion association is an aggregate of early type stars centered at $RA \cong 5^h 34^m$ and $\delta \cong -2^\circ$. Two principal subgroups will be referred to repeatedly in this investigation: a) the 'Belt' system, which includes ζ , ϵ , and δ Orionis and extends from $\delta = +1^\circ$ to -3° (see Figure 12); and b) the 'Sword' system, which is centered on the Great Orion Nebula (NGC 1976) and includes ι , θ^1 , θ^2 , and ν Orionis. The mean distance of the whole association is between 400 and 500 parsecs (Blaauw, 1964). The Orion Nebula region is the youngest part of the aggregate with an age of 2×10^4 years (Vandervoort, 1964). The star θ^1 Orionis, the Trapezium, is actually four early-type stars. $\theta^1(C)$, an O 6 star, is the primary source of excitation for the nebulosity. Since NGC 1976 is the brightest nebula in the northern hemisphere, it has been the subject of numerous detailed investigations. The results of many of these studies will be discussed in other parts of this paper.

2. Extinction in the Orion Nebula

For nearly thirty years, the outstanding enigma in interstellar extinction has been the Orion Nebula region. While this mystery has certainly had a disconcerting effect on our general understanding of the phenomenon, it has also been somewhat beneficial since it has stimulated many

studies in this field. Recent results indicate that any previous doubts about a uniform extinction law for all parts of the galaxy, inspired solely by the Orion observations, were probably justified.

The history of the extinction problem in the Orion Nebula region begins with the early work of Baade and Minkowski (1937b). These authors, who obtained both photometric and spectrophotometric data, found that the extinction in and near the Trapezium was notably different from that in other areas. The differences found were: 1) the extinction curve from 4,000 Å to 6,000 Å appeared somewhat flatter than 'normal,' and 2) the extinction from 9,000 Å to 6,000 Å increased much more rapidly than in other areas. Stebbins and Whitford (1945) confirmed the infrared anomaly with their six-color work and noted that the deviations from a $1/\lambda$ dependence are twice as large here as those seen elsewhere. Sharpless (1952), who obtained UBV photometry for a large number of stars throughout the I Orion association, concluded that the reddening law for the 'Sword' region in the UBV spectral range ($\lambda \approx 3,000$ Å to 6,000 Å) was not anomalous, but also found evidence for a high ratio of total to selective absorption-- $R = 6.0 \pm 0.2$ (p.e.). A 'normal' reddening law from $\lambda = 3,130$ Å to 6,100 Å for the Trapezium was also found by Divan (1954), who made a thorough study of reddened stars in all parts of the galaxy. Recently,

Johnson and Borgman (1963) and Johnson (1966a) obtained infrared data for the Trapezium area and found that the extinction curve here exhibits a very large gradient in the infrared and a correspondingly high value of R . Johnson and Borgman (1963) give $R = 7.37 \pm 0.25$ (m.e.) for the Orion Nebula. In this same context, Mendez (1965) utilized a different method involving the intensities of the nebular Balmer and Paschen lines, and found an extinction curve for this region which gives $R = 4.8$. Johnson and Mendoza (1964) studied a highly reddened star, NGC 2024 No. 1, in the 'Belt' portion of the association and found that $R = 5.5$ for this star.

The work summarized above yields the following information regarding the extinction law in the neighborhood of θ^1 Orionis:

- 1) The reddening law from 3,000 Å to 6,000 Å very closely resembles that found elsewhere.
- 2) The extinction in the near and far infrared appears to be decidedly 'non-normal' in the sense that the increase in extinction with increasing $1/\lambda$ is much greater than that given by the 'normal' relation.
- 3) The ratio of total to selective absorption is high--perhaps twice the 'normal' value of 3.0.

If it were not for several puzzling complications, these conclusions would provide an adequate answer to the observational portion of this problem. These complicating factors, however, so confuse the interpretation that some astronomers believe these results are by no means definite and are not the final answer.

One of the uncertainties is the question of the intrinsic colors of the Trapezium stars. All four stars are very young and all exhibit peculiar spectra. Furthermore, all have been classified as spectroscopic binaries (Plaskett and Pearce, 1935), and the effects of unseen red companions upon the unreddened infrared indices of the composite star are not precisely known. The nearby star θ^2 Orionis (O 9.5 Vp) exhibits an extinction curve that is very similar to that of the Trapezium, but it too is a recognized spectroscopic binary. Stebbins and Kron (1956) showed that if an unseen K O III-type companion were present with θ^2 Orionis, the extinction law for this star would then be 'normal.' On the other hand, these authors were unable to find a similar such companion for θ^1 Orionis that would make its extinction 'normal.' Certainly some combination of invisible components can probably be found for the Trapezium which would reduce the extinction anomaly here, but as Johnson and Borgman (1963) remark, it is curious that the additional infrared emission required to produce a 'normal' extinction law for these stars is very closely proportional to their color

excesses. Infrared observations of additional stars in this same area should clarify this question.

Another problem is that the stars in and near the Trapezium are imbedded in bright nebulosity and are rather difficult to observe. The location of the diaphragm when the sky measures are made may affect the photometry somewhat, particularly in the infrared where the distribution of the nebular intensity is not so well known. Hallam (1959), however, found that in no case in the 2,950 Å to 11,000 Å spectral region does the nebulosity amount to more than a few percent of the intensity of the Trapezium. The distribution of the nebular radiation in the infrared can be easily seen on infrared photographs of this area.

Finally, other sources of infrared emission in this region must be considered. An infrared plate of the Orion Nebula (Baade and Minkowski, 1937a) shows a pronounced clustering of faint red stars centered on the Trapezium. The cluster is very compact--containing 80 stars within a 3' diameter--and is not visible on a plate taken in visual light. Two similar infrared plates, taken by Dr. G. Haro with the 48-in. Schmidt telescope, show these stars even more clearly and will be reproduced in a later part of this work. These faint red stars are an interesting phenomenon by themselves, but it is their role as a possible contaminant of the photometry of the brighter stars in this region that

is of interest here. The distribution of these red stars, as seen from infrared photographs of this area, should reveal to what extent they are contributing to the anomalous extinction law found here.

The factors discussed above certainly tend to obscure the interpretation of the existing extinction data for the Orion Nebula. Furthermore, in many instances the results of previous investigations are limited since they are based on observations of θ^1 and θ^2 Orionis only. Therefore, I feel that additional infrared data, both in the immediate vicinity of θ^1 Orionis and in other parts of the I Orion association, together with a careful reanalysis of the complicating factors for the Trapezium region will yield definitive answers regarding the true extinction law in this region and the general tendencies of the phenomenon throughout the galaxy.

II

OBSERVATIONAL DATA

A. Selection of Stars

Since the purpose of this study is to obtain information about interstellar extinction in the Orion association, the most highly reddened stars in this region are the best suited for observational investigation. A somewhat uniform distribution of stars was also desired so that some conclusions concerning extinction could be made for all parts of the association. The stars were selected from lists of members of the association given by Sharpless (1952, 1962), Parenago (1954), and Hardie, Heiser, and Tolbert (1965). Since the extinction was found to be almost negligible in some areas, some stars with little reddening were also included. All recognized, early-type members of the Orion association with $m_V < 10.0$ and $E_{B-V} > 0.25$ were observed here.

B. Equipment and Techniques

The observing work was done during the 1964-65 and 1965-66 seasons with the 21-in., 28-in., and 60-in.

photometric telescopes of the Lunar and Planetary Laboratory of the University of Arizona. These instruments are located in the Santa Catalina Mountains (elevation 8,300 ft.) some thirty miles northeast of Tucson, Arizona. The observations consist of wide-band photoelectric photometry on the UBVRIJKL system (Johnson, 1965; Johnson, et al., 1966), extending from 0.36 μ to 3.4 μ . The effective wavelengths, defined in (4), as well as the reciprocal of the effective wavelengths are given in Table 1 for the various filters.

$$(4) \quad \lambda_o = \frac{\int \lambda F(\lambda) d\lambda}{\int F(\lambda) d\lambda}$$

($F(\lambda)$ = normalized filter-cell response function)

Table 1

Effective Wavelengths and Reciprocal Effective Wavelengths for the Photometric Filters

<u>Filter</u>	<u>λ_o (μ)</u>	<u>$1/\lambda_o$ (μ^{-1})</u>
U	0.36	2.78
B	0.44	2.27
V	0.55	1.82
R	0.70	1.43
I	0.88	1.14
J	1.25	0.80
K	2.2	0.45
L	3.4	0.29

The normalized response functions of the filters are shown in Figure 4.

Two separate photometers, one for the UBVRI measures and another for the JKL observations, were required for this work. The UBVRI photometer contains two photocells, a RCA 1P21 (UBV) and a RCA 7102 (RI), cooled by dry ice. Conventional photometric procedures are used with this instrument. The JKL photometer has a PbS photocell with a very high sensitivity and a small effective area ($\frac{1}{4}$ mm \times $\frac{1}{4}$ mm), and is refrigerated with liquid nitrogen. Since the sky brightness is considerable in the far infrared, a special sky-cancellation procedure is required for measures made at these wavelengths. The JKL photometer has two diaphragms aligned in a north-south direction; the star is observed alternately in one diaphragm and then in the other. The sky measure is taken both north and south of the star as the reading is made simultaneously through the diaphragm in which the star is not located. During each integration, the signals received through the two diaphragms are electronically subtracted from each other, and the net integrated deflection is punched out on paper tape. A motorized declination drive system moves the telescope back and forth, the star thereby moving automatically from one hole to the other. The observation is terminated by the observer when the desired precision is obtained. For example, if the

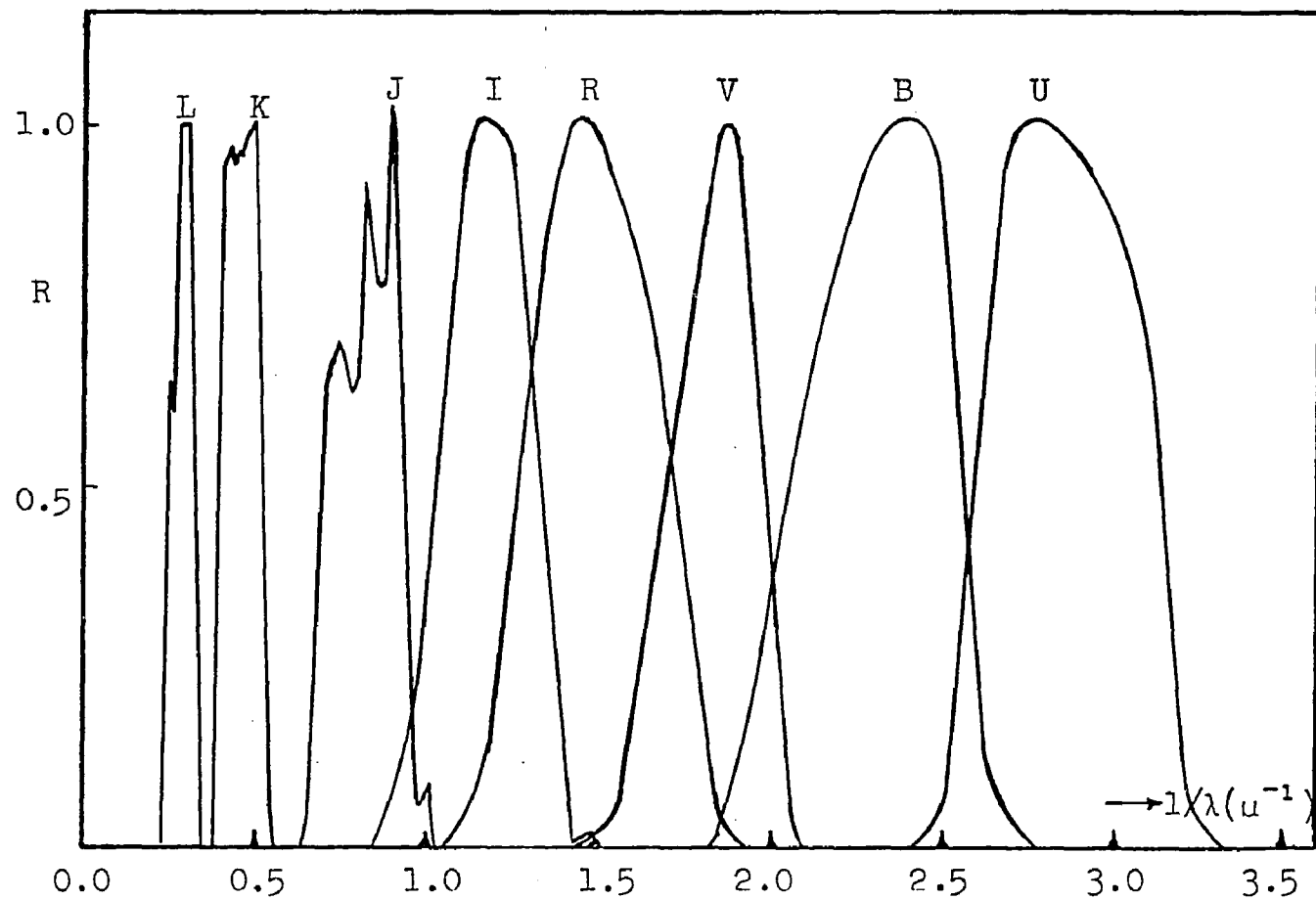


FIGURE 4

Normalized Filter-Cell Response Functions

60-in. telescope is used for the $L(3.4\ \mu)$ measure of an unreddened B-type star whose $m_K > 8^m.0$, one must normally continue the integrations for at least one hour if a probable error of 10% or less is to be realized. Observations of the brighter stars, of course, take much less time.

All of the stars included in this study were observed with the UBVRI photometer, with an average of 3.1 observations per star being obtained. The additional integration time required per observation for the JKL measures restricted this work to 44 of the above stars. Priority for the JKL data was given to the most highly reddened stars, but all of the brighter stars in Orion were also observed since they required very little telescope time. A limited number of observations of the brighter stars were taken from the photometry files of the Lunar and Planetary Laboratory and incorporated into this study so that the best possible values of the colors and magnitudes could be used here.

The photometric reductions were carried out on the IBM 7072 computer of the Numerical Analysis Laboratory of the University of Arizona. The reduction procedure and other details of the observing apparatus and method have been described by Johnson and Mitchell (1962). A least squares adjustment for the extinction coefficients is made whenever possible, but mean coefficients are used occasionally when sky conditions are marginal or few standard stars

are observed. The design of the photometers and associated equipment is such that all data necessary for the reduction, such as star names, coordinates, integrations, filter and gain positions, times, etc., are punched onto paper tape at the telescope. The information is then transferred to IBM cards which are processed by the computer, with only a minimum of manual handling and editing required.

C. The Data

The observational data are presented in Tables 2 and 3. Those stars having only UBVRI photometry are found in Table 2, while those observed at 2.2 μ and 3.4 μ are given in Table 3. The data of Table 2 are as follows:

- | | |
|----------|--|
| Column 1 | <u>Star Name</u> . Either Henry Draper (HD), Bonner Durchmusterung (BD), or Parenago (P) numbers are given. Bayer designations are also given for the brightest stars. An asterisk (*) indicates a note is included at the end of the table. |
| Column 2 | <u>Region Designation</u> . N, B, or S indicate that the star is located in the northern, 'Belt,' or 'Sword' regions of the association. |
| Column 3 | <u>Number of Observations</u> . |

Column 4	<u>Apparent Visual Magnitude.</u>
Column 5-8	<u>Color Indices.</u>
Column 9	<u>Spectral Type.</u> The types have been taken from many sources: Sharpless (1952), Parenago (1954), Johnson and Morgan (1953), Hiltner (1956), Johnson and Borgman (1963), Straizys (1963, 1964), and Bartkus (1964). The more uncertain spectral types are given in parentheses.
Column 10	<u>Intrinsic (B-V).</u> (See Section IV B)
Column 11	<u>E_{B-V}.</u> Blank means $E_{B-V} < 0^m.05$.
Column 12	<u>E_{V-I}/E_{B-V}.</u>

Table 3 is organized in a similar manner except the two numbers given in Column 3 refer to the number of UBVRI and JKL observations respectively.

Table 2
UBVRI Observations

Star	R	N	V	U-V	B-V	V-R	V-I	Sp.	(B-V) ₀	E _{B-V}	$\frac{E_{V-I}}{E_{B-V}}$
31237* (π^5)	N	3	3.73	-1.01	- .19	- .06	- .26	B 2 III	-.24	+.05	1.6
-3° 1013	S	3	10.08	+ .25	+ .20	+ .23	+ .40	B 9 V	-.04	+.24	1.83
33647	N	2	6.67	- .41	- .07	+ .01	- .10	B 8 V	-.09	--	
34179	B	3	8.04	- .50	- .06	+ .01	- .07	B 8 V	-.14	+.08	1.5
34317	N	2	6.42	.00	- .02	+ .05	+ .02	A 0 V	.00	--	
34511	B	2	7.38	- .82	- .14	- .04	- .20	B 5 V	-.20	+.06	1.2
34959	N	4	6.62	- .56	- .09	+ .03	- .02	B 5 p			
35007	B	3	5.69	- .77	- .11	- .02	- .17	B 3 V	-.20	+.09	1.1
35203	N	3	7.98	- .56	- .09	- .02	- .10	B 6 V	-.15	+.06	1.7
35298*	N	2	7.89	- .71	- .12	- .04	- .20	B 9 V	-.18	+.06	0.7
35299	B	9	5.70	-1.09	- .21	- .08	- .27	B 1 V	-.26	+.05	1.8
35407	N	3	6.32	- .78	- .15	- .05	- .21	B 5 V	-.16	--	
35439	N	5	4.96	-1.13	- .20	- .08	- .30	B 1 Vp			
35501	N	2	7.42	- .44	- .05	+ .02	- .08	B 8 V	-.13	+.08	1.2
35575	B	3	6.43	- .89	- .17	- .05	- .22	B 3 V	-.20	--	
35588	B	3	6.16	- .93	- .18	- .06	- .26	B 3 V	-.20	--	
35640	S	2	6.23	- .28	- .05	+ .01	- .04	B 9 V	-.06	--	
35715 (ψ)	N	5	4.60	-1.14	- .21	- .11	- .33	B 2 IV	-.24	--	

Table 2--Continued

Star	R	N	V	U-V	B-V	V-R	V-I	Sp.	(B-V) ₀	E _{B-V}	$\frac{E_{V-I}}{E_{B-V}}$
35718	S	2	8.69	+ .02	+ .06	+ .09	+ .10	(B 8-9)	-.03	+.09	1.4
35730	N	2	7.20	- .80	- .13	- .05	- .23	B 5 p			
35762	N	2	6.75	- .90	- .16	- .06	- .25	B 2 V	-.22	+.06	0.8
35777	B	3	6.62	- .91	- .15	- .03	- .20	B 2 V	-.23	+.08	1.2
35792	B	2	7.21	- .77	- .14	- .05	- .19	B 3 V	-.19	+.05	1.4
35834	N	3	7.70	- .36	- .03	+ .05	.00	B 8 V	-.11	+.08	1.9
35881	N	2	7.80	- .55	- .07	.00	- .09	B 8 V	-.15	+.08	1.4
35882	B	2	7.81	- .53	- .07	+ .01	- .02	(B 8)	-.15	+.08	2.2
35899	B	3	7.51	- .74	- .12	- .05	- .18	B 5 V	-.19	+.07	1.1
35901	S	2	9.03	- .16	- .03	+ .09	+ .08	(B 8-9)	-.03	--	
35912	N	2	6.40	- .92	- .17	- .06	- .24	(B 2)	-.22	+.05	1.2
36012	N	2	7.33	- .69	- .11	- .05	- .15	(B 2-B 5)	-.18	+.07	1.3
36013	N	3	6.91	- .77	- .14	- .04	- .18	B 2 V	-.19	+.05	1.6
36120	S	3	7.97	- .40	- .05	+ .04	- .01	(B 8-9)	-.11	+.06	2.3
36133	N	6	7.12	- .78	- .11	- .06	- .23	B 2 V	-.21	+.10	0.5
36151	S	2	6.67	- .70	- .11	- .02	- .14	B 5 V	-.18	+.07	1.4
36166	N	4	5.78	-1.04	- .20	- .06	- .26	B 1.5 V	-.25	+.05	1.6
36219	B	2	7.65	- .38	- .06	- .02	- .08	(B 8-9)	-.10	--	
36234	S	3	8.65	- .43	- .06	- .01	- .10	(B 8-9)	-.12	+.06	1.2

Table 2--Continued

Star	R	N	V	U-V	B-V	V-R	V-I	Sp.	(B-V) ₀	E _{B-V}	$\frac{E_{V-I}}{E_{B-V}}$
36285	S	3	6.32	-1.03	- .19	- .07	- .24	B 1.5 V	-.25	+.06	1.7
36324	S	3	9.03	+ .14	+ .06	+ .08	+ .10	(A 0-A 2)	+.06	--	
-3° 1119	S	2	10.31	+ .32	+ .20	+ .21	+ .36	(B 9-A 0)	-.02	+.22	1.73
36366	S	3	8.18	+ .01	+ .05	+ .10	+ .11	(B 9-A 0)	-.03	+.08	1.8
36392	N	4	7.54	- .75	- .12	- .04	- .19	B 3 V	-.19	+.07	1.0
36411	S	4	9.71	+ .15	+ .09	+ .14	+ .12	(B 8-9)	.00	+.09	1.3
36412	S	3	9.47	+1.24	+ .72	+ .69	+1.20	(A 7)	+.15	+.57	1.70
36429	N	4	7.56	- .75	- .12	.00	- .12	B 5 V	-.19	+.07	2.0
36430	S	2	6.21	- .92	- .18	- .06	- .24	B 2 V	-.20	--	
36487	S	3	7.78	- .63	- .11	- .01	- .13	B 5 V	-.16	+.05	1.8
36513	S	3	9.49	- .05	+ .02	+ .04	+ .02	(B 8-9)	-.04	+.06	1.0
36527	S	2	9.49	+ .25	+ .15	+ .24	+ .29	(A 0)	.00	+.15	1.93
36540*	S	3	8.14	- .42	+ .06	+ .17	+ .22	(B 8-9)	-.18	+.24	1.91
36541	S	2	7.67	- .54	- .10	+ .03	- .07	(B 8-9)	-.12	--	
36550	S	3	9.35	- .04	+ .02	+ .05	+ .02	(B 8-9)	-.03	+.05	1.0
36559	S	3	8.81	- .26	- .03	+ .07	- .04	(B 8-9)	-.08	+.05	1.2
36560	S	2	8.25	- .46	- .08	- .01	- .11	(B 9)	-.11	--	
36591	B 10		5.35	-1.12	- .19	- .05	- .24	B 1 V	-.27	+.08	1.8
36607	S	2	9.19	- .18	- .03	+ .04	- .02	(B 8-9)	-.04	--	
-5° 1287	S	2	10.02	+ .35	+ .28	+ .23	+ .36	(A 8)	+.28	--	

Table 2--Continued

Star	R	N	V	U-V	B-V	V-R	V-I	Sp.	(B-V) ₀	E _{B-V}	$\frac{E_{V-I}}{E_{B-V}}$
36627	N	3	7.58	- .64	- .10	- .05	- .14	B 6 V	-.17	+.07	1.3
36655	S	2	8.61	- .31	- .05	+ .11	+ .08	(B 8-9)	-.06	--	
36670	S	2	8.94	- .05	+ .02	+ .09	+ .03	(B 8-9)	-.03	+.05	1.2
36697	S	3	8.63	+ .03	+ .07	+ .11	+ .13	(B 8-9)	-.03	+.10	1.6
P 1212	S	2	11.36	+1.06	+ .68	+ .66	+1.23	(A 0)	.00	+.68	1.81
36741	N	4	6.58	- .96	- .16	- .07	- .28	B 2 V	-.24	+.08	0.5
36779	B	3	6.20	- .97	- .16	- .06	- .24	B 3 V	-.24	+.08	1.0
36783	S	2	9.49	- .08	+ .01	+ .05	+ .07	(B 8-9)	-.04	+.05	2.2
-3° 1140	S	2	10.18	+ .36	+ .27	+ .30	+ .50	(B 8-9)	-.04	+.31	1.74
36841	B	2	8.58	- .30	+ .04	+ .08	+ .11	(B 9)	-.13	+.17	1.71
36842	S	2	8.12	- .59	- .08	.00	- .11	(B 3)	-.16	+.08	1.4
36863	B	3	8.28	+ .47	+ .27	+ .31	+ .39	(A 0-A 2)	+.03	+.24	1.46
36865	S	2	7.41	- .48	- .05	+ .04	- .04	(B 8-9)	-.14	+.09	1.7
36867	S	2	9.28	- .14	.00	+ .02	- .01	(B 8-9)	-.06	+.06	0.8
-5° 1302	S	3	10.27	+ .38	+ .25	+ .24	+ .36	A 7 V	+.20	+.05	1.2
36883	S	3	7.26	- .55	- .09	+ .05	- .05	(B 8-9)	-.15	+.07	2.8
36898	B	3	7.11	- .50	- .08	+ .01	- .08	(B 5)	-.13	+.05	2.0
36899	S	2	9.59	+ .01	+ .05	+ .02	+ .02	(B 8-9)	-.03	+.08	0.7
36916	S	3	6.75	- .67	- .14	.00	- .14	(B 8-9)	-.14	--	

Table 2--Continued

Star	R	N	V	U-V	B-V	V-R	V-I	Sp.	(B-V) ₀	E _{B-V}	$\frac{E_{V-I}}{E_{B-V}}$
36917*	S	3	7.94	+ .17	+ .13	+ .24	+ .46	(A 0)	-.02	+.15	3.2
36918	S	3	8.32	- .63	- .10	- .04	- .17	(B -)	-.16	+.06	0.8
36936	S	3	7.57	- .68	- .11	- .02	- .16	(B 5-6)	-.17	+.06	1.2
36938	S	2	8.85	- .14	+ .06	+ .12	+ .18	(B 8-9)	-.09	+.15	2.0
36939	S	2	8.97	- .30	- .04	.00	- .03	(B 8-9)	-.08	--	
-5° 1309	S	3	10.91	+ .71	+ .41	+ .38	+ .65	(A 0)	.00	+.41	1.59
-5° 1310	S	2	10.43	+ .78	+ .54	+ .52	+ .90	(B 9)	-.06	+.60	1.58
36954	B	2	6.97	- .75	- .11	- .02	- .13	B 3 V	-.20	+.09	1.6
36957	S	3	8.84	+ .03	+ .06	+ .10	+ .07	(B 8-9)	-.03	+.09	1.1
36958*	S	3	7.32	- .72	- .10	+ .04	- .04	(B 3)	-.19	+.09	2.4
36959	S	3	5.67	-1.15	- .24	- .07	- .28	B 1 V	-.26	--	
36960	S	7	4.78	-1.27	- .25	- .11	- .35	B 0 V	-.27	--	
-3° 1143	S	4	9.87	+ .22	+ .13	+ .20	+ .35	(B 8-9)	.00	+.13	2.69
36982*	S	4	8.43	- .52	+ .10	+ .24	+ .45	B 1.5 Vp			
36983	S	3	9.15	- .22	.00	- .02	- .06	(B 8-9)	-.09	+.09	0.7
36998	S	2	9.02	- .21	- .01	+ .12	+ .05	(B 8-9)	-.07	+.06	2.2
36999	S	3	8.43	- .55	- .11	- .02	- .14	(B 8-9)	-.12	--	
37000	S	3	7.42	- .80	- .14	- .03	- .17	(B 5)	-.20	+.06	1.7
37001	S	3	8.88	- .30	- .04	+ .03	- .04	(B 8-9)	-.09	+.05	1.6
37016	S	2	6.25	- .85	- .15	- .01	- .18	B 3 V	-.21	+.06	1.7

Table 2--Continued

Star	R	N	V	U-V	B-V	V-R	V-I	Sp.	(B-V) ₀	E _{B-V}	$\frac{E_{V-I}}{E_{B-V}}$
37017	S	3	6.55	- .89	- .13	- .05	- .19	B 1.5 V	-.23	+.10	1.2
37018	S	7	4.59	-1.13	- .19	- .08	- .26	B 2 III	-.24	--	
-4° 1181	S	3	9.51	- .10	+ .34	+ .49	+ .94	(B 3)	-.23	+.57	2.19
37019	S	2	9.34	- .06	+ .02	+ .06	+ .03	(B 8-9)	-.04	+.06	1.2
37020	S	2	6.72	- .86	.00	+ .31	+ .52	B 0.5 Vp	-.29	+.29	3.14
37023	S	3	6.70	- .74	+ .08	+ .31	+ .51	B 0.5 Vp	-.30	+.38	2.42
37040	S	3	6.32	- .84	- .13	- .02	- .18	(B 2-3)	-.21	+.08	1.2
37055	S	3	6.40	- .76	- .12	- .01	- .14	B 3 V	-.19	+.07	1.7
37056	S	3	8.37	- .41	- .05	+ .04	- .02	(B 8-9)	-.12	+.07	2.1
37057	S	3	9.29	- .11	+ .01	+ .14	+ .14	(B 8-9)	-.05	+.06	3.2
37058*	S	3	7.32	- .93	- .15	- .04	- .24	B 2 Vp			
37059	S	3	9.07	- .28	- .02	.00	- .06	(B 8-9)	-.09	+.07	0.9
37060	S	3	9.35	- .07	- .01	+ .05	+ .03	(B 8-9)	-.02	--	
37062*	S	5	8.17	- .45	+ .04	+ .15	+ .24	B 5 V	-.18	+.22	2.18
-5° 1328	S	3	9.86	+ .08	+ .05	+ .12	+ .11	(A 0)	.00	+.05	2.2
-5° 1324*	S	2	9.78	+ .61	+ .46	+ .42	+ .70	(A 8-F 0)	+.30	+.16	1.88
37078	S	2	9.44	+ .19	+ .09	+ .09	+ .10	(A 0)	.00	+.09	1.1
37129	S	3	7.14	- .87	- .17	- .05	- .21	(B 2-3p)			
37130	S	3	9.97	+ .02	+ .11	+ .24	+ .45	(B 8-9)	-.06	+.17	3.0
37131	S	2	8.13	- .40	- .07	+ .05	+ .02	(B 8-9)	-.13	+.06	3.3

Table 2--Continued

Star	R	N	V	U-V	B-V	V-R	V-I	Sp.	(B-V) ₀	E _{B-V}	$\frac{E_{V-I}}{E_{B-V}}$
37209	S	2	5.74	-1.13	- .22	- .06	- .30	(B 2)	-.25	--	
-3° 1154	S	2	9.67	- .14	- .04	+ .06	+ .01	(B 8-A0)	-.03	--	
37258	S	2	9.60	+ .15	+ .11	+ .15	+ .27	(A 0)	-.02	+.13	2.23
37273	S	4	9.92	+ .20	+ .15	+ .20	+ .33	(B 8-9)	-.02	+.17	2.06
37303	S	2	6.06	-1.13	- .21	- .07	- .32	B1 V	-.27	+.06	1.0
37321	B	2	7.13	- .58	- .08	.00	- .08	B 3 V	-.16	+.08	1.8
37322	S	2	9.80	+ .09	+ .07	+ .07	+ .08	(A 0)	-.01	+.08	1.1
37330	N	3	7.46	- .62	- .10	+ .01	- .11	B 6 V	-.16	+.06	1.8
37357	S	3	8.87	+ .17	+ .09	+ .12	+ .22	(B 8-A 0)	.00	+.09	2.4
P 2603	S	3	10.87	+ .55	+ .30	+ .32	+ .55	(A 2-5)	+.10	+.20	1.95
37373	S	2	8.33	- .47	- .11	- .01	- .12	(B 8-9)	-.09	--	
37390	S	3	9.42	+ .10	+ .15	+ .22	+ .39	(B 8-9)	-.06	+.21	2.14
-6° 1270	S	3	9.78	+ .15	+ .08	+ .08	+ .14	(A 0-A 2)	+.06	--	
P 2652	S	2	11.45	+1.22	+ .88	+ .84	+1.42	(B 9)	-.10	+.98	1.59
37411	S	3	9.79	+ .24	+ .12	+ .19	+ .34	(B 8-9)	.00	+.12	2.8
-6° 1273	S	3	10.23	+ .29	+ .29	+ .30	+ .60	(B 8-9)	-.07	+.36	1.89
37469	S	3	9.62	+ .23	+ .19	+ .26	+ .44	(B 8-9)	-.04	+.23	2.09
37470	S	3	8.24	- .21	+ .02	+ .13	+ .17	(B 8-9)	-.09	+.11	2.64
-0° 1046	B	3	10.39	+ .68	+ .39	+ .38	+ .69	(A 2)	+.06	+.33	1.82
37526	S	2	7.60	- .66	- .14	- .03	- .17	(B 3 V)	-.14	--	

Table 2--Continued

Star	R	N	V	U-V	B-V	V-R	V-I	Sp.	(B-V) ₀	E _{B-V}	$\frac{E_{V-I}}{E_{B-V}}$
37547	S	3	9.28	- .11	- .03	+ .01	- .02	(B 8-9)	-.03	--	
-5° 1352	S	3	10.45	+1.03	+ .61	+ .56	+ .99	(A 8-F 0)	+.15	+.46	1.43
37642	S	3	8.06	- .71	- .14	.00	- .12	(B 8-9)	-.15	--	
37700	S	2	8.04	- .57	- .11	- .01	- .14	(B 8-9)	-.12	--	
-4° 1211	S	3	10.26	+ .24	+ .14	+ .10	+ .24	(A 2)	+.14	--	
P 2942	S	3	12.24	+1.25	+ .70	+ .66	+1.13	(A 0)	.00	+.70	1.61
37807	S	2	7.90	- .72	- .11	- .04	- .15	(B 2)	-.19	+.08	1.1
37888	S	2	9.21	.00	+ .02	+ .08	+ .10	(B 8-9)	.00	--	
37889	S	2	7.67	- .80	- .13	- .01	- .13	B 2 V	-.20	+.07	2.0
38087	B	3	8.30	- .33	+ .11	+ .23	+ .40	(B 3)	-.18	+.29	2.21
38088	S	3	9.68	+ .23	+ .16	+ .20	+ .34	(A 0)	.00	+.16	2.12
38120	S	2	9.05	- .04	+ .03	+ .12	+ .16	(B 8-9)	-.04	+.07	2.9
38165	B	2	8.84	+ .05	+ .25	+ .30	+ .50	(B 9)	-.12	+.37	1.81
38239	S	2	9.22	+ .05	+ .04	+ .07	+ .03	(A 0)	.00	--	
-5° 1377	S	3	9.78	+ .78	+ .44	+ .39	+ .72	(A 2)	+.06	+.38	1.66

Notes to Table 2

HD 31237	π^5	Orionis	Variable Star
35298			Sp. type too late
36540			Sp. type too late
36917	V372	Orionis	Variable Star
36958	KX	Orionis	Variable Star
36982	LP	Orionis	Variable Star
37058	V359	Orionis	Variable Star
37062	V361	Orionis	Variable Star
-5° 1324	NV	Orionis	Variable Star

Table 3

UBVRIJKL Observations

Star	R	N	V	U-V	B-V	V-R	V-I	V-J	V-K	V-L	Sp.	(B-V) ₀	E _{B-V}	
30836 (π^4)	N	7	4	3.68	- .96	- .16	- .07	- .22	- .38	- .47	- .52	B 2 III	- .23	+ .07
34748	B	3	6	6.35	- .86	- .11	+ .01	- .13	- .30	- .37	- .26	B 1.5 V	- .23	+ .12
34989	N	3	4	5.80	-1.01	- .13	+ .01	- .12	- .33	- .47	- .49	B 1 V	- .27	+ .14
35039	B	7	3	4.74	- .95	- .16	- .05	- .23	- .35	- .49	- .49	B 2 IV	- .24	+ .08
35079	B	4	6	7.07	- .56	- .04	+ .03	- .03	- .07	- .10	+ .06	B 3 V	- .17	+ .13
35149	N	5	2	5.00	-1.01	- .14	- .05	- .23	- .36	- .56	- .66	B 1 V	- .27	+ .13
35411* (η)	B	6	7	3.35	-1.10	- .17	- .05	- .30	- .40	- .52	- .57	B 0.5 V	- .28	+ .11
35502	B	2	5	7.34	- .58	- .04	+ .02	- .06	- .13	- .19	.00	B 5 V	- .18	+ .14
35673	N	3	4	6.53	- .20	.00	+ .07	+ .04	+ .03	+ .02		B 9 V	- .08	+ .08
35910	N	2	5	7.57	- .62	- .10	- .03	- .15	- .27	- .23		B 6 V	- .16	+ .06
36267	N	3	3	4.21	- .70	- .13	- .05	- .20	- .37	- .45	- .43	B 5 V	- .16	--
36351	N	2	4	5.46	- .99	- .17	- .07	- .26	- .46	- .53	- .48	B 1.5 V	- .24	+ .07
36486* (δ)	B	6	10	2.24	-1.28	- .22	- .08	- .30	- .45	- .63	- .63	O 9.5 II	- .30	+ .08
36512 (ν)	S	5	4	4.63	-1.33	- .26	- .12	- .37	- .67	- .90	-1.03	B 0 V	- .30	--
36629	S	4	5	7.65	- .64	+ .02	+ .12	+ .12	+ .04	+ .07		B 2 V	- .24	+ .26
36646	B	2	5	6.53	- .75	- .10	.00	- .11	- .27	- .33		B 3 V	- .20	+ .10
36695*	B	8	4	5.34	-1.09	- .18	- .05	- .25	- .46	- .57	- .69	B 1 V	- .27	+ .09
36781	B	3	3	8.51	- .40	.00	+ .07	+ .07	.00	- .07		(B 9)	- .14	+ .14
36811	B	2	2	7.07	+ .29	+ .17	+ .13	+ .23	+ .36	+ .50	+ .49	(A 0)	.00	+ .17
36822 (φ^1)	N	3	2	4.41	-1.12	- .15	- .01	- .18	- .38	- .54	- .56	B 0 IV	- .30	+ .15
36824	N	2	4	6.71	- .85	- .14	- .02	- .18	- .46	- .54	- .49	B 3 V	- .21	+ .07
36861 (λ)	N	3	3	3.39	-1.20	- .18	- .06	- .23	- .38	- .53		O 8	- .30	+ .12
36981	S	4	3	7.84	- .71	- .13	- .03	- .16	- .25	- .37		(B 3)	- .16	--
37020-3 (θ^1)	S	2	4	4.58	- .81	+ .05	+ .22	+ .43	+ .45	+ .83	+1.26	O-	- .31	+ .36
37022 ($\theta^1(c)$)	S	4	1	5.13	- .95	.00	+ .22	+ .40	+ .55	+ .77	+ .98	O 6p	- .32	+ .32
37025	S	2	3	7.13	- .78	- .14	- .04	- .16	- .25	- .36		(B 3)	- .19	+ .05
-5° 1318	S	3	2	9.71	- .07	+ .27	+ .36	+ .90	+1.23	+2.14	+3.04	(B 2)	- .19	+ .46
37041 (θ^2)	S	6	6	5.07	-1.02	- .09	+ .09	+ .09	+ .01	+ .08	+ .61	O 9.5 Vp	- .30	+ .21
37042	S	5	5	6.41	- .98	- .08	+ .04	.00	+ .01	+ .01	+ .33	B 1 V	- .29	+ .21

Table 3--Continued

Star	R	N	V	U-V	B-V	V-R	V-I	V-J	V-K	V-L	Sp.	(B-V) ₀	E _{B-V}	
37043	S	5	5	2.76	-1.31	- .25	- .08	- .29	- .52	- .72	- .75	O 9 III	- .30	+ .05
37061*	S	3	4	6.80	- .39	+ .27	+ .39	+ .70	+ .92	+1.30	+1.57	B 1 V	- .30	+ .57
37128 (ε)	B	9	12	1.69	-1.21	- .18	- .07	- .24	- .37	- .48	- .46	B 0 Ia	- .27	+ .09
37140	B	3	5	8.56	- .31	+ .10	+ .18	+ .24	+ .35	+ .43	+ .88	(B 5)	- .17	+ .27
37428	S	4	3	8.68	- .05	+ .11	+ .19	+ .31	+ .32	+ .25	+ .19	(B 8-9)	- .09	+ .20
37468	B	6	2	3.80	-1.25	- .24	- .08	- .32	- .54	- .70	- .73	O 9.5 V	- .29	+ .05
37490 (w)	N	5	5	4.59	- .86	- .10	+ .02	- .08	- .17	- .23	- .21	B 3 IIIe	- .20	+ .10
-0° 1050	B	3	2	10.13	+ .71	+ .59	+ .57	+ .99	+1.16	+1.43		(B 8-A 0)	- .11	+ .70
37742 (ζ)	B	7	10	1.77	-1.27	- .21	- .08	- .28	- .44	- .56	- .54	O 9.5 Ib	- .27	+ .06
NGC 2024 No. 1	B	3	3	12.17	+1.70	+1.41	+1.80	+3.46	+4.79	+6.24	+7.09	O-	- .31	+1.72
37903	B	5	7	7.83	- .51	- .11	+ .19	+ .31	+ .35	+ .42	+ .83	B 1.5 V	- .25	+ .36
38051	S	4	3	8.48	+ .05	+ .35	+ .38	+ .64	+ .72	+ .79		B 3	- .20	+ .55
38563A	B	5	3	10.42	+ .51	+ .58	+ .66	+1.25	+1.35	+1.82	+2.78	(B 5)	- .18	+ .76
38563B*	B	5	4	10.56	+1.53	+1.14	+1.23	+2.31	+3.00	+3.85	+3.99	(B 1)	- .18	+1.32
38771 (η)	S	3	6	2.06	-1.18	- .18	- .04	- .21	- .41	- .53	- .56	B 0.5 Ia	- .25	+ .07
41117 (χ ²)	N	4	4	4.63	- .39	+ .28	+ .31	+ .53	+ .59	+ .77	+ .92	B 2 Ia	- .18	+ .46

*Notes to Table 3

HD 35411 η Orionis	Variable Star
36486 δ Orionis	Variable Star
36695 VV Orionis	Variable Star
37061 NU Orionis	Variable Star (??)
38563B	Sp. Type too early (?)

III

INTRINSIC COLORS OF EARLY-TYPE STARS

A. Unreddened Early-Type Stars

The study of interstellar extinction requires knowledge of the intrinsic (unreddened) color indices of early-type stars. The importance of these intrinsic colors to this investigation justifies a discussion of this subject in some detail. The greatest difficulty encountered in the determination of the unreddened colors of O and B-type stars is the scarcity of these stars in the solar neighborhood. Because of this low spatial density, we must base some of our conclusions on observations of stars that are more distant and slightly reddened, and correct for the reddening in some appropriate manner. Some of the brighter unreddened or slightly reddened early-type stars, whose colors have been used in the following discussions, are listed in Table 4.

B. The U-B and B-V Color Indices

Analysis of the U-B and B-V intrinsic colors was first carried out by Johnson and Morgan (1953). Though their initial study included only a limited number of stars

Table 4
Unreddened Early-Type Stars

<u>Star</u>	<u>Type</u>
ζ Puppis	O 5 f
ν Orionis	B 0 V
τ Scorpii	B 0 V
ξ Canis Majoris	B 0.5 V
α Virginis	B 1 V
γ Pegasi	B 2 V
ν Centauri	B 2 V
η Hydrae	B 3 V
η Ursae Majoris	B 3 V
ν Andromedae	B 5 V
λ Canis Majoris	B 5 V
λ Cassiopeiae	B 8
β Librae	B 8 V
α Delphini	B 9 V

and was necessarily somewhat subjective, the results obtained agree well with those of subsequent investigations (Serkowski, 1963; Johnson, 1966b). The values of the U-V and B-V intrinsic colors adopted for this study are taken from Johnson (1966b) and are given for the various spectral types in Columns 2 and 3 of Tables 5 and 6.

The colors for the O-type stars are found from the intersection of the extrapolation of the O-star reddening line and the established B-star main sequence, and therefore, the colors of these earliest-type stars are somewhat more uncertain. Some authors (Serkowski, 1963; Whiteoak, 1966) have suggested that the colors given in Tables 5 and 6 for the O-type stars are slightly too red. This criticism finds

Table 5

Intrinsic Color Indices of Early-Type
Main Sequence Stars

Type	U-V	B-V	V-R	V-I	V-J	V-K	V-L
O 5-7	-1.46	-0.32	-0.15	-0.47	-0.73	-0.94	-1.01
O 8-9	-1.44	-0.31	-0.15	-0.47	-0.73	-0.94	-1.01
O 9.5	-1.40	-0.30	-0.14	-0.46	-0.73	-0.94	-1.00
B 0	-1.38	-0.30	-0.13	-0.42	-0.70	-0.93	-0.99
B 0.5	-1.29	-0.28	-0.12	-0.39	-0.66	-0.88	-0.93
B 1	-1.19	-0.26	-0.11	-0.36	-0.61	-0.81	-0.86
B 2	-1.10	-0.24	-0.10	-0.32	-0.55	-0.74	-0.77
B 3	-0.91	-0.20	-0.08	-0.27	-0.45	-0.61	-0.63
B 5	-0.72	-0.16	-0.06	-0.22	-0.35	-0.47	-0.48
B 6	-0.63	-0.14	-0.06	-0.19	-0.30	-0.41	-0.41
B 7	-0.54	-0.12	-0.04	-0.17	-0.25	-0.35	-0.34
B 8	-0.39	-0.09	-0.02	-0.12	-0.17	-0.24	-0.22
B 9	-0.25	-0.06	0.00	-0.06	-0.09	-0.14	-0.11
A 0	-0.00	0.00	+0.02	0.00	-0.01	-0.03	0.00
A 2	+0.12	+0.06	+0.08	+0.09	+0.11	+0.13	+0.16

Table 6

Intrinsic Color Indices of Early-Type
Supergiants

Type	U-V		B-V	V-R	V-I	V-J	V-K	V-L
	Ia	Ib						
O 9	-1.46	-1.46	-0.31	-0.15	-0.47	-0.73	-0.94	-1.00
O 9.5	-1.44	-1.44	-0.30	-0.13	-0.45	-0.70	-0.90	-0.96
B 0	-1.38	-1.37	-0.27	-0.11	-0.38	-0.62	-0.79	-0.84
B 0.5	-1.32	-1.30	-0.25	-0.09	-0.32	-0.54	-0.70	-0.74
B 1	-1.26	-1.24	-0.22	-0.08	-0.27	-0.47	-0.60	-0.62
B 2	-1.15	-1.10	-0.18	-0.05	-0.20	-0.36	-0.45	-0.46
B 3	-1.03	-0.98	-0.14	-0.02	-0.14	-0.29	-0.36	-0.36
B 5	-0.86	-0.78	-0.10	+0.02	-0.05	-0.20	-0.22	-0.20
B 6	-0.80	-0.74	-0.08	+0.02	-0.03	-0.16	-0.16	-0.13
B 7	-0.73	-0.67	-0.06	+0.02	-0.01	-0.12	-0.10	-0.06
B 8	-0.64	-0.57	-0.03	+0.02	+0.02	-0.08	-0.03	+0.01
B 9	-0.58	-0.50	-0.01	+0.02	+0.05	-0.03	+0.03	+0.08
A 0	-0.47	-0.40	+0.01	+0.03	+0.08	+0.01	+0.10	+0.15
A 1	-0.35	-0.29	+0.03	+0.05	+0.11	+0.06	+0.16	+0.21
A 2	-0.22	--	+0.05	+0.07	+0.14	+0.10	+0.22	+0.27

some support in the observations of the two stars given below:

<u>Star</u>	<u>V</u>	<u>B-V</u>	<u>U-B</u>
SA 4 #197	9.56	-.36	-1.17 (one obs.)
+28° 4211	10.50	-.33	-1.26

These colors are bluer than any given in Tables 5 and 6. Whether these two stars, both O-type subdwarfs, are representative of main sequence O-type stars is not known, but the intrinsic colors of some O-type stars in clusters, as obtained from the mean excesses of the later-type stars, are not as blue as those given above. Therefore, the answer to the question is not clear-cut. Perhaps some intrinsic dispersion in these colors can be expected. In any case, the errors in the values adopted here should be small and will not appreciably affect the calculated extinction curves of moderately reddened stars.

C. The Infrared Color Indices

The infrared intrinsic color indices of early-type stars have been investigated by Johnson and Borgman (1963) and Johnson (1966b), and are currently under study at the Lunar and Planetary Laboratory. The far-infrared colors pose additional problems since the intensity of the radiation from blue stars drops off considerably at these wavelengths, thus making observational uncertainties somewhat

larger. Also, since the JKL system is a relatively new one, the observational data on hand are less complete than are those for the UBVRI system.

Two methods can be used to find these intrinsic colors. The first approach was used by Johnson and Borgman (1963) and consists of plotting the observed indices, (V-R), (V-I), (V-J), (V-K), and (V-L), against (B-V) for stars of the same approximate spectral type. Three diagrams of this sort are shown in Figures 5, 6, and 7. The points in these diagrams are seen to form a wedge-shaped pattern, and the coordinates of the apex of the wedge represent the respective intrinsic colors for this spectral type. The wedge shape is produced by variations in the extinction law at these infrared wavelengths. For a given B-V excess, stars in different regions will often have different infrared excesses; stars located on the boundaries of the wedge pattern exhibit extreme extinction laws. Prior knowledge of the intrinsic B-V for this particular spectral type is the guide in locating the apex in this procedure. However, this method is actually useful for only the earliest spectral types.

A second procedure for obtaining the intrinsic colors of early type stars involves correcting the observed colors of slightly reddened stars on the basis of an assumed or previously determined extinction law. For example, if the photometry and spectral type indicate a given star is slightly reddened, then one can compute the infrared color excesses

Figure 5. V-R versus B-V for O and B O Stars

All of the stars represented in this diagram have essentially the same intrinsic (unreddened) colors. The wedge-shape is produced by variations in the wavelength dependence of interstellar extinction. The apex of the wedge represents the intrinsic colors of the stars. Similar diagrams for the V-I and V-K indices are given in Figures 6 and 7.

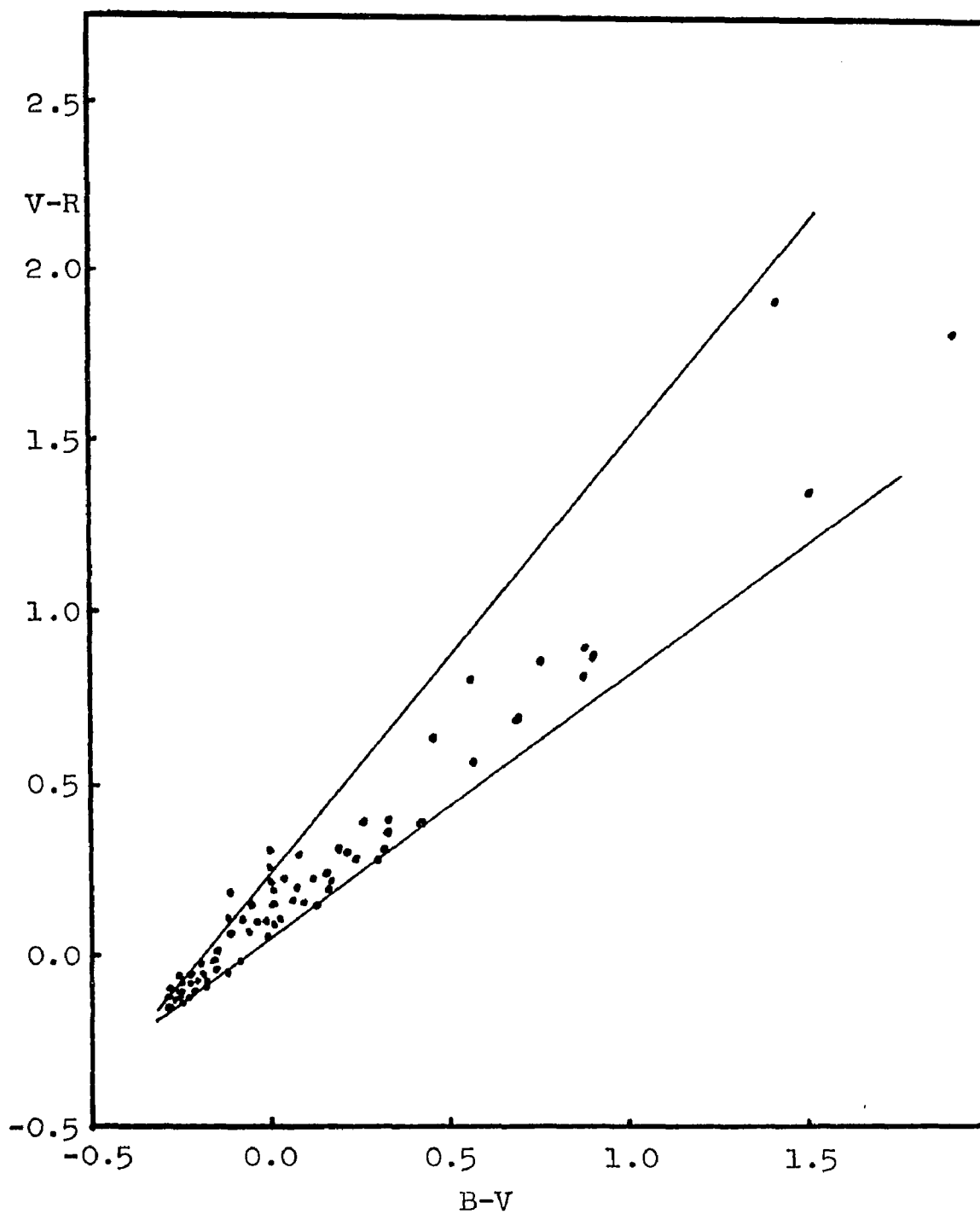


FIGURE 5

V-R versus B-V for O and B 0 Stars

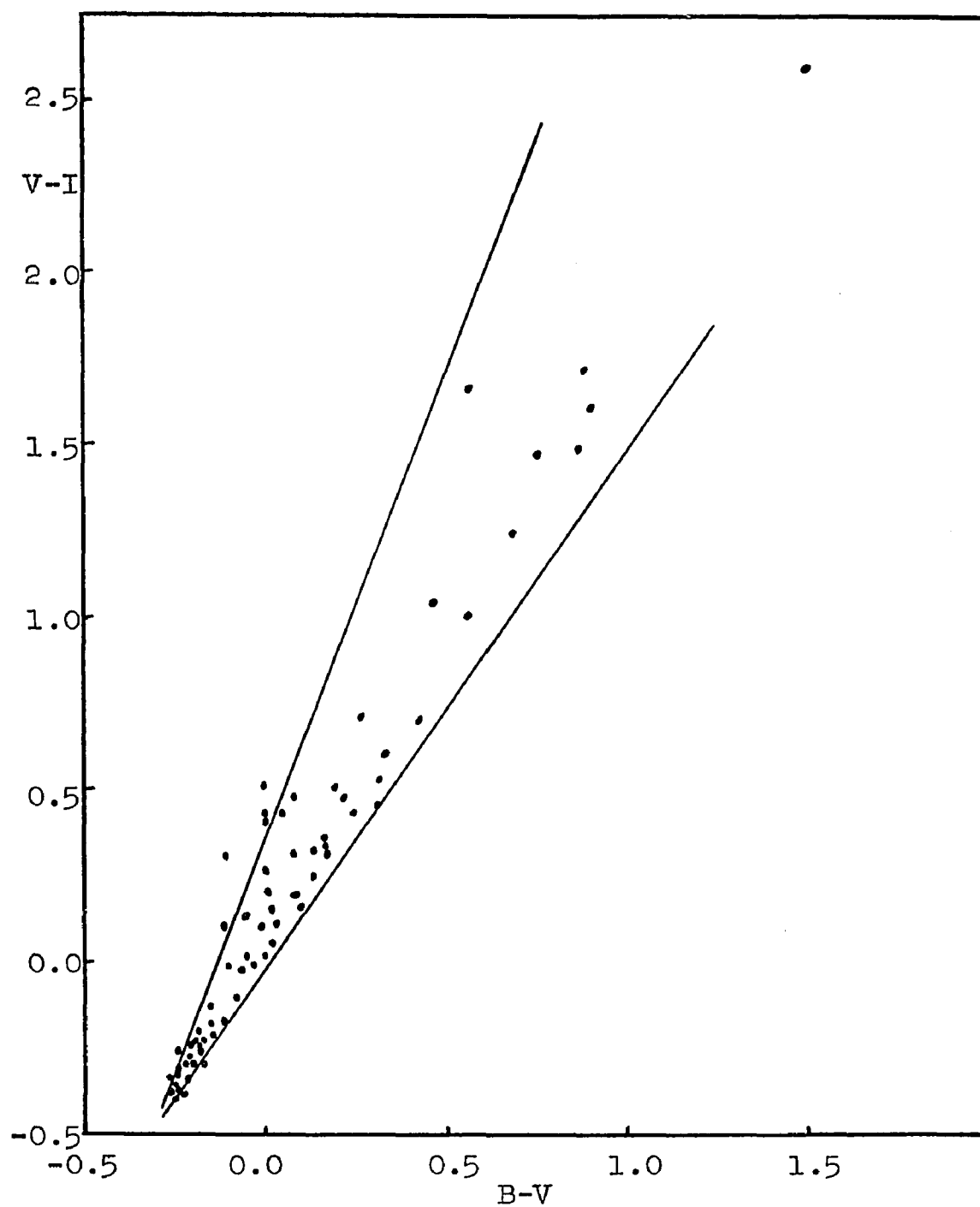


FIGURE 6

V-I versus B-V for O and B 0 Stars

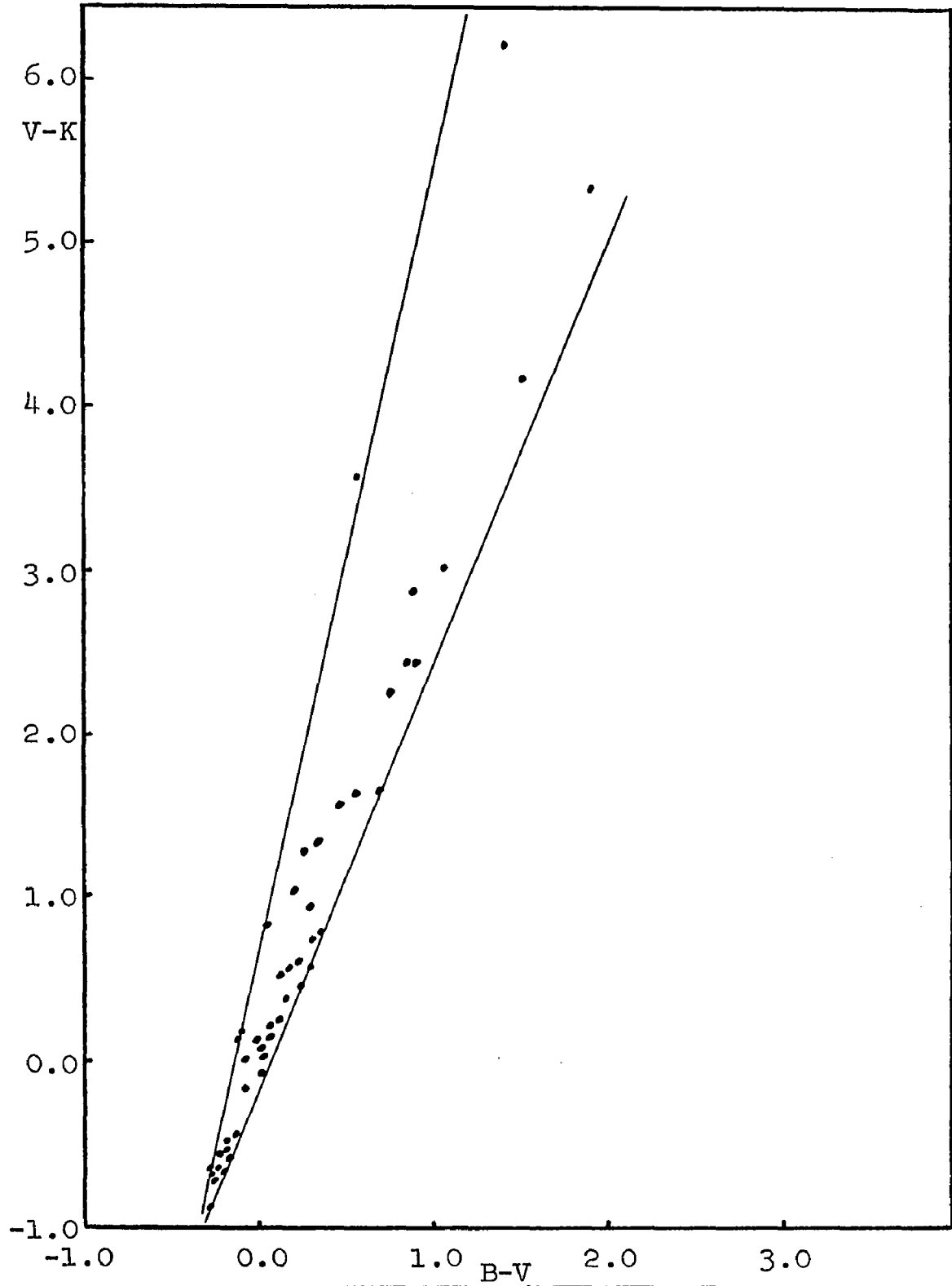


FIGURE 7

$V-K$ versus $B-V$ for O and B 0 Stars

from E_{B-V} and an extinction law, and thus find the unreddened color indices. This method may appear somewhat circular since the intrinsic colors must be known before an extinction law can be determined. For highly reddened stars, however, the derived extinction law is quite insensitive to the intrinsic colors assumed. Similarly, the errors in the derived intrinsic colors of slightly reddened stars, arising from errors in the adopted extinction law, are also small. For a general sample of slightly reddened O and B stars, the 'normal' extinction law is adequate. The values of the V-R, V-I, V-J, and V-K indices given in Tables 5 and 6 were found by smoothing the values obtained by the procedures discussed above.

D. The V-L Index

The V-L intrinsic color index of the earliest-type stars has been the most difficult to determine. Both observational uncertainties and some problematical extinction effects (not atmospheric) seem to be contributing to the difficulties. A preliminary study, based on the methods described above, indicated that the K-L intrinsic color for O-type stars was slightly positive and remained nearly constant from spectral type O to A 0. This result was accepted with some reserve since a black-body distribution, which should be an excellent approximation at such high

temperatures and long wavelengths, yields a negative value for this index. A more recent study of this problem has found evidence favoring the black-body result. Plotted in Figure 8 are the I-K and K-L observed colors of all B 1 and earlier-type stars having L (3.4 μ) measures. The I-K color was chosen because it is nearly constant over the spectral range O to B 1. Therefore, the principal cause of the scatter in Figure 8, excluding observational uncertainties, is interstellar extinction. Though the wedge-shaped diagram has no well-defined apex, the limits drawn do indicate a probable negative value for K-L at I-K = $-0^m.51$ (I-K = $-0^m.51$ for type B 0). Further evidence favoring a negative value for the K-L color of O-type stars was found by Johnson (1966a), who noted that if a positive value of this intrinsic color was assumed, the E_{V-L}/E_{V-K} ratio was correlated with E_{B-V} . This dependence suggested that the V-L color used previously for these stars was slightly too red. Therefore, on the basis of these arguments, the V-L intrinsic colors of the earliest-type stars given in Tables 5 and 6 have been determined from the V-K colors found observationally and the K-L colors calculated from the Rayleigh - Jeans approximation to Plank's radiation law.

Estimates of the probable errors of the intrinsic colors used here will be given in Section V.

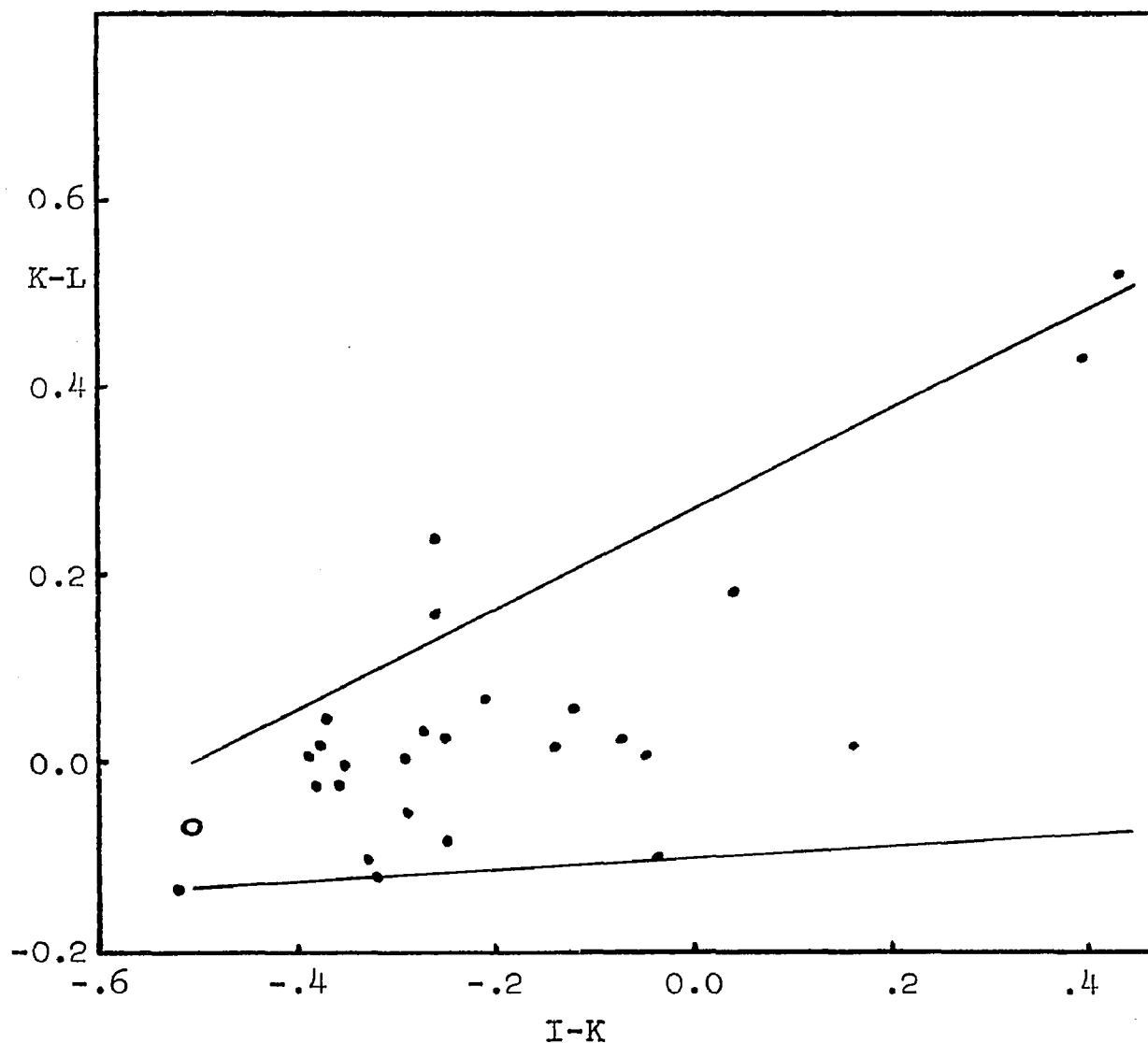


FIGURE 8

K-L versus I-K for B 1 and Earlier-Type Stars

Although the scatter in this diagram is considerable, a negative value for the intrinsic K-L index is indicated. The I-K color index is nearly constant from type O to B 1. The colors of the circle are those of a 30,000 degree black-body.

IV

EXTINCTION CURVE CALCULATIONS

A. Method

1. Color Excesses

An interstellar extinction curve can be obtained from a comparison of the observed (reddened) and the intrinsic (unreddened) color indices of a reddened star. The series of color excesses, E_{U-V} , E_{B-V} , E_{V-R} , E_{V-I} , E_{V-J} , E_{V-K} , and E_{V-L} , represent the differences in the extinction in the U, B, R, I, J, K, L, and V filters respectively. Therefore, when the color excesses are plotted against the filter effective wavelengths, the wavelength dependence of interstellar extinction is obtained. The extinction curve found in this manner will be a smoothed curve that may differ slightly from the monochromatic relation due to the finite pass bands of the filters. A discussion of monochromatic extinction laws will be given in Section VII.

2. Normalization and Scaling

To facilitate direct comparisons of the extinction curves of stars with varying degrees of reddening, one must normalize the curves in some manner. The normalization procedure adopted here (see Figure 2), which has been used by

Johnson (1966a), produces one magnitude of differential extinction between the B and V filters (E_{B-V}) and sets the extinction in the V filter to zero. The normalized extinction, ΔM , is plotted against $1/\lambda_0$, where λ_0 is given by (4). The value of the ratio of total to selective absorption, R , can be read directly from the absolute value of ΔM at $1/\lambda_0 = 0$. Since the photometric data do not extend to $\lambda = \infty$, the value of R must usually be found from an extrapolation of the observed portion of the curve to $1/\lambda_0 = 0$. From this normalization scheme, one sees that the normalized extinction is just the color excess ratio.

$$(5) \quad \Delta M_i = \frac{E_{V-i}}{E_{B-V}}$$

Therefore the color excess ratios become the significant parameters for these extinction laws.

B. The E_{U-V}/E_{B-V} Ratio

The so-called reddening line in the two-color diagram has been the subject of several investigations. Hiltner and Johnson (1956) observed 262 O-type stars and found that the mean reddening line can be represented by the relation

$$(6) \quad \frac{E_{U-B}}{E_{B-V}} = 0.72 + .05E_{B-V}$$

Lindholm (1957) showed that due to the position of the U filter and the Balmer discontinuity, this ratio is somewhat

dependent upon spectral type. Johnson (1958) included this spectral type dependence in his treatment of the problem of finding the intrinsic colors of reddened B-type stars from UBV photometry. Regional deviations from the relation given in (6), the most notable being in Cygnus, have been studied by Johnson and Morgan (1955) and Wampler (1961). A value of 0.81 for E_{U-B}/E_{B-V} was found for the O-type stars in the Cygnus region, with a small change with galactic longitude also suspected.

The photographic spectrophotometry of Divan (1954) showed that in the UBV spectral region the extinction law is everywhere the same--including the Trapezium of the Orion Nebula--and that (6) is correct for O-type stars. Sharpless' (1952) photometric study of the Orion association also has found 'normal' reddening here. The most heavily reddened stars observed in the present investigation were used to check the validity of this result. The E_{U-V}/E_{B-V} ratio was determined from the observed and intrinsic colors of 31 stars whose spectral types are all well established. The intrinsic colors were taken from Tables 5 and 6. The mean color excess ratios with their probable errors are given below in Table 7. The mean ratio for the whole Orion region agrees well with the results of Divan (1954) and Sharpless (1952). The value for the immediate Trapezium region is slightly lower, but it is not clear that this difference is real. A recent study by Whiteoak (1966) suggests that the

Table 7
The E_{U-V}/E_{B-V} Ratio in Orion

	E_{U-V}/E_{B-V}	No. of Stars	P.E. of Mean
Whole Orion Assoc.	1.71	31	.019
Trapezium Region	1.66	8	.044

extinction in the ultraviolet may be slightly less in the Orion Nebula than that found in most other areas, and hence, the lower value of E_{U-V}/E_{B-V} found above may be valid. On the other hand, the difference found here, when compared to the errors, does not justify this conclusion, and therefore, the assumption that the reddening in the UBV spectral range in the Orion Nebula is basically the same as that found elsewhere (excluding Cygnus) is hereby adopted. This assumption allows us to employ the modified 'Q Method' given by Johnson (1958) for the calculation of $(B-V)_0$ of the main sequence early-type stars. The other intrinsic colors follow directly since they are tabulated as a function of $(B-V)_0$ in Table 5. The intrinsic colors of recognized high-luminosity stars are taken directly from their spectral types as given in Table 6. The agreement between $(B-V)_0$ found photometrically and that following from a well-determined spectral type is generally excellent. Since many of the stars included in this study have only poorly known spectral types obtained from objective prism spectra, the

photometric method is often the preferred way of obtaining the intrinsic colors of early-type stars.

The errors made in this procedure are relatively small for moderately reddened stars since the color excess ratios become more insensitive to the intrinsic colors as E_{B-V} increases. However, by forcing $E_{U-V}/E_{B-V} \cong 1.7$ for all stars, we will be unable to detect any small variations--and the above discussion has shown that these variations are small within the Orion region--in the wavelength dependence of the extinction in the ultraviolet.

V

REGIONAL MEAN EXTINCTION LAWS

A. Probable Errors and Weights

The color excess ratios for the stars for which UBVRIJKL data are obtained are tabulated in Table 8. The values of $(B-V)_0$, E_{B-V} , and E_{V-I}/E_{B-V} for those stars having only UBVRI observations have been included in Table 2. Since the reddening in the Orion association is not uniformly large, the uncertainties of the excess ratios for some of the stars in Table 8 will be sizable. For this reason, regional mean extinction laws will be constructed from the data for the individual stars. The tacit assumption made here is that the various physical parameters of the interstellar absorbing material are reasonably constant in a limited area and that the wavelength dependence of the regional extinction will reflect any significant variations in these parameters from one area to another.

Due to the varying degree of reddening for these stars, it is essential that the individual extinction laws are weighted appropriately before the mean laws are computed. Weights will be ascribed to each color excess ratio for all stars included in Table 8, and the series of weighted mean

Table 8

Color Excess Ratios

Star	Sp.	U-V	B-V	V-R	V-I	V-J	V-K	V-L	E _{B-V}
30836	B 2 III	1.6	1.0	0.4	1.3	2.0	3.4	3.1	+ .07
34748	B 2 V	1.58	1.0	0.92	1.50	1.83	2.83	4.00	+ .12
34989	B 1 V	1.64	1.0	0.93	1.86	2.21	2.64	2.93	+ .14
35039	B 2 IV	1.9	1.0	0.6	1.1	2.5	3.1	3.5	+ .08
35079	B 3 V	1.62	1.0	0.69	1.54	2.38	3.08	4.46	+ .13
35149	B 1 V	1.77	1.0	0.54	1.15	2.15	2.15	1.85	+ .13
35411	B 0.5 V	1.72	1.0	0.64	0.91	2.55	3.45	3.55	+ .11
35502	B 5 V	1.71	1.0	0.64	1.28	1.93	2.50	4.00	+ .14
35673	B 9 V	1.8	1.0	1.0	1.8	2.1	2.9	--	+ .08
35910	B 5-6 V	1.7	1.0	0.5	1.2	1.3	4.0		+ .06
36351	B 1.5 V	1.6	1.0	0.4	0.9	1.3	3.0	4.1	+ .07
36486	O 9.5 II	1.8	1.0	0.6	1.9	3.1	3.4	4.1	+ .08
36629	B 2 V	1.77	1.0	0.85	1.69	2.19	3.12	--	+ .26
36646	B 3 V	1.6	1.0	0.8	1.6	1.8	2.8	--	+ .10
36695	B 1 V	1.7	1.0	0.7	1.4	2.0	3.0	2.3	+ .09
36781	~B 6-9	1.64	1.0	0.93	1.86	2.14	2.43	--	+ .14
36811	A 0	1.71	1.0	0.65	1.35	2.18	3.12	2.88	+ .17
36822	B 0 IV	1.73	1.0	0.80	1.60	2.13	2.60	2.87	+ .15
36824	B 3 V	1.6	1.0	0.9	1.4	0.3	1.4	2.6	+ .07

Table 8--Continued

Star	Sp.	U-V	B-V	V-R	V-I	V-J	V-K	V-L	E _{B-V}
36861	O 8-9	1.67	1.0	0.67	1.92	2.92	3.42	--	+ .12
37020-3	~O 9	1.75	1.0	1.03	2.50	3.28	4.92	6.31	+ .36
37022	O 6p	1.59	1.0	1.16	2.72	4.00	5.34	6.22	+ .32
37025	~B 3	1.6	1.0	0.8	2.0	3.4	4.4	--	+ .05
-5° 1318	~B 2	1.72	1.0	0.96	2.52	3.59	5.91	7.89	+ .46
37041	O 9.5 Vp	1.71	1.0	1.05	2.43	3.38	4.81	7.62	+ .21
37042	B 1 V	1.71	1.0	0.76	1.40	3.28	4.33	6.14	+ .21
37043	O 9 III	1.6	1.0	1.0	2.6	3.6	4.2	4.8	+ .05
37061	B 0-1 V	1.74	1.0	0.91	1.96	2.84	3.91	4.49	+ .57
37128	B 0 Ia	1.9	1.0	0.4	1.6	2.8	3.4	4.2	+ .09
37140	B 5	1.70	1.0	0.89	1.74	2.70	3.48	5.19	+ .27
37428	~B 8-9	1.70	1.0	1.05	2.15	2.45	2.45	2.05	+ .20
37468	B 0 V	1.8	1.0	0.8	1.6	2.8	4.0	4.6	+ .05
37490*	B 3 IIIe	0.8	1.0	1.0	1.9	2.8	3.8	4.2	+ .10
-0° 1050	~B 8	1.71	1.0	0.86	1.63	1.97	2.49	--	+ .70
37742	O 9.5 Ib	1.7	1.0	0.5	1.7	3.0	3.8	5.0	+ .06
NGC 2024 No. 1	~O	1.83	1.0	1.13	2.28	3.21	4.17	4.71	+1.72
37903	B 1.5 V	1.75	1.0	0.81	1.81	2.58	3.33	4.58	+ .36
38051	B 3	1.75	1.0	0.84	1.65	2.13	2.55	--	+ .55
38563A	~B 5	1.75	1.0	0.96	1.96	2.30	3.11	4.52	+ .76

Table 8--Continued

Star	Sp.	U-V	B-V	V-R	V-I	V-J	V-K	V-L	E_{B-V}
38563B*	~B 1-5	1.78	1.0	0.98	1.93	2.58	3.33	3.44	+1.32
38771	B 0.5 Ia	1.7	1.0	0.7	1.6	1.9	2.4	2.6	+ .07
41117	B 2 Ia	1.65	1.0	0.78	1.59	2.07	2.65	3.00	+ .46

*Notes to Table 8

HD 37490 Spectral type B 3 IIIe; Low E_{U-V}/E_{B-V} results from emission in ultraviolet.

HD 38563B Spectral type from Sharpless (1952) is B 1. Spectral type from forcing $E_{U-V}/E_{B-V} = 1.7$ is ~ B 5. Star is faint and imbedded in nebulosity.

excess ratios for stars in a given area will represent the regional mean extinction law for the area. The proper weighting factors, w_i , are proportional to the inverse square of the probable errors (Chauvenet, 1960), and therefore, the probable errors of the excess ratios must be determined.

In the discussion that follows, the E_{V-K}/E_{B-V} ratio will be used explicitly, but the other excess ratios, E_{V-R}/E_{B-V} , E_{V-I}/E_{B-V} , E_{V-J}/E_{B-V} , and E_{V-L}/E_{B-V} , will be treated in an identical manner. The notation used here is the following:

$$R_K = E_{V-K}/E_{B-V} \text{ for a given star}$$

$$\sigma(R_K) = \text{probable error of } R_K \\ \text{(p.e. of mean of } N \text{ observations)}$$

$$w(R_K) = \text{weight for } R_K$$

We have:

$$(7) \quad w(R_K) = (1/\sigma(R_K))^2$$

And from the definition of R_K , it follows that:

$$(8) \quad \sigma(R_K) \leq \sqrt{\frac{(\sigma(E_{V-K}))^2 + R_K^2 (\sigma(E_{B-V}))^2}{E_{B-V}}}$$

The inequality here results from ignoring a correlation term relating $\sigma(E_{V-K})$ and $\sigma(E_{B-V})$. The correlation is such that the omission of this term results in an estimate of the error that is only an upper limit of the true error. Since

$\sigma(E_{V-K})$ and $\sigma(E_{B-V})$ are not completely correlated, the error introduced in (8) should always be less than 25%. Knowledge of the probable errors to this accuracy is sufficient for the weight calculations. The error dependence on E_{B-V} should be noted as it is the dominant term in (8). Since the weight, $w(R_K)$, varies as $(E_{B-V})^2$, the most heavily reddened stars will dominate in the calculation of the mean extinction laws.

Equation (8) shows that the calculation of the weights of the color excess ratios requires knowledge of the probable errors of the color excesses. Since the intrinsic and observed colors are essentially independent, we have:

$$(9) \quad (\sigma(E_{V-K}))^2 = (\sigma(V-K))^2 + (\sigma(V-K)_o)^2$$

$$(10) \quad (\sigma(E_{B-V}))^2 = (\sigma(B-V))^2 + (\sigma(B-V)_o)^2$$

The observational errors in (9) and (10), summarized in Table 9, have been determined from an extensive study of the UBVRIJKL photometric data of the Lunar and Planetary Laboratory. The errors of the (U-V), (B-V), (V-R), and (V-I) colors are seen to be independent of the brightness of the star for $m_V < 12.0$. The (V-J), (V-K), and (V-L) colors, however, do have errors that become larger for fainter stars. The quoted errors of these infrared colors for those stars having $m_K > 7.0$ refer to observations that average one half-hour of integrations per filter. The errors given in

Table 9
Observational Errors

<u>Color</u>	<u>Probable Error of Single Observation</u>							
U-V	$\pm 0^m.020$ (not magnitude dependent)							
B-V	$\pm 0^m.013$ (not magnitude dependent)							
V-R	$\pm 0^m.020$ (not magnitude dependent)							
V-I	$\pm 0^m.025$ (not magnitude dependent)							

	<u>M_K</u>							
	<u>2</u>	<u>2 - 3</u>	<u>3 - 4</u>	<u>4 - 5</u>	<u>5 - 6</u>	<u>6 - 7</u>	<u>7 - 8</u>	<u>8 - 9</u>
V-J	$\pm^m.045$	$\pm.045$	$\pm.045$	$\pm.051$	$\pm.071$	$\pm.076$	$\pm.090$	$\pm.113$
V-K	$\pm^m.038$	$\pm.044$	$\pm.048$	$\pm.064$	$\pm.076$	$\pm.086$	$\pm.120$	$\pm.198$
V-L	$\pm^m.064$	$\pm.064$	$\pm.064$	$\pm.085$	$\pm.127$	$\pm.170$	$\pm.212$	$\pm.354$

Table 10
Errors of Intrinsic Colors of O and B Stars

<u>Color Index</u>	<u>Standard Deviation</u>	<u>Probable Error</u>
U-V	$\pm 0^m.055$	$\pm 0^m.037$
B-V	$\pm 0^m.026$	$\pm 0^m.018$
V-R	$\pm 0^m.032$	$\pm 0^m.022$
V-I	$\pm 0^m.047$	$\pm 0^m.032$
V-J	$\pm 0^m.058$	$\pm 0^m.039$
V-K	$\pm 0^m.071$	$\pm 0^m.048$
V-L	$\pm 0^m.091$	$\pm 0^m.061$

Table 9 are the probable errors of a single observation and are related to the probable error of the mean of N observations by (11).

$$(11) \quad \begin{array}{l} \text{P.E. of Mean} \\ \text{of N Obs.} \end{array} = \frac{\text{P.E. of Sing. Obs.}}{\sqrt{N}}$$

The errors of the intrinsic colors of early type stars, which were discussed in Section III, are given in Table 10. They were found in the following manner: The probable error of $(B-V)_0$ was determined from a sample of 38 O-type and B-type stars in the Orion region for which good spectral types are available. The error was obtained from the residuals between the value of $(B-V)_0$ following from known spectral types (Tables 5 and 6) and that resulting from forcing E_{U-V}/E_{B-V} to ~ 1.7 . The errors of the other intrinsic colors of the O-type and B-type stars were found from a larger sample of unreddened or slightly reddened stars that have both photometric data and known spectral types. For each star, E_{B-V} was found from the observed $(B-V)$ and the value of $(B-V)_0$ that follows from the given spectral type. The other observed colors were corrected for reddening by the use of a mean extinction law. The corrections used are:

$$\begin{array}{ll} \Delta(U-V) = -1.7 E_{B-V} & \Delta(V-J) = -2.3 E_{B-V} \\ \Delta(V-R) = -0.8 E_{B-V} & \Delta(V-K) = -2.9 E_{B-V} \\ \Delta(V-I) = -1.6 E_{B-V} & \Delta(V-L) = -3.1 E_{B-V} \end{array}$$

The residuals between the corrected colors and the intrinsic colors consistent with the known spectral types were then used to find the errors given in Table 10. Since all of the stars used in this discussion are only slightly reddened ($E_{B-V} < 0.^m14$), the errors introduced by adopting a mean extinction law for this purpose should be minimal.

The probable errors given in Tables 9 and 10 suffice for the calculation of the color excess errors according to (9) and (10). These probable errors are given in Table 11 and are seen to depend only on the number of observations, N , for the (U-V), (B-V), (V-R), and (V-I) colors, but are also a function of m_K for (V-J), (V-K), and (V-L). Finally, the errors of the color excesses allow us to compute the desired weighting factors given by (7). The probable errors and weights of the excess ratios of all stars having JKL observations are found in Appendix A. The weights vary over a considerable range due to the $(E_{B-V})^2$ dependence noted earlier. For a given region, therefore, one may expect most of the weight of the mean extinction law to come from a limited number of highly reddened stars.

The weighted excess ratios were grouped and averaged for stars in localized areas. The boundaries of the regions were determined from a study of the errors of the mean excess ratios and from the E_{V-I}/E_{B-V} ratio of those stars having only UBVRI observations. Due to the finite number of stars observed, the actual boundaries of the regions must

Table 11
Probable Errors of Color Excesses
for N Observations

N =	1	2	3	4	5	6	7	∞
EB-V	.022	.020	.019	.019	.019	.019	.019	.018
EU-V	.042	.040	.039	.038	.038	.038	.038	.037
EV-R	.030	.026	.025	.024	.024	.023	.023	.022
EV-I	.041	.037	.035	.034	.034	.034	.033	.032
<u>EV-J</u>								
$m_K = < 5.0$.063	.053	.049	.046	.045	.044	.043	.039
5 - 6	.080	.063	.056	.052	.050	.048	.047	.039
6 - 7	.089	.069	.060	.056	.053	.051	.049	.039
7 - 8	.098	.075	.065	.060	.056	.054	.052	.039
8 - 9	.145	.106	.090	.080	.074	.069	.066	.039
<u>EV-K</u>								
$m_K = < 3.0$.062	.056	.053	.052	.051	.051	.050	.048
3 - 4	.069	.060	.056	.054	.053	.052	.052	.048
4 - 5	.077	.064	.059	.057	.055	.054	.053	.048
5 - 6	.085	.069	.063	.059	.057	.056	.055	.048
6 - 7	.093	.074	.067	.062	.060	.058	.057	.048
7 - 8	.129	.097	.084	.077	.072	.069	.066	.048
8 - 9	.206	.149	.125	.111	.101	.947	.090	.048
<u>EV-L</u>								
$m_K = < 4.0$.086	.074	.070	.068	.067	.066	.065	.061
4 - 5	.101	.083	.077	.073	.071	.069	.068	.061
5 - 6	.144	.110	.097	.089	.084	.081	.078	.061
6 - 7	.181	.135	.115	.105	.097	.092	.089	.061
7 - 8	.219	.161	.136	.121	.112	.105	.100	.061
8 - 9	.355	.255	.211	.185	.168	.155	.146	.061

remain somewhat uncertain. The total weights, probable errors of the mean, and the mean excess ratios for the various regions are given in Table 12; and the extinction laws are shown in Figures 9, 10, and 11. The error bars on the curves represent $2.5 \times$ probable error of the mean points, which, assuming the errors are normally distributed, will include 91% of the probability. Figure 12 shows a schematic map of the I Orion association with the boundaries of the regions and other salient features indicated.

B. Properties of the Regional Laws

East 'Belt' Region

The extinction law for this region (Figure 9) was obtained from the data for five stars: HD 37742 (ζ), HD 37903, HD 37468 (σ), HD 37140, and HD 37128 (ϵ). HD 37903 and HD 37140 are the most highly reddened of the group with $E_{B-V} = +0.^m36$ and $0.^m27$ respectively; most of the weight for the regional curve comes from these two stars. The L (3.4μ) measure for HD 37903 is somewhat uncertain, although seven JKL observations have been made for this star. The average E_{V-L}/E_{B-V} ratio for the three stars that are only slightly reddened is 4.5 as compared to 4.64 for the weighted mean, and therefore, the steep rise from the K to L points on the mean curve is characteristic of the extinction of all five stars. The average E_{V-I}/E_{B-V} ratio for eight other stars in this area is 1.8, which agrees well with the weighted mean.

Table 12
Regional Extinction Data

Region	No. of Stars		$\frac{E_{V-R}}{E_{B-V}}$	$\frac{E_{V-I}}{E_{B-V}}$	$\frac{E_{V-J}}{E_{B-V}}$	$\frac{E_{V-K}}{E_{B-V}}$	$\frac{E_{V-L}}{E_{B-V}}$
East 'Belt'	5	Mean	0.80	1.78	2.65	3.39	4.64
		Wts.	262	94	38	22	10
		P. E.	± 0.04	± 0.02	± 0.04	± 0.04	± 0.09
		2.5x(P.E.)	± 0.10	± 0.05	± 0.10	± 0.10	± 0.22
NGC 2024 No. 1		Mean	1.13	2.28	3.21	4.17	4.71
		Wts.	2500	918	384	269	149
		P. E.	± 0.02	± 0.03	± 0.05	± 0.06	± 0.08
		2.5x(P.E.)	± 0.05	± 0.08	± 0.13	± 0.15	± 0.20
North- western Region	21	Mean	0.81	1.58	2.05	2.68	3.08
		Wts.	1134	447	146	91	41
		P. E.	± 0.02	± 0.02	± 0.04	± 0.05	± 0.06
		2.5x(P.E.)	± 0.05	± 0.05	± 0.10	± 0.12	± 0.15
M 78 A, B	2	Mean	0.97	1.94	2.56	3.30	3.54
		Wts.	2548	915	376	253	124
		P. E.	± 0.01	± 0.01	± 0.07	± 0.05	± 0.21
		2.5x(P.E.)	± 0.02	± 0.03	± 0.18	± 0.13	± 0.52
Outer 'Sword'	6	Mean	0.86	1.70	2.17	2.66	2.57
		Wts.	504	189	72	44	2
		P. E.	± 0.02	± 0.04	± 0.05	± 0.07	± 0.39
		2.5x(P.E.)	± 0.05	± 0.10	± 0.12	± 0.18	± 0.98
HD 37061		Mean	0.91	1.96	2.84	3.91	4.49
		Wts.	356	123	58	36	21
		P. E.	± 0.05	± 0.09	± 0.13	± 0.17	± 0.22
		2.5x(P.E.)	± 0.13	± 0.22	± 0.33	± 0.42	± 0.54
Immediate Trapezium Region	5	Mean	1.00	2.47	3.51	5.14	6.76
		Wts.	541	153	65	32	19
		P. E.	± 0.04	± 0.08	± 0.09	± 0.17	± 0.25
		2.5x(P.E.)	± 0.10	± 0.20	± 0.22	± 0.42	± 0.62

Figure 9. Normalized Extinction Laws for the Orion East 'Belt' and NGC 2024 No. 1

The normalized extinction, ΔM , is plotted against the inverse wavelength. The photometric filter positions are also given. The error bars represent five times the probable errors of the mean excess ratios. If a normal distribution of the errors is assumed, the error bars include 91% of the probability. Similar curves for other regions are shown in Figures 10 and 11.

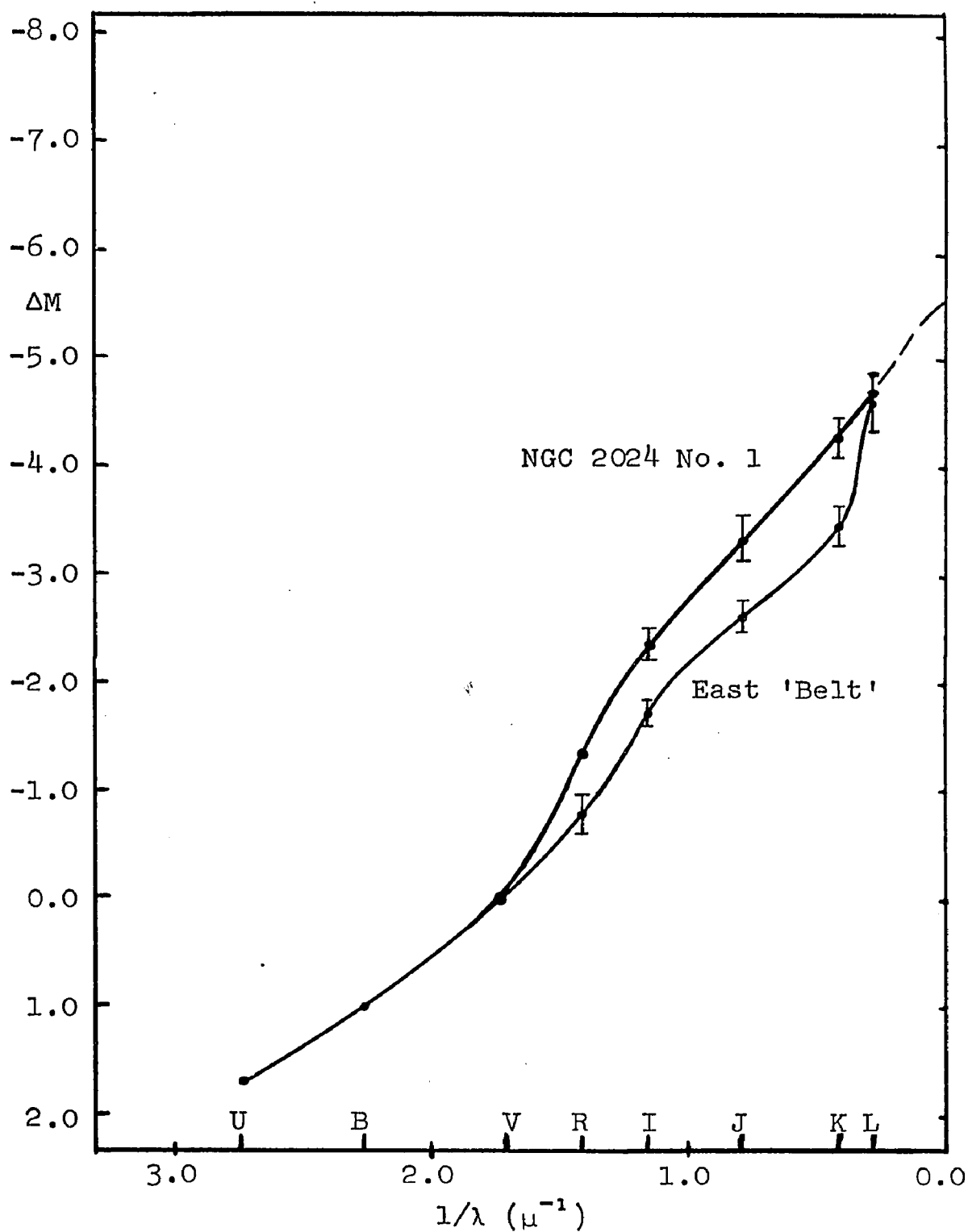


FIGURE 9

Normalized Extinction Laws for the Orion East 'Belt'
and NGC 2024 No. 1

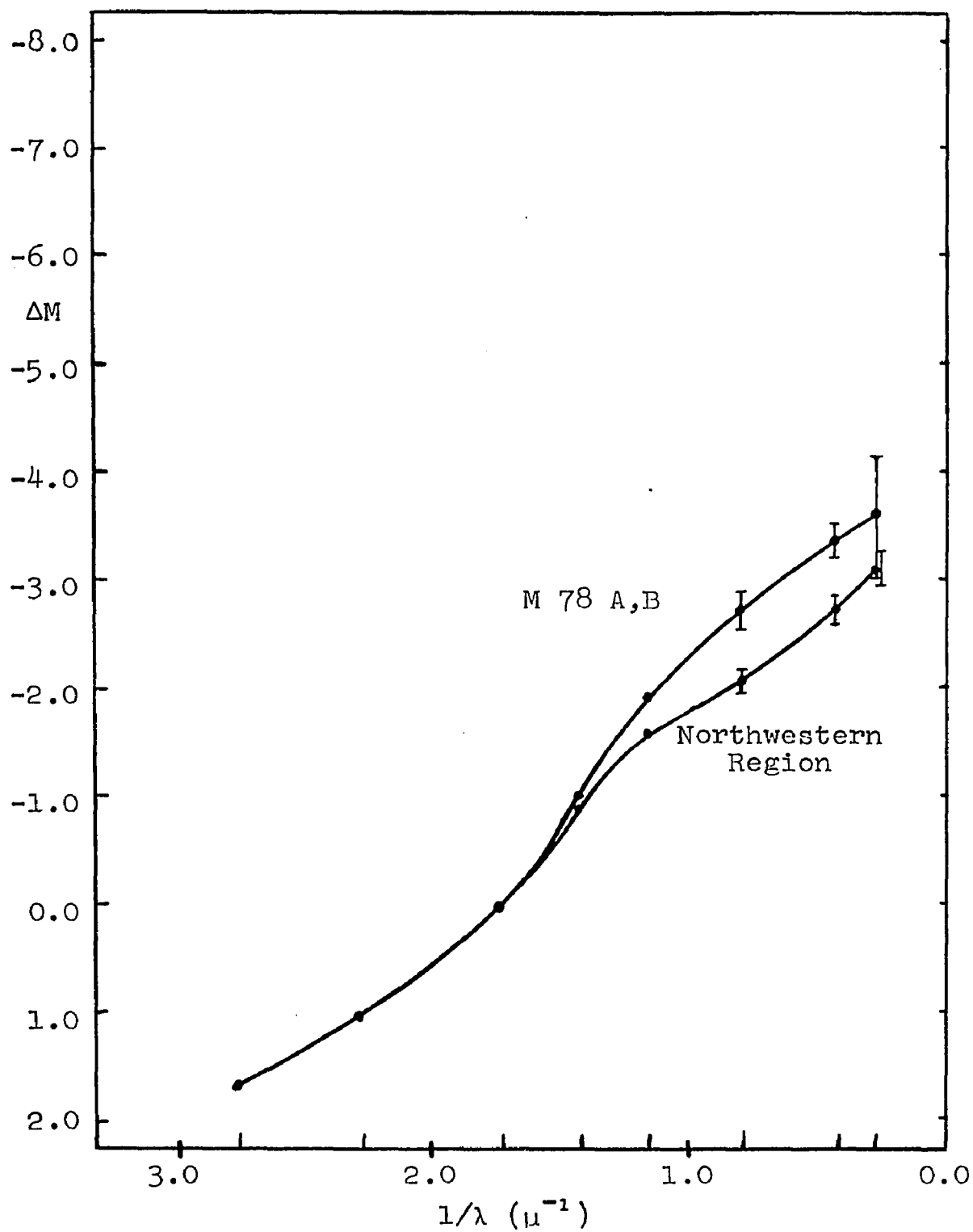


FIGURE 10

Normalized Extinction Laws for M 78 A, B and the Northwestern Region

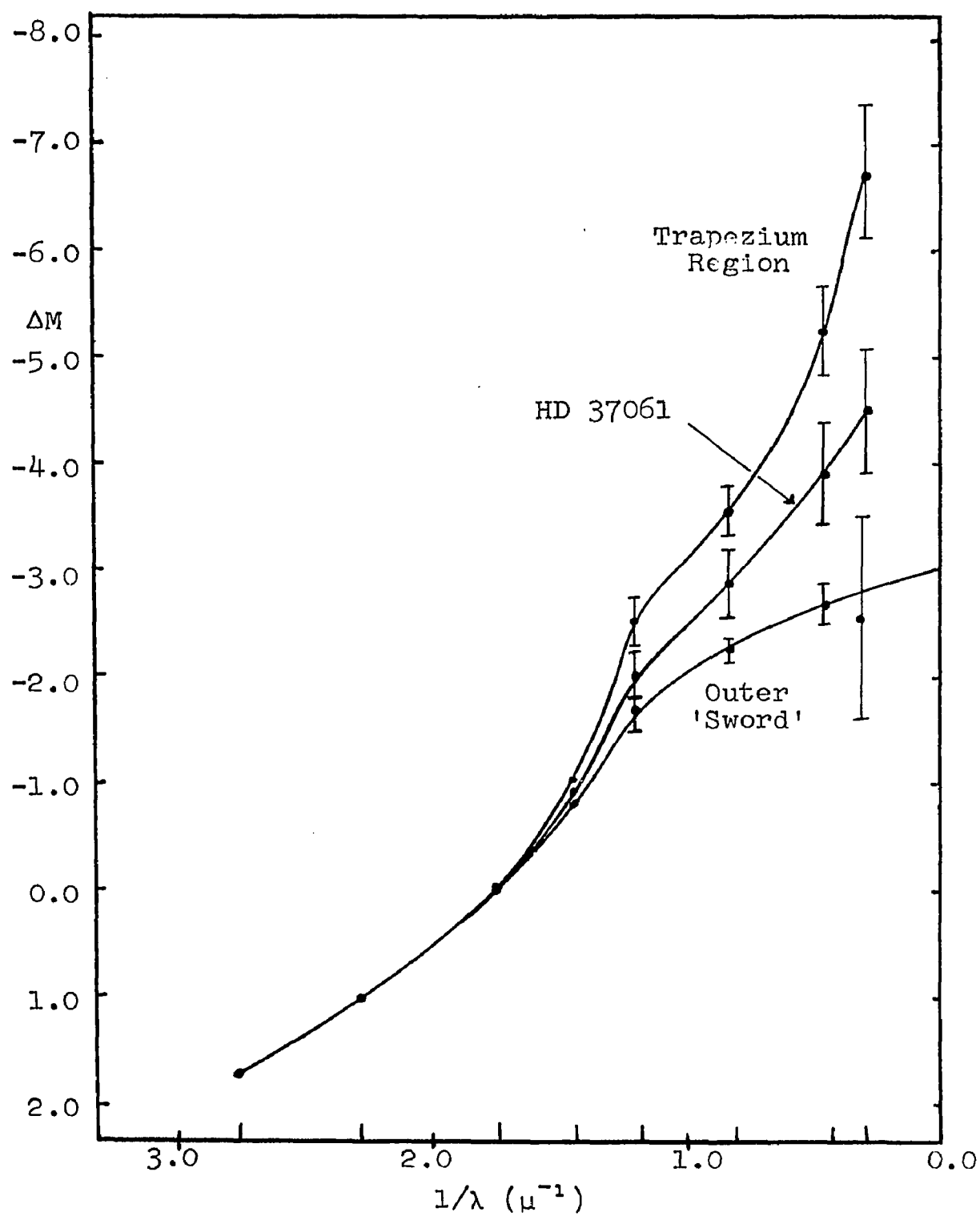


FIGURE II

Normalized Extinction Laws for the Outer 'Sword,'
HD 37061, and the Trapezium Region

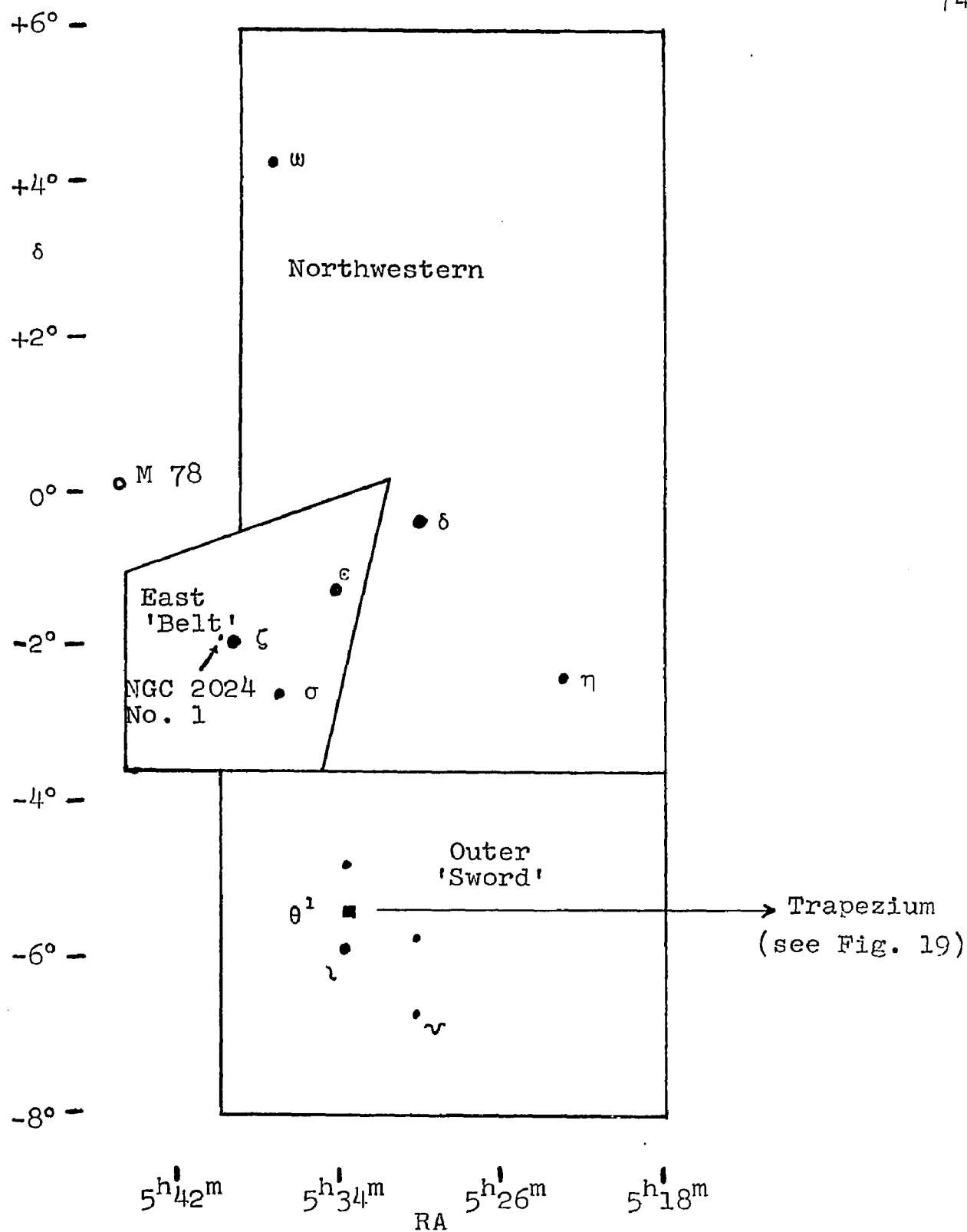


FIGURE 12

Schematic Map of Extinction Regions in the I Orion Association

NGC 2024 No. 1

This is the most highly reddened star known in the Orion association. The spectral type has been investigated by Johnson and Mendoza (1964), who found it to be an early O-type or B-type star. The extinction curve shown in Figure 9 results from assuming O-type intrinsic colors, but the star is so heavily reddened that the extinction law is quite insensitive to the intrinsic colors used. In fact, if a spectral type as late as F 5 is assumed, the infrared excess ratios remain high and only E_{U-V}/E_{B-V} changes significantly. The curve, as given in Figure 9, shows a rapid rise between the R and I points and then a steady increase to $E_{V-L}/E_{B-V} = 4.7$. The enormous reddening causes the error bars to be small even though the curve refers to a single star. An estimate of 5.5 for the ratio of total to selective absorption, made by Johnson and Mendoza (1964) from the reddening and apparent distance modulus, agrees well with that found by extrapolating the curve in Figure 10 to $1/\lambda = 0$.

Northwestern Region

One sees from Figure 12 that this region is a large one that includes many stars. Determining the extinction law here is complicated because of the very low reddening throughout this region. Studies of smaller regions within this area showed no significant localized variations in the extinction law, and therefore, the mean law given in Figure

10 adequately represents this whole portion of the association. The curve is similar to that of the 'normal' law, but has a steeper slope in the infrared and a slightly higher ratio of total to selective absorption. The mean value of E_{V-I}/E_{B-V} from 28 additional stars is 1.4, which is slightly lower than the weighted mean value of 1.58.

M 78 A, B (NGC 2068)

These two stars, which are highly reddened and imbedded in a reflection nebulosity, are located about 2° northeast of ζ Orionis. They are classified as early B-type stars (Sharpless, 1952) and have a mean reddening of $E_{B-V} = 1.0$. The high reddening makes knowing the exact spectral types unnecessary. The weighted mean extinction curve for these two stars is given in Figure 10. The curves for the individual stars are in very good agreement out to $\lambda = 2.2 \mu$, but the L points are somewhat discordant. The infrared photometric data for M 78 A are not as good as that for M 78 B, and this is no doubt the cause of the discordance at 3.4μ . But since the most highly reddened of the two stars is M 78 B, this uncertainty in the L measure of M 78 A has only a minimal effect on the weighted mean law. The curve in Figure 10 shows a steep rise from the R to I points, but it also indicates a probable ratio of total to selective absorption of no greater than 4.

Orion 'Sword' (Outer Part)

The extinction curve for the outer portion of the Orion 'Sword' region, which excludes the immediate Trapezium area, was obtained from the data of six stars and is shown in Figure 11. The error of the L point is very large since only three slightly reddened stars were observed in this filter. The extinction in this area is variable, being heavy in some places and nearly zero in others. The ratio of total to selective absorption was estimated from a color-magnitude diagram (corrected for extinction) for the highly reddened and the unreddened stars in this region. By assuming all stars are at approximately the same distance, one can estimate R by forcing the highly reddened stars to lie along the same sequence defined by the unreddened stars. The uncertainty in this method is large, but $R = 3.0$ is consistent with the data while $R > 4.0$ is not, and moreover, $R = 3.0$ fits well with the observed part of the mean curve given in Figure 11.

HD 37061

This early B-type star is located northeast of the Trapezium, some 8' distant, and is imbedded in the nebula NGC 1982. The star is supposedly variable (NU Orionis), but the photometric data listed below, which extend over 14 years, show no great variation in brightness. Moreover, the spectral classifications by Sharpless (1952), Divan (1954), and Strand (1958), B 1 V, B 0 V, and B 1 V respectively,

<u>Source</u>	<u>m_v</u>	<u>No. of Obs.</u>
Sharpless (1952)	6.86	2
Johnson (1957)	6.81	2
Johnson and Borgman (1963)	6.85	2
TL (1966)	6.80	3

disclosed no spectral peculiarity or variability. Therefore, the variable nature of this star must be regarded with suspicion. The extinction law presented in Figure 11 results from adopting normal B 1 V-type intrinsic colors. The curve exhibits a more rapid rise in the infrared than that shown by the law for the outer 'Sword' stars, and the size of the errors indicates that the differences at these wavelengths are real.

Trapezium Region

The extinction curve for the Trapezium region, shown in Figure 11, was determined from data for the following stars:

<u>Star</u>	
HD 37020-23 (θ^1 (ABCD))	~ 0 9
HD 37022 (θ^1 (C))	0 6 p
HD 37041 (θ^2)	0 9.5 Vp
HD 37042	B 1 V
Bond 669 (-5° 1318)	B 2-3

The relative positions of these stars are shown in Figure 19. The infrared data for all stars except θ^1 (C) are very good-- θ^1 (C) was observed only once, but the percentage errors of

the deflections of this single measure are low. The curve in Figure 11 was found by assuming normal intrinsic colors commensurate with the spectral types given above. The spectral types themselves are adequately known, but the effect of the peculiar designation given some of the stars is a subject that will require additional discussion in the chapter to follow. At this juncture, however, we do note that the individual extinction laws for all five stars show the sharp turn up in the far infrared seen in Figure 11, since all have $E_{V-L}/E_{B-V} > 6.0$. Also of interest is the fact that the deviations from the 'normal' curve are already apparent at the I point, and that they increase at longer wavelengths until a ratio of total to selective absorption of greater than twice the normal value is indicated.

VI

RELATED PHENOMENA MODIFYING THE EXTINCTION INTERPRETATION

A. The 'Belt' Region

The extinction curves determined in this study indicate a variation in the extinction law in the Orion 'Belt.' The probable values of the ratio of total to selective absorption in the east and west parts of the 'Belt,' as indicated from the curves given in Figures 9 and 10, are 5.5 and 3.5 respectively. The error bars on the curves are such that if the interpretation is correct, this variation must be real.

The work of Hardie, Heiser, and Tolbert (1964) is of considerable interest here. These authors obtained UBV photometry for 93 B-type stars in the 'Belt' area and found, when a 'normal' ratio of total to selective absorption was assumed for all stars, that the average distance modulus for stars in the east 'Belt' region was $0^m.9$ larger than that for the stars in the western part. The conclusion reached by Hardie et al. was that this distance modulus difference is the result of the true spatial distribution of the stars, the mean distance of the stars in the east being 525 parsecs

as compared to 350 parsecs for those in the west. The change is the ratio of total to selective absorption found in the present study is seen to be compatible with the mean moduli found by Hardie et al. That is, a distance modulus difference in the sense observed by these authors would result from assuming a 'normal' uniform extinction law if, in fact, the actual ratio of total to selective absorption does vary in the manner proposed here. The effect is augmented by the greater reddening in the eastern region, near ζ Orionis. Although a change in the ratio of total to selective absorption from 5.5 to 3.5 is not sufficient to remove completely the modulus difference present in the data of Hardie et al., no such effect is seen in the data of this study. Figure 13 shows the corrected visual magnitude as a function of intrinsic (B-V) for stars in the east and west parts of the 'Belt.' The division of the two regions is shown in Figure 14. No significant vertical displacement of one group of stars with respect to the other is seen in Figure 13, and hence, there is no apparent difference in the mean distance of the two groups. Therefore, the change in the mean distance of the stars in the east and west parts of the Orion 'Belt' that was found by Hardie et al. appears to arise primarily from a heretofore unrecognized variation in the interstellar extinction law in this region, and moreover, the data obtained by these authors add, in some

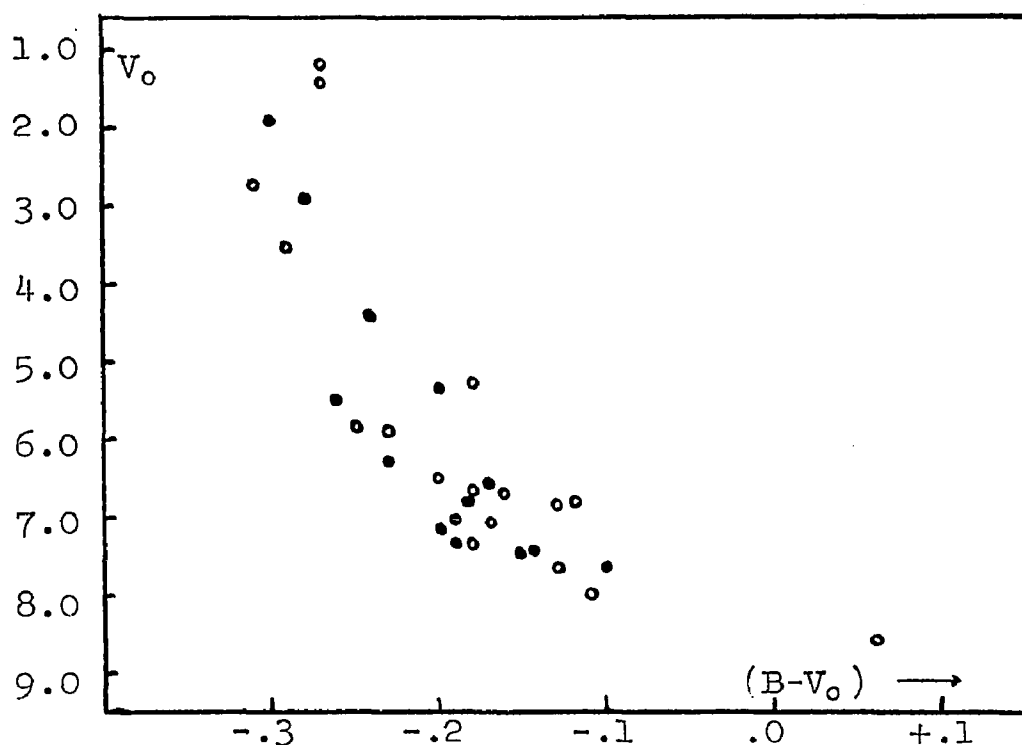


FIGURE 13

Orion 'Belt' Color-Magnitude Diagram--Corrected
for Extinction

Circles refer to stars in the east, while solid dots represent stars in the west.

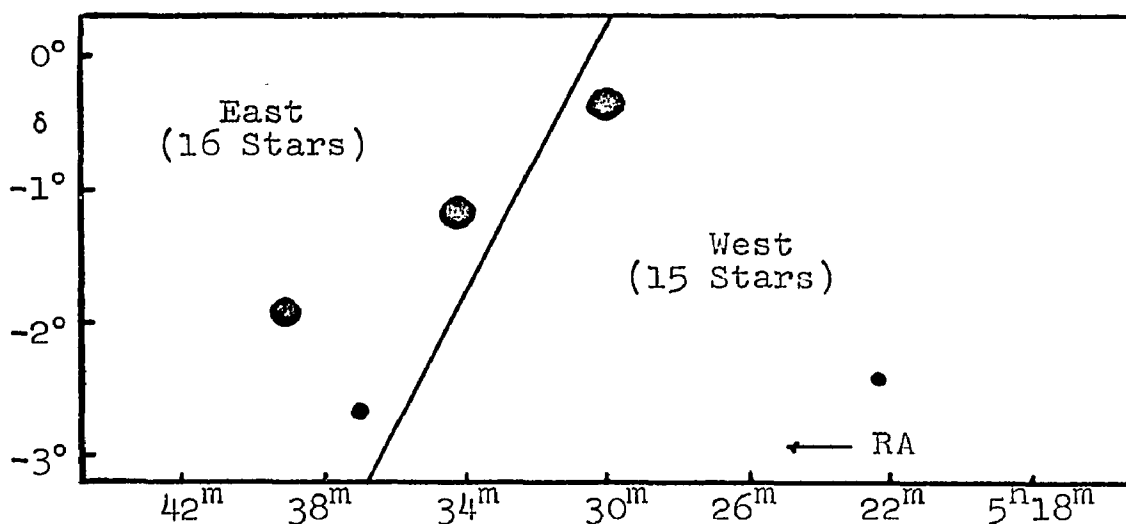


FIGURE 14

East-West Division of the 'Belt' Region

degree, to the credibility of the extinction curves presented in Figures 9 and 10.¹

The mean distance modulus for stars in the 'Belt' region and in the northern part of the association, determined from a fit of the color magnitude diagram (corrected for extinction) with the zero age main sequence (Johnson, 1963), is $7^m.9$; the corresponding distance is 380 parsecs.

B. The 'Sword' Region

1. Anomalous Energy Distributions

We shall now undertake a detailed analysis of the several factors, mentioned briefly in Chapter I, that could invalidate the extinction laws derived for the region immediately adjacent to θ^1 Orionis. The possible effects of abnormal energy distributions of the stars in this region will be discussed first. All four components of θ^1 Orionis and θ^2 Orionis are recognized as spectroscopic binaries and have peculiar designations attached to their spectral types. Underhill (1964) suggested that these facts vitiate the extinction laws obtained from the assumption of normal intrinsic colors for these stars. The effects of possible

1. Morgan (1958) pointed out a possible change in the evolutionary state of the stars in the Orion 'Belt,' the evolution being more advanced in the west than in the east. Recently however, Crawford and Barnes (1966) found that this effect, if indeed it exists at all, is small. In any case, such a change in the evolution in this region would also modify the interpretation of Hardie, Heiser, and Tolbert (1964).

unseen red companions were investigated by adopting the absolute magnitudes of Blaauw (1963) and the intrinsic color indices of Johnson (1966b), and calculating what extinction law would result for θ^1 Orionis if certain types of unseen stars were present. The intrinsic colors of the composite star, the resulting color excess ratios, and the change in the color excess ratios produced by the presence of the red companions are summarized for four cases in Table 13. If θ^1 (ABCD) Orionis had four unseen K 0 III companions, the intrinsic colors (3 B 0 V + 0 6 + 4 K 0 III) would change very little from the values obtained for the Trapezium stars alone (3 B 0 V + 0 6), and therefore, the extinction law would change only slightly. Even with the presence of 10 unrecognized K 0 III companions, the extinction would still be significantly 'non-normal'-- $E_{V-L}/E_{B-V} > 5$. An unreasonable number of M 2 V stars is required if the ratio of total to selective absorption here is really less than 4.0, whereas only one M 4 III companion will greatly reduce the infrared excess ratios and, hence, the extinction anomaly for this star. Clearly, some combination of one or more late-type companions, most probably evolved M-type, can be found that will produce the correct amount of infrared radiation involved in the large infrared excesses observed for θ^1 Orionis. However, on infrared spectrograms extending to $\lambda = 9,000 \text{ \AA}$, obtained by Sharpless (1963) for θ^1 (ABCD) and

Table 13

Extinction Laws for θ^1 Orionis if Unseen Companions
Are Present

θ^1 with no companion	<u>U-V</u>	<u>B-V</u>	<u>V-R</u>	<u>V-I</u>	<u>V-J</u>	<u>V-K</u>	<u>V-L</u>
Intrinsic Colors	-1.44	-.31	-.15	-.47	-.73	-.94	-1.01
E/E_{B-V}	1.75	1.00	1.03	2.50	3.28	4.92	6.31
<hr/>							
<u>$\theta^1 + 4 \text{ K O III}$</u>							
Intrinsic Colors	-1.43	-.31	-.14	-.43	-.67	-.82	-.87
$\Delta E/E_{B-V}$	-0.03		-.03	-.08	-.17	-.34	-.39
E/E_{B-V}	1.72	1.00	1.00	2.42	3.11	4.58	5.92
<hr/>							
<u>$\theta^1 + 10 \text{ K O III}$</u>							
Intrinsic Colors	-1.42	-.30	-.12	-.37	-.56	-.59	-.60
$\Delta E/E_{B-V}$	-0.01		-.06	-.19	-.39	-1.15	-1.00
E/E_{B-V}	1.74	1.00	0.97	2.31	2.89	3.77	5.31
<hr/>							
<u>$\theta^1 + 3 \times 10^4 \text{ M 2 V}$</u>							
Intrinsic Colors	-1.42	-.30	-.11	-.28	-.35	-.11	-.03
$\Delta E/E_{B-V}$	-0.01		-.09	-.44	-1.00	-2.24	-2.63
E/E_{B-V}	1.74	1.00	0.94	2.06	2.28	2.68	3.68
<hr/>							
<u>$\theta^1 + \text{one M 4 III}$</u>							
Intrinsic Colors	-1.43	-.31	-.12	-.30	-.32	-.01	+.09
$\Delta E/E_{B-V}$	-0.03		-.09	-.47	-1.14	-2.59	-3.06
E/E_{B-V}	1.72	1.00	0.94	2.03	2.14	2.33	3.25

θ^2 Orionis and by Hallam (1959) for $\theta^1(c)$ Orionis, no evidence of any late-type companions is seen. If the required number of red companions or sufficiently strong stellar emission features are present to account for these deviations from the 'normal' extinction law--which are already appreciable in the I filter, accounting for 34% of the intensity for $\theta^1(ABCD)$ if the extinction is truly 'normal'--then some evidence of these late-type stars or emission lines should be seen in the infrared spectra of these stars. Moreover, the extinction curves for three other stars near the Trapezium--HD 37042, HD 37061, and $-5^\circ 1318$ (Bond 669), all of which appear to have perfectly normal B-type spectra and are not recognized spectroscopic binaries--show the same steep gradient in the infrared that is characteristic of the laws of θ^1 and θ^2 Orionis. Therefore, in the light of present data and information, any explanation of the observed extinction law in the neighborhood of θ^1 Orionis in terms of anomalous intrinsic energy distributions for the stars in this region appears to be untenable.

2. Nebular Radiation

The stars in the immediate Trapezium region, θ^1 and θ^2 Orionis, HD 37042, and $-5^\circ 1318$ are imbedded in the Orion Nebula (NGC 1976), while HD 37061 is located in NGC 1982. The nebular radiation from this region has been the subject of several investigations in recent years. Osterbrock and

Flather (1959) used the intensities of the forbidden oxygen lines and obtained a spherical model for the Orion Nebula that is characterized by electron densities of 1.8×10^4 at the center (θ^1) and 2.6×10^2 at the edge, $24'$ from the center. Menon (1961) used 3.75-cm measures to construct a similar model having considerably lower electron densities, 2.3×10^3 at the center and 1×10^1 at the edge. Local density fluctuations, shown very well in a photograph by Münch and Wilson (1962), can apparently reconcile the results of these two models. Mendez (1965) studied the continuum radiation from $\lambda = 3,500 \text{ \AA}$ to $11,000 \text{ \AA}$ and determined the component that is due to scattered star light. The albedo variation with wavelength is consistent with an index of refraction of $n = 1.11 - 0.02i$ for the grains in this region. O'Dell and Hubbard (1965) have made photometric observations of the continuum and find that the continuous radiation becomes bluer in the outer parts of the nebula, and that the gas to dust ratio appears to decrease with increasing distance from the Trapezium. Also Reitmeyer (1965), again from photometric data, found some evidence indicating that the nebula may be optically thin in the Lyman lines, and that the electron temperature varies considerably in some regions.

Our primary interest in the radiation from the nebulosity, in this study, is in its role as a possible contaminant of the photometric measures of the stars in this

area. The following considerations will show that the general nebular radiation cannot significantly affect the measured stellar colors and magnitudes:

1. The observations are made with the utmost care in an effort to minimize these effects. The smallest possible diaphragm is used for the UBVRI measures, and the sky readings are made very close to the star and at four positions: to the north, south, east, and west. The JKL sky readings are taken both north and south of the star. Therefore, if the nebular emission is to affect the photometric measures, it must be strongly peaked and very near the star.

2. Hallam (1959) found that in no case in the spectral range from 2,950 Å to 11,000 Å does the intensity of the nebulosity amount to more than a few percent of that of the Trapezium.

3. Figures 15 and 16 show the central parts of two infrared 48-in. Schmidt plates (hypersensitized 1 N + #89 Wratten filter) of the Orion 'Sword' region taken by Dr. G. Haro. The spectral response of these plates should approximate that of the I photometric band. The two exposures show different details in the various regions. The distribution of nebular radiation seen in Figure 16 as well as that seen in the short-exposure color photograph of θ^1 Orionis shown in Figure 17 show no pronounced maxima at the positions of the stars in question. Even in the very center of the nebula, one sees that the peak of the nebular intensity is

Figure 15. Infrared Photograph of the Orion 'Sword'

The original plate--hypersensitized 1N with Wratten #89 filter--was taken by Dr. G. Haro with the 48-in. Schmidt telescope. North is at the top, east is to the left. The clustering of faint stars in the neighborhood of the Orion Nebula is quite conspicuous. The spectral response of this plate approximates the I photometric band.

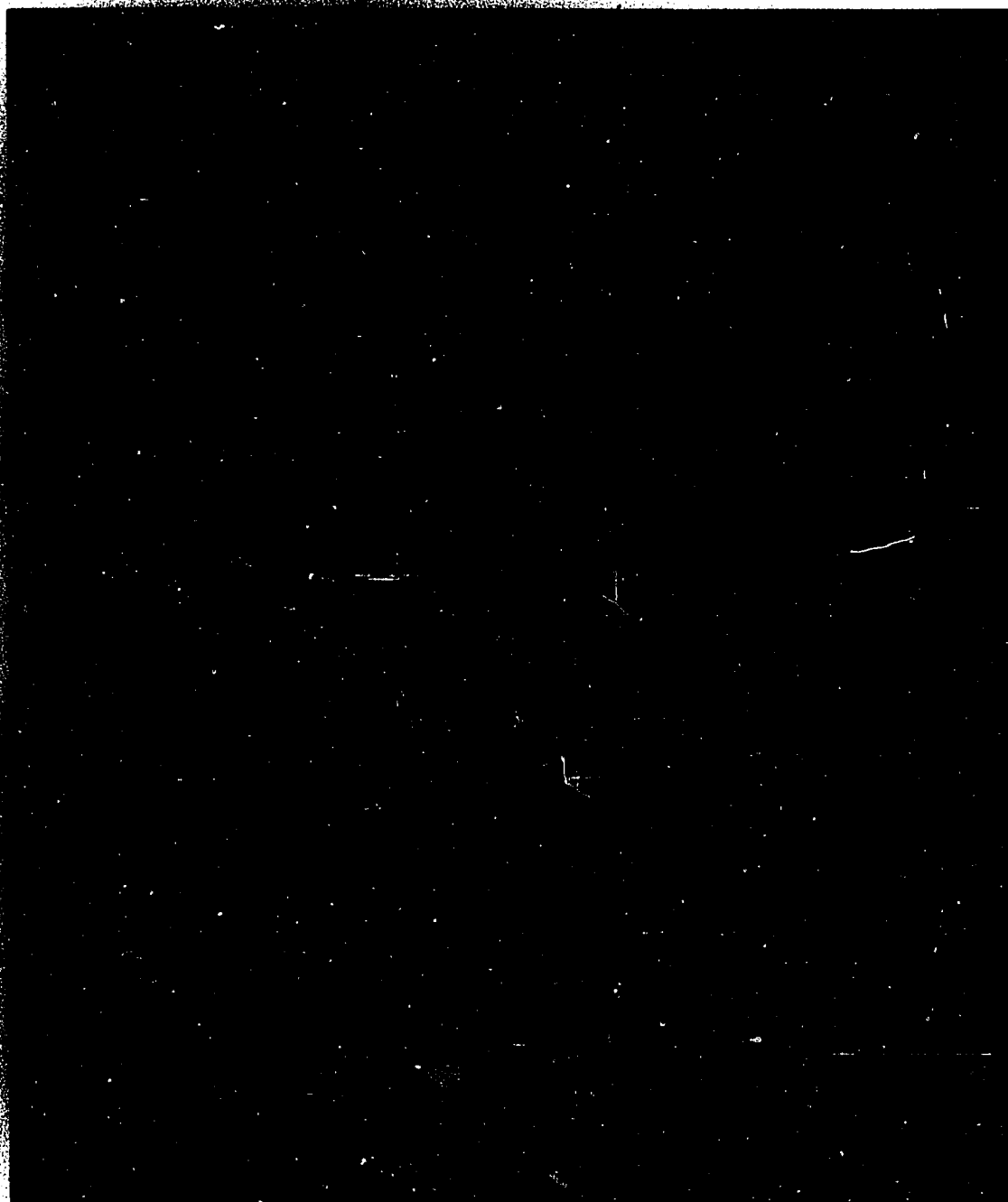


FIGURE 15

Infrared Photograph of the Orion 'Sword'

Figure 16. Infrared Photograph of the Orion Nebula

This plate is similar to Figure 15 and was also taken by Dr. Haro, but it is a shorter exposure and is enlarged to a larger scale. North is at the top and east is to the left. The shorter exposure allows greater detail to be seen in the very center of the nebula.

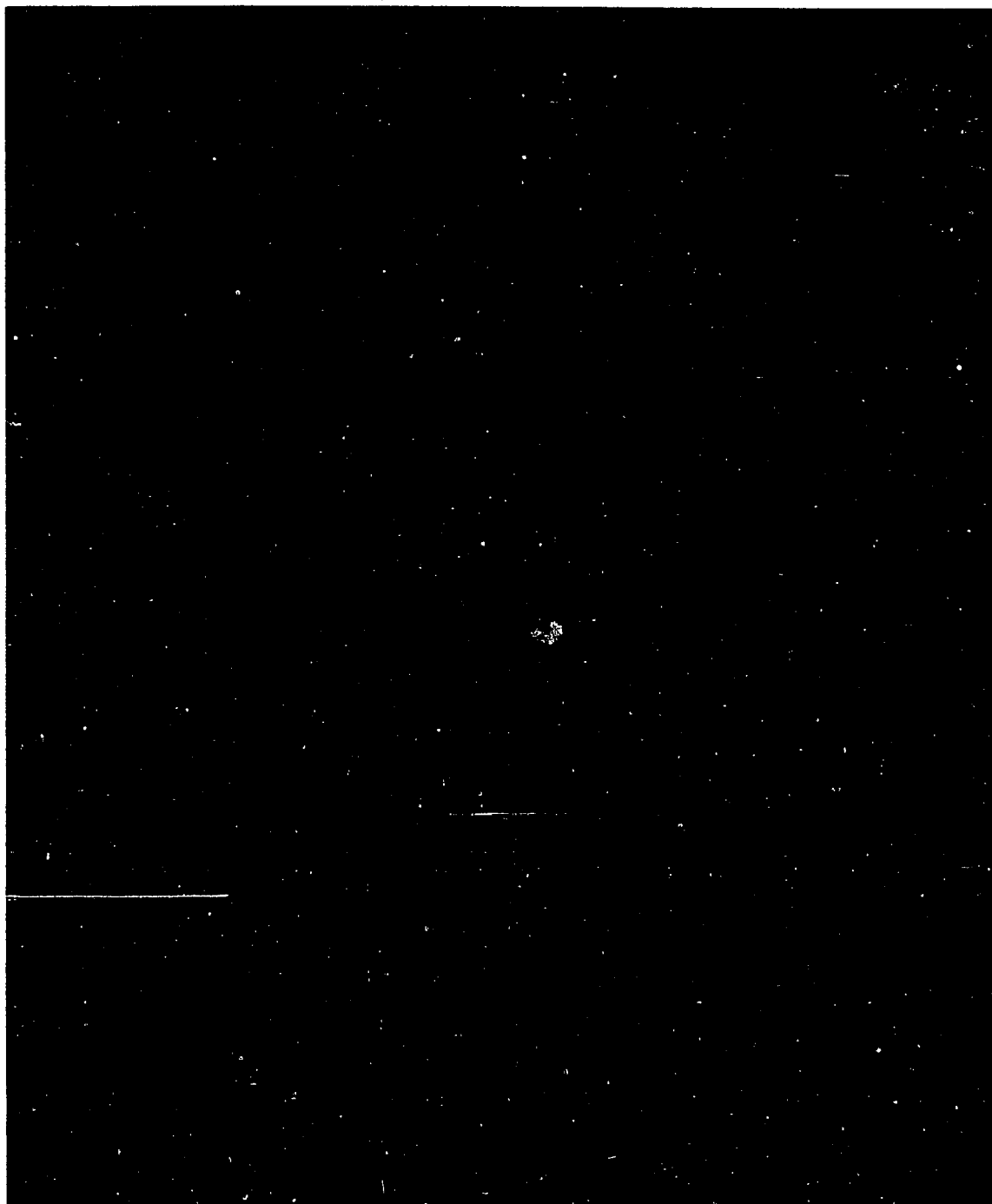


FIGURE 16

Infrared Photograph of the Orion Nebula

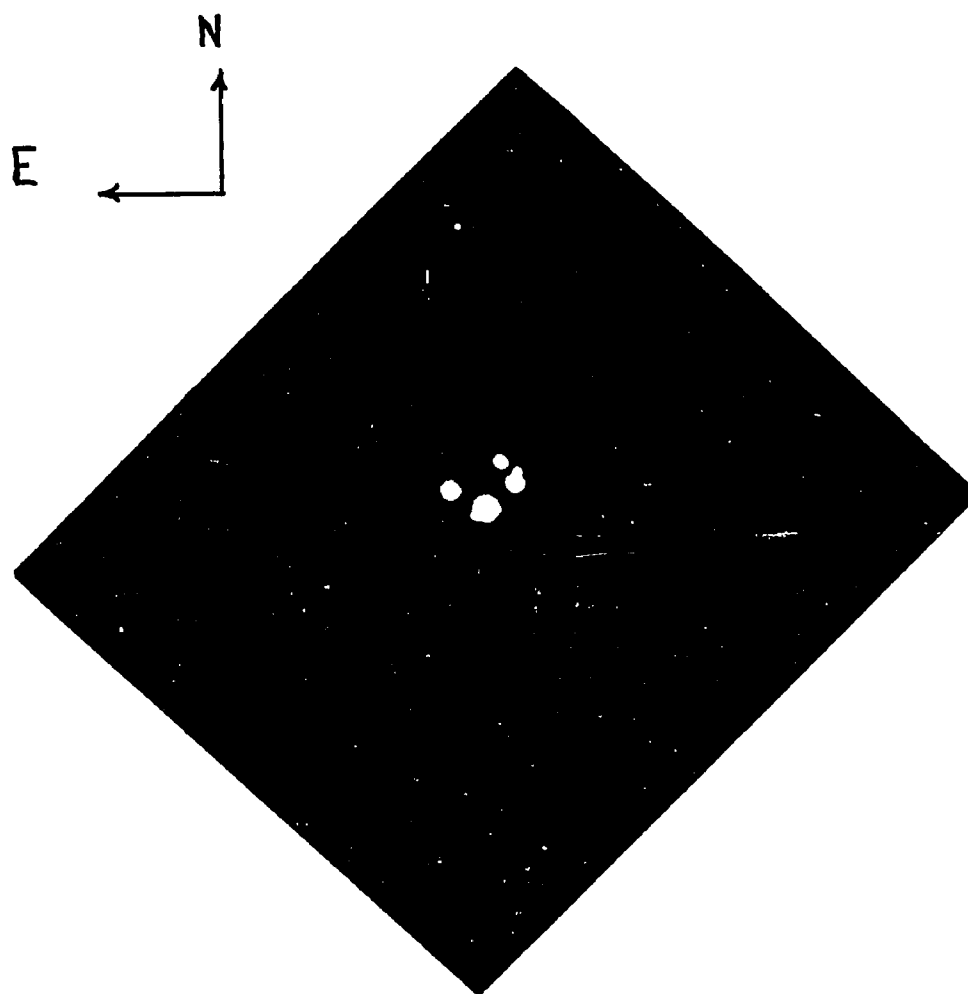


FIGURE 17

θ^1 Orionis

The 35mm color exposure was taken at F/13 with the 61-in. telescope of the Lunar and Planetary Laboratory by Dennis Milon. The exposure time was 15 seconds and no filter was used. The distribution of the nebular radiation near the Trapezium is easily seen.

not coincident with θ^1 Orionis, but is located somewhat to the southwest. The nebulosity near HD 37042 is very weak and uniform, while for θ^2 Orionis, the emission in the northern sky position is much stronger than that near the star. We recall again that the 'non-normal' character of the extinction law for these stars is already very significant in the I spectral band, and hence, any nebular radiation producing this abnormality should be seen in Figure 16 unless it is extremely near the stars.

4. The hypothetical emission spectrum that must exist if the extinction law in this region were truly 'normal' has been computed. The six stars near the Trapezium for which individual extinction curves have been determined in this study, as well as NGC 2024 No. 1 and Herschel #36 in NGC 6530 (Johnson, 1966c), were included in this calculation. The last two stars exhibit extinction curves that closely resemble those of the stars in the Orion Nebula. The 'normal' extinction law was assumed for each star and the excess radiation in the R, I, J, K, and L filters was computed from E_{B-V} and the absolute calibration given by Johnson (1966b).² The intensity distributions of the excess radiation were then corrected for extinction, again using the 'normal' relation and the appropriate value

2. The mean of two 5 μ measures of θ^1 (C) Orionis was also included here.

of E_{B-V} . The emission spectral distributions, corrected for extinction, were found to be remarkably similar. The normalized mean spectrum is plotted in Figure 18 and shows a definite maximum in the I filter, near $\lambda = 9,000 \text{ \AA}$, and a steady decrease toward longer wavelengths. The intensity at $1/\lambda = 1.82$, the position of the V filter, should be small since the reddening in the UBV spectral region is essentially 'normal' for these stars. The mean intensity distribution of the nebular continuum in the $\lambda = 7,000 \text{ \AA}$ to $10,000 \text{ \AA}$ range found by Mendez (1965) shows a steady decrease with increasing wavelength; such a distribution is markedly different from that shown in Figure 18.

From the arguments presented above, we see that the general nebular radiation cannot produce the large infrared intensities of the stars in the Orion Nebula. However, some emission mechanism could still produce this result if it were actually circumstellar, since then the source would be undetectable photographically. Stein (1966) discussed the problem of circumstellar emission from large dust particles in the far infrared ($\lambda = 5 \mu - 10 \mu$), but his results do not satisfactorily explain such excesses at shorter wavelengths. Underhill (1966) suggested that the observed phenomenon could arise from "the tail of a synchrotron emission distribution generated near the stars," yet the distribution seen in Figure 18 is hardly reminiscent of any normal synchrotron spectrum. In fact, a synchrotron radiation distribution

Figure 18. Mean Normalized Emission Spectrum Required for 'Normal' Extinction in the Orion Trapezium

The spectrum was determined from observations made with a 25" diaphragm, and has been corrected for extinction. The intensity in the V filter ($1/\lambda = 1.82$) must be small since the UBV reddening is essentially 'normal' for these stars. The distribution shows a definite maximum near $\lambda = 1\mu$.

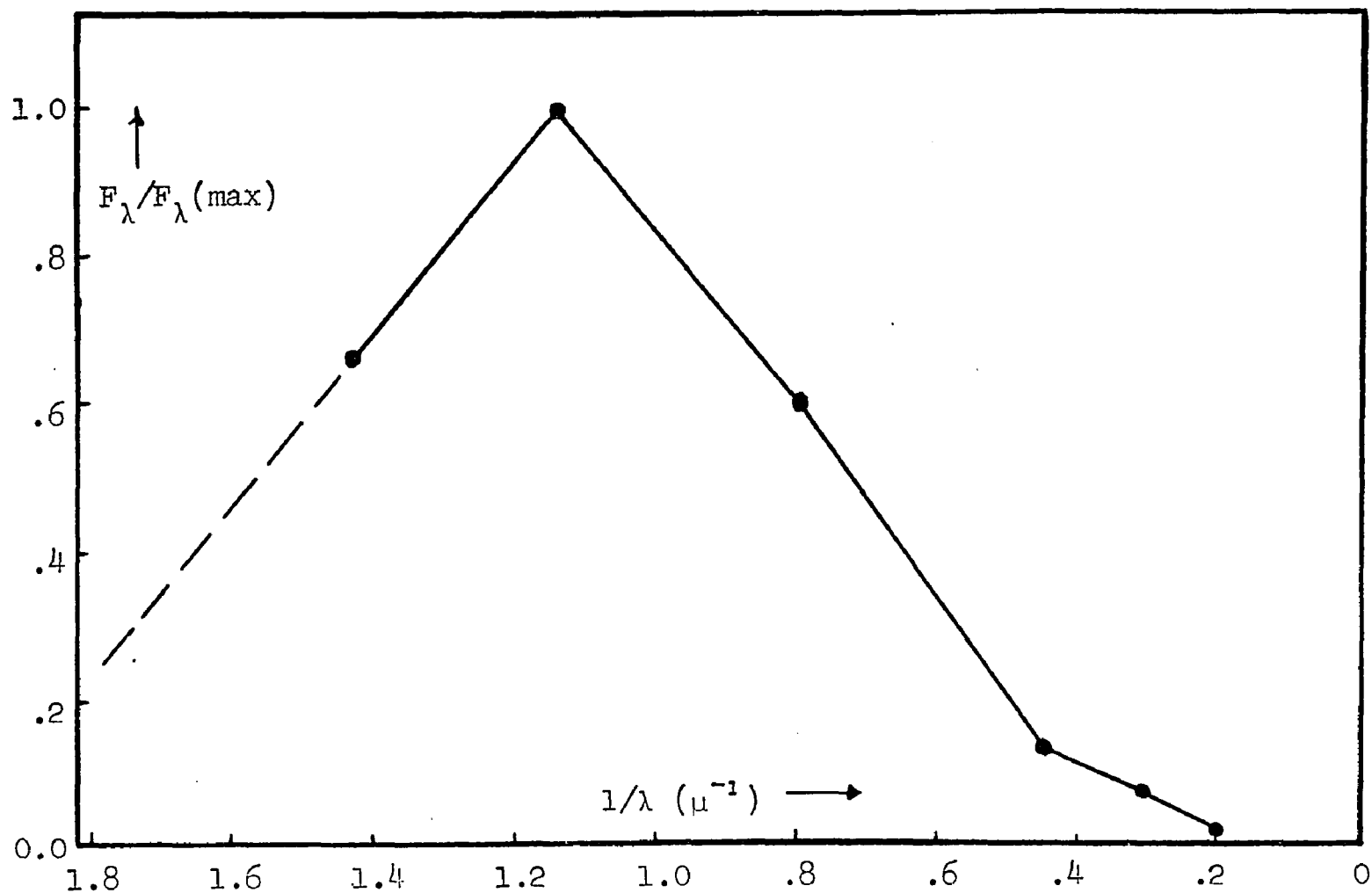


FIGURE 18

Mean Normalized Emission Spectrum Required for 'Normal' Extinction in the Orion Trapezium

similar to that of Figure 18 would require either a) the matter to be optically thick at wavelengths greater than 1μ , or b) the existence of many high-energy electrons and a sharp low-energy cutoff in their distribution. The first alternative is extremely unlikely in a configuration as small as a circumstellar envelope, and the second is unobserved in any synchrotron source (Williams, 1966).

3. Faint Red Stars in the Orion Nebula

The existence of a compact cluster of faint, late-type stars in the Orion Nebula was first noted by Baade and Minkowski (1937a). On an infrared plate of this region these authors counted 80 stars within a 3' diameter. The star charts published by Parenago (1954) and Strand and Teska (1958) clearly show the distribution of these stars. The long-exposure infrared photograph in Figure 15 shows the clustering in the outer nebulous regions, while the shorter exposure of Figure 16 allows greater detail to be seen in the center of the nebula. The redness of the faint cluster stars seen on these photographs is indicated by the fact that many of them are not visible on the blue 48-in. Palomar plate of this region.

H. M. Johnson (1961, 1966) made an extensive study of this cluster of stars. He found that the system is centered on θ^1 Orionis and has a mean central density of 750 stars per cubic parsec. The total mass of all the material

in the cluster is thought to be about 800 solar masses, and the mean density for the whole cluster is 21 solar masses per cubic parsec. Blanco (1963) obtained spectral types for 16 stars in the outer part of the cluster and found no types later than M 4. These objects were seen to form a continuation of the sequence of bluer stars ($B-V > 0.0$) that were observed by Johnson (1957) to lie above the main sequence in a color-magnitude diagram. Many have been found to be variable and show $H\alpha$ in emission (Haro, 1953). They are most probably young objects in the process of gravitational contraction.

Johnson (1966a) suggested that the ratio of total to selective absorption for the central part of the Orion Nebula may be about 5.0, and that the excess infrared radiation observed for the bright stars in this region might be caused by emission from these faint, red objects that are unavoidably included in the diaphragm when the observations are made. This possibility was explored by studying the distribution and the estimated colors and magnitudes of these faint stars. The charts of Strand and Teska (1958), the photographic B-V colors of Parenago (1954), and the I magnitudes estimated from Figure 16 were used in this analysis. A random sample of 30 of these stars near θ^1 Orionis yielded mean values for B-V and V-I of $+1.^m50$ and $+2.^m50$ respectively. If these objects are normal stars, then

a spectral type no later than M 3 would be indicated by these colors. However, the I magnitudes are simply estimates based on the images of several of the brighter stars that were photometrically observed, and therefore, the mean V-I color is quite uncertain. If the estimates are systematically in error, the mean V-I for these objects could be as large as $+4.0^m$, which would correspond to a M 5 - M 6 spectral type. The B-V color is of little value in this respect since it is nearly constant in the M 0 to M 8 range. A mean spectral type of M 3 for these stars would suggest that they are similar to the objects studied by Blanco (1963) in the outer part of the cluster, but the temperature of an M 3 star is considerably higher than the $1,300^\circ$ black-body emission spectrum required if the true ratio of total to selective absorption were 5.0 in this region (Johnson, 1966a). When an average type of M 3 is assumed, the infrared emission from these objects, in all but one instance, is found to make a negligible contribution to the measured intensities of the brighter stars in this region. The lone exception, $-5^\circ 1318$, is not as bright as the others and has several faint red stars nearby. The correction to the measured V-L for this star may be as large as 0.2^m ; such a correction would change E_{V-L}/E_{B-V} from 7.89 to 7.46--still highly 'non-normal'--and the corresponding change in the weighted

mean value for the region would be less than 0.1, which is less than one probable error.³

However, recent infrared work in the Orion Nebula by Becklin and Neugebauer (1966) tend to complicate the above discussion. These authors discovered an extremely red object only one minute of arc from θ^1 Orionis. This object, the reddest known to date, has a K magnitude of $5^m.2$ and K-L of $+3^m.2$ and shows broad wings extending more than $30''$ from the central source. The energy distribution closely approximates that of a 700° black body. The position of the source coincides with a pair of 16th (V) magnitude stars on the charts of Strand and Teska (1958) and Parenago (1954) (Parenago numbers 1820 and 1821). The position is shown on a reproduction of the Parenago chart in Figure 19. These two stars are visible on the infrared photograph in Figure 16, but they are by no means conspicuous when compared to the other cluster stars. This object does not appear to be typical of the other faint stars found here, since infrared scans of the region by Becklin and Neugebauer and by Low (1966) revealed no other conspicuous sources except θ^1

3. Haro and Moreno (1954) found another cluster of red stars in NGC 2024, near ζ Orionis. The magnitudes and colors of these stars are difficult to estimate, but only one very red star is seen near NGC 2024 #1, and it is located at the position of one of the sky measures. Thus, the measured colors of NGC 2024 #1 are probably correct, but may be slightly too blue.

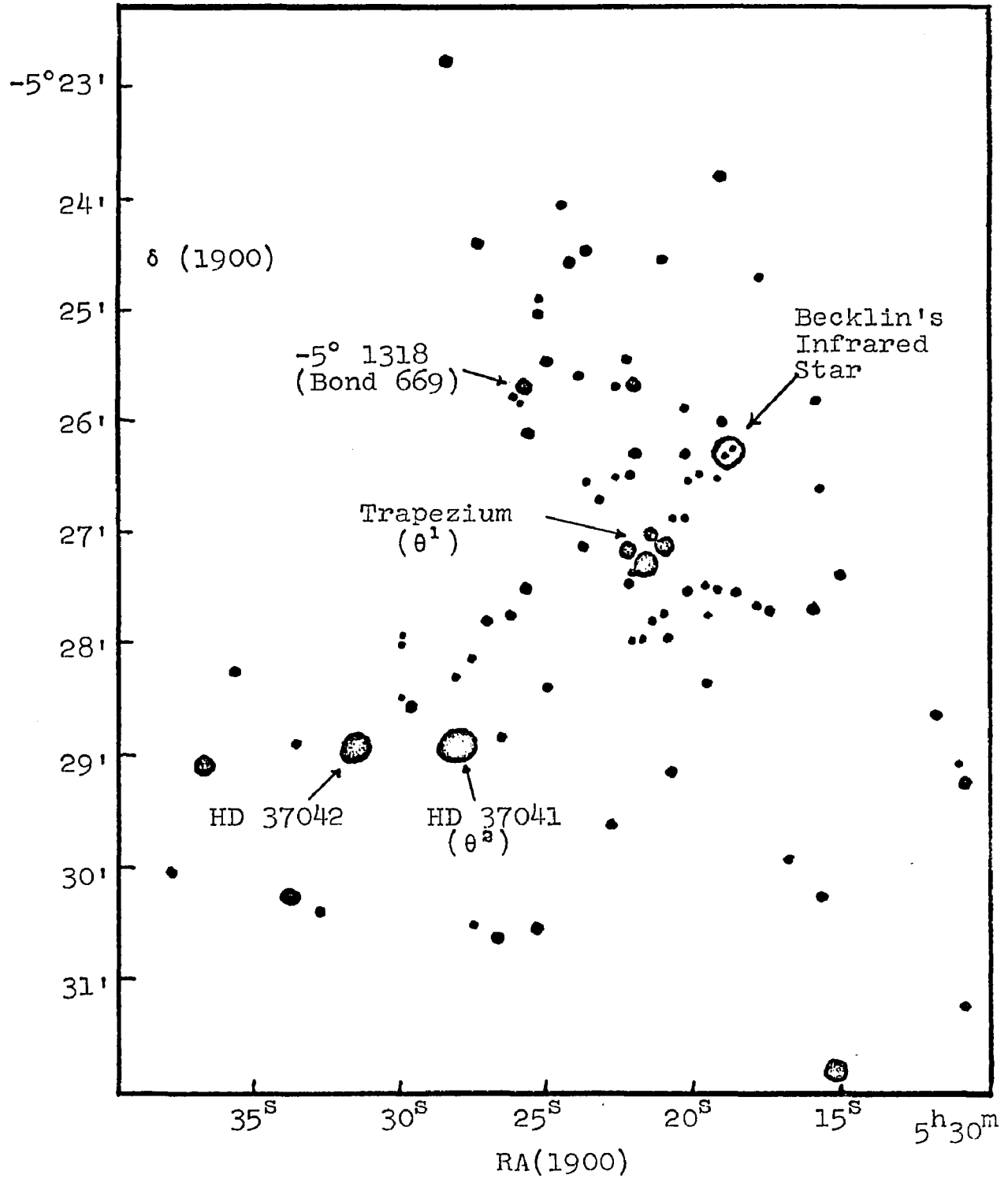


FIGURE 19

Map of the Orion Trapezium Region (Parenago, 1954)

Orionis itself. Nevertheless, the presence of a single strong infrared radiator in this region is significant since if this source is truly associated with the association, additional fainter sources of this type may also be present and the effects of these objects on the infrared measures made here could be non-negligible.

Of additional importance in this context is the fact that infrared scans made with the 200-in. telescope by Becklin and Neugebauer detected an increase in the infrared radiation at 2.2μ near the Trapezium. The wings found here are similar to those seen around the 700° source described above. For this object the mean intensity at 2.2μ is $12.0 \pm 0.5 \times 10^{-9}$ Watts $\text{cm}^{-2} \mu^{-1}$ steradian $^{-1}$ within $30''$ of the object, and $7.0 \pm 0.5 \times 10^{-9}$ Watts $\text{cm}^{-2} \mu^{-1}$ steradian $^{-1}$ between $30''$ and $50''$ away. If the gradient near θ^1 Orionis is similar to this, then a sizable fraction of the 2.2μ radiation measured for the Trapezium--perhaps as much as 50%-- could be due to this nonstellar component. However, neither HD 37042 nor HD 37041, nor any of the other stars in this area showed similar emission wings, and so the significance of this effect as observed for the Trapezium is not at all clear. The possibility that some of the hot young stars in the Orion Nebula have some form of protoplanetary systems associated with them, similar to that suggested by Low and Smith (1966) for R Monocerotis, cannot be ruled out at this juncture.

Therefore, the present evidence regarding the true interstellar extinction law in the neighborhood of the Orion Trapezium is not one hundred percent conclusive. The additional observations presented in this study for HD 37041, HD 37042, HD 37061, and -5° 1318 certainly strengthen the extinction interpretation since an emission process that produces the proper amount of infrared radiation for each of these stars, which span a considerable range in brightness, spectral type, and reddening, appears somewhat improbable. The work of Becklin and Neugebauer (1966), however, suggests that the Trapezium itself may be affected in this manner. The conclusion of this author, based on the data of this investigation and on previous results (Sharpless, 1952; Johnson, 1966a; and Mendez, 1965), is that the extinction law here is decidedly 'non-normal' and is characterized by a ratio of total to selective absorption of 5.0 or greater; the evidence for a ratio as high as that indicated by the mean curve given in Figure 11 is somewhat less convincing. In the analysis that follows we shall assume that the mean law for the Trapezium area in Figure 11 is correct, but the uncertainty of this assumption must be implicit in any additional conclusions realized for this region in the remaining chapters of this study.

VII

Regional Monochromatic Extinction Laws

A. Method

Because of the bandwidths of the UBVRIJKL filters, the extinction laws obtained directly from the observational data may differ somewhat from the corresponding monochromatic laws. King (1952) showed that in the first approximation, the wavelength λ_e , given in (12), is the effective wavelength for extinction-law determinations.

$$(12) \quad \lambda_e = \frac{\int \lambda I(\lambda) F(\lambda) d\lambda}{\int I(\lambda) F(\lambda) d\lambda}$$

where $I(\lambda)$ is the incident intensity distribution,
and $F(\lambda)$ is the filter-cell response function

Thus the monochromatic law, to first order, is represented by the plot of Δm against λ_e for the various filters used. This procedure has been the conventional one for obtaining the monochromatic extinction law from an observed heterochromatic (wide band) relation.

An alternate method that eliminates the use of the effective wavelength will be used in this study. The

response of a photometer with the i -th filter is:

$$(13) \quad L_i(k) = \int_0^{\infty} I(\nu) F_i(\nu) e^{-kE(\nu)} d\nu$$

where $I(\nu)$ = intrinsic intensity dist. of star

$F_i(\nu)$ = normalized response function of i -th filter

$E(\nu)$ = monochromatic extinction efficiency factors

= $\frac{\text{true extinction cross section of particle}}{\text{geometrical cross section } (\sigma)}$

k = total number of particles in line of sight \times geometrical cross section

= $N\sigma$

$(\tau_\nu = kE(\nu) = \text{optical depth of cloud})$

The total attenuation in magnitudes at the i -th filter becomes:

$$(14) \quad \Delta m_i(k) = -2.5 \text{ Log } \left\{ \frac{L_i(k)}{L_i(k=0)} \right\}$$

The series of $\Delta m_i(k)$ for the various filters then represents the observed extinction law produced by a certain amount of material (characterized by k) whose monochromatic extinction is given by $E(\nu)$. By varying the monochromatic law, which is the input for this routine, one can, after several trials, reproduce a particular observed extinction law. The monochromatic law determined in this manner will be smoothed since no structure finer than the filter bandwidths will be ascertainable.

Since the parameters in the integrand of (13) are continuous and well-behaved, an eleven-point Simpson-type integration was used for the solution. The normalized filter-cell response functions were taken from Johnson (1965). The intrinsic intensity distribution was assumed to be that of a black-body. This assumption should be adequate for this investigation--except possibly at the U point--since all the data here refer to hot early-type stars. The solutions for each monochromatic extinction law were computed for four black-body intensity distributions, $T = 30,000^\circ$, $20,000^\circ$, $10,000^\circ$, and $3,500^\circ$. The numerical work was carried out on the IBM 7072 of the Numerical Analysis Laboratory of the University of Arizona. The printed output from the computer consists of eight pages of data--two for each intensity distribution--for each monochromatic law. Two sets of sample solutions are given in Appendix B. The first solutions refer to the 'normal' monochromatic law, while the second group represents a law which has greater extinction in the infrared and a higher ratio of total to selective absorption. For each black-body temperature, the first page of output includes the monochromatic efficiency factors used, as well as the total attenuation in each of the 10 filters as a function of the parameter k , which is incremented from 0.0 to 8.0. Also given here is the ratio of total to selective absorption. The second page gives the

total visual extinction, E_{B-V} , and the normalized extinction law (the observed color excess ratios) as a function of k .

B. General Properties of Wideband Extinction Laws

Some comments regarding the numerical solutions described above are appropriate at this point. The ultraviolet portion of the derived monochromatic laws must be taken with some reserve for the following reasons: a) By forcing $E_{U-V}/E_{B-V} = 1.7$, we have eliminated the possibility of detecting any variations in the extinction law in the ultraviolet spectral region, albeit the observational data indicate that such variations within the Orion association must be small. b) The U observation represents the last point on this end of the spectrum, and therefore, the precise nature of the extinction curve here cannot be well determined. c) Finally, the use of a black-body intensity distribution in the neighborhood of the Balmer discontinuity may partially vitiate the results in this spectral region.

The sample solutions in Appendix B indicate some significant relationships. The observed ratio of total to selective absorption always increases as one goes from hot to cool stars, but the ratio is nearly constant for stars whose temperatures are in the $10,000^\circ$ to $30,000^\circ$ range. The E_{U-V}/E_{B-V} ratio increases with increasing extinction

(larger k) and with decreasing star temperature.⁴ The dependence of the ratio of total to selective absorption and of the other excess ratios upon the amount of reddening is not consistent, but depends on the particular monochromatic law and also somewhat on the temperature of the star. These general characteristics are in qualitative agreement with the results of Blanco and Lennon (1961) who treated only the 'normal' monochromatic law. However, it is clear that not all of their conclusions regarding these functional dependences for the 'normal' monochromatic relation can be adopted for other laws.

The monochromatic extinction laws producing the mean regional curves obtained earlier in this study have been determined by the method outlined above. In accord with the theoretical work of van de Hulst (1949), the condition $E(\nu=0) = 0$ has been imposed for all the monochromatic laws. The fitting of the color excess ratios to the values obtained from the monochromatic relation is done at the values of E_{B-V} and color temperature that approximate the mean values of these parameters for the stars in the region. The lack of a strong dependence of the excess ratios on either

4. The dependence of E_{U-V}/E_{B-V} on the amount of extinction is in qualitative accord with the observed curvature in the O-star reddening line, and the second-order term present in (6). The reality of this curvature has been debated for many years; the above consideration adds somewhat to its validity.

E_{B-V} or T_c (for $T_c > 10,000^\circ$), as indicated by the solutions given in Appendix B, shows that the method of normalization and the use of stars with varying degrees of reddening for the mean extinction law calculations cannot significantly affect the results. Further evidence to this effect can be found in the observational data obtained at the Lunar and Planetary Laboratory for stars in the Cygnus region.

Figures 20 and 21 show the dependences of E_{V-R} and E_{V-I} on E_{B-V} for a sample of O-type stars in Cygnus. The linearity of the relations over a considerable range in E_{B-V} is in agreement with that predicted by the first set of sample solutions in Appendix B, which employs a monochromatic law similar to that of the Cygnus region. A similar degree of linearity should apply to the other excesses. For monochromatic laws showing greater extinction in the infrared and a larger ratio of total to selective absorption, however, the changes in the measured excess ratios with reddening are more significant; but since the normal range of reddening in Orion is from 0.1^m to 0.6^m in E_{B-V} , these changes will still be small when compared to the uncertainties of the mean values. If late-type stars had been included in this study, additional care in the calculation of the regional extinction curves would have been required, since the differences in the excess ratios of two equally reddened stars whose color temperatures are $3,500^\circ$ and $30,000^\circ$ are more significant. This is shown in Figure 22.

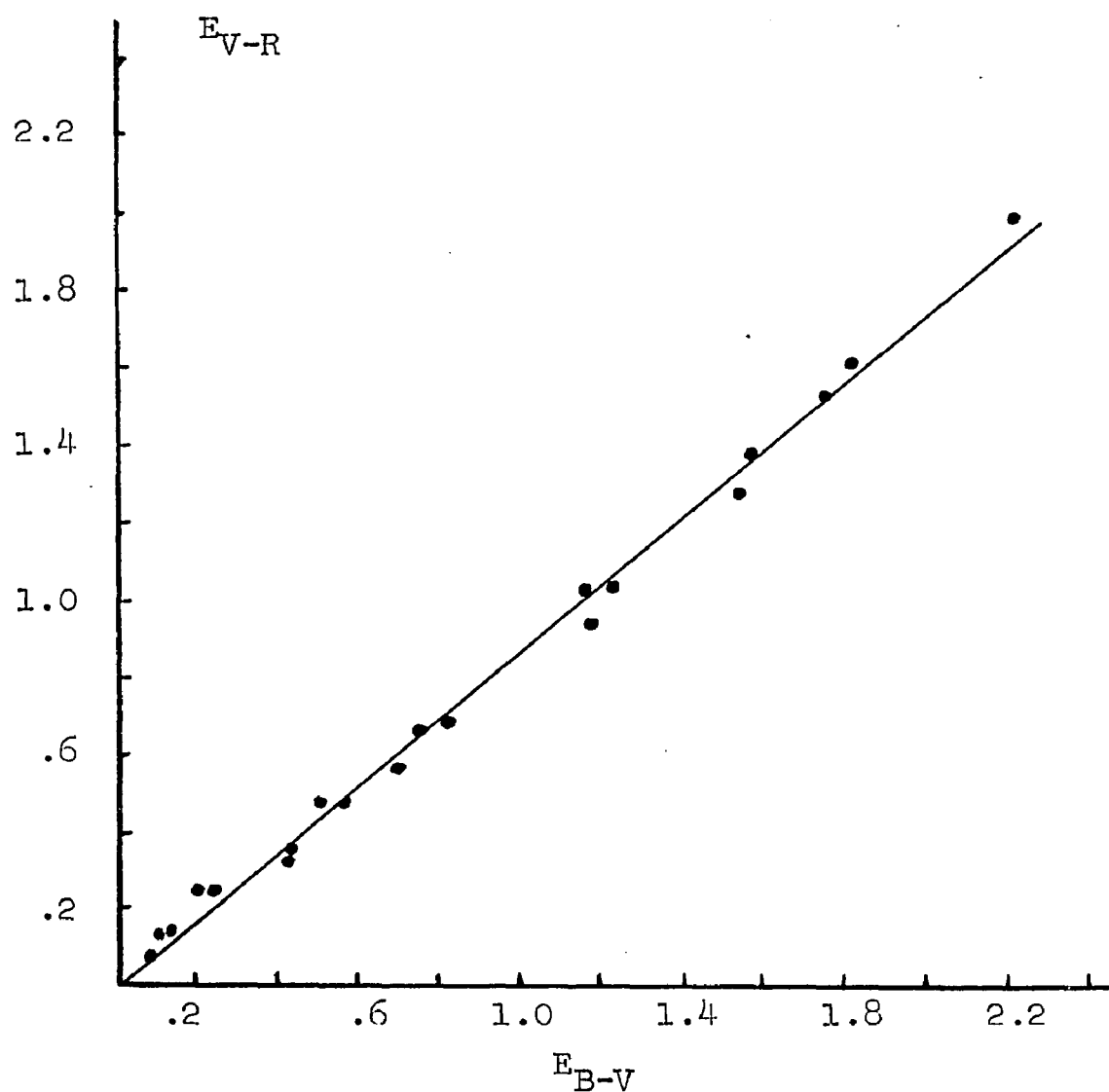


FIGURE 20

E_{V-R} versus E_{B-V} for O-type Stars in Cygnus

The linear relation indicates no significant changes of E_{V-R}/E_{B-V} with reddening.

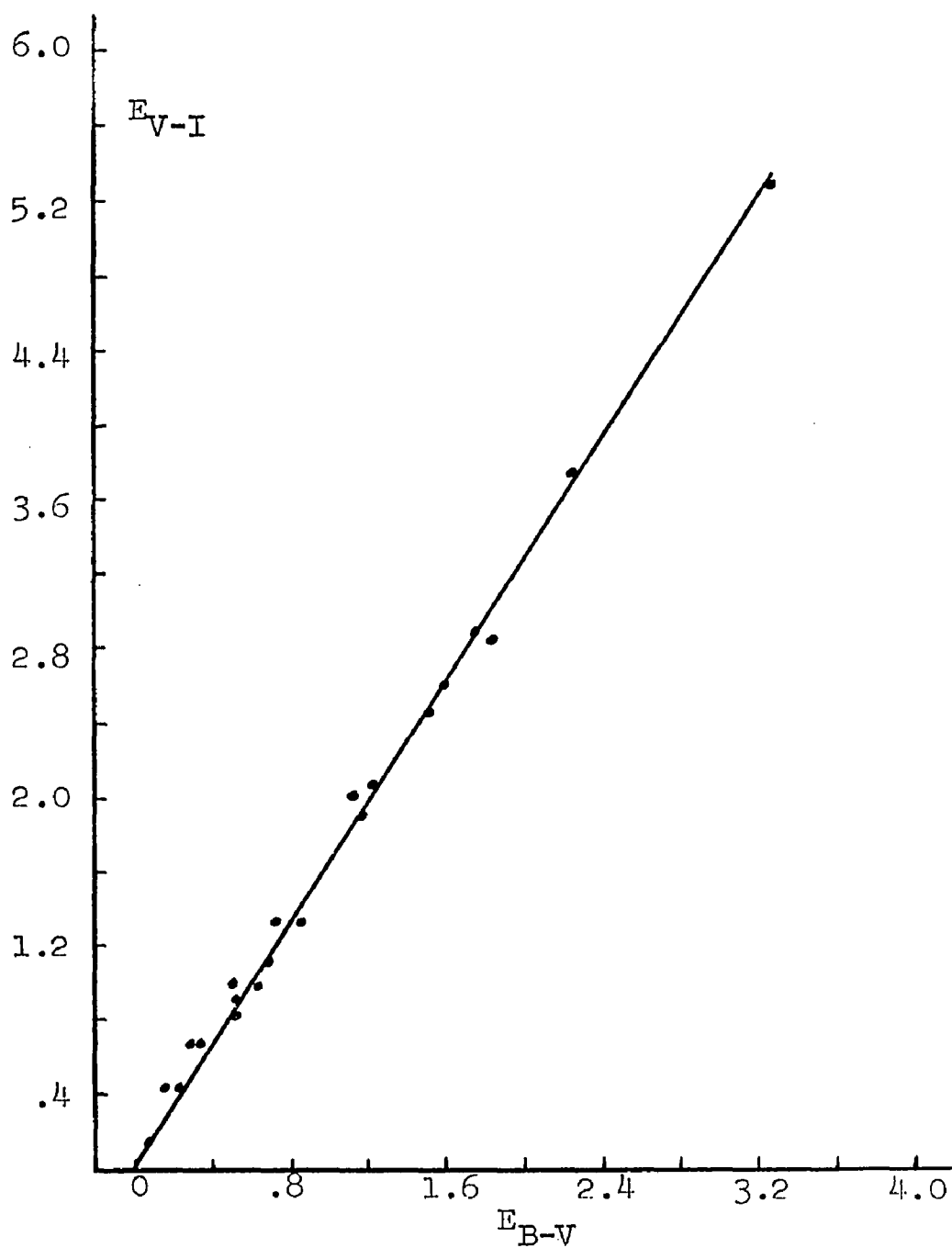


FIGURE 21

E_{V-I} versus E_{B-V} for O-type Stars in Cygnus

The linear relation indicates no significant changes of E_{V-I}/E_{B-V} with reddening.

Figure 22. Normalized Extinction Curves for Two Stars whose Color Temperatures are 3,500 and 30,000 Degrees

The reddening (E_{B-V}) and the monochromatic extinction law are the same for both stars. The differences in the curves, which arise from bandwidth effects, are noticeable but not large.

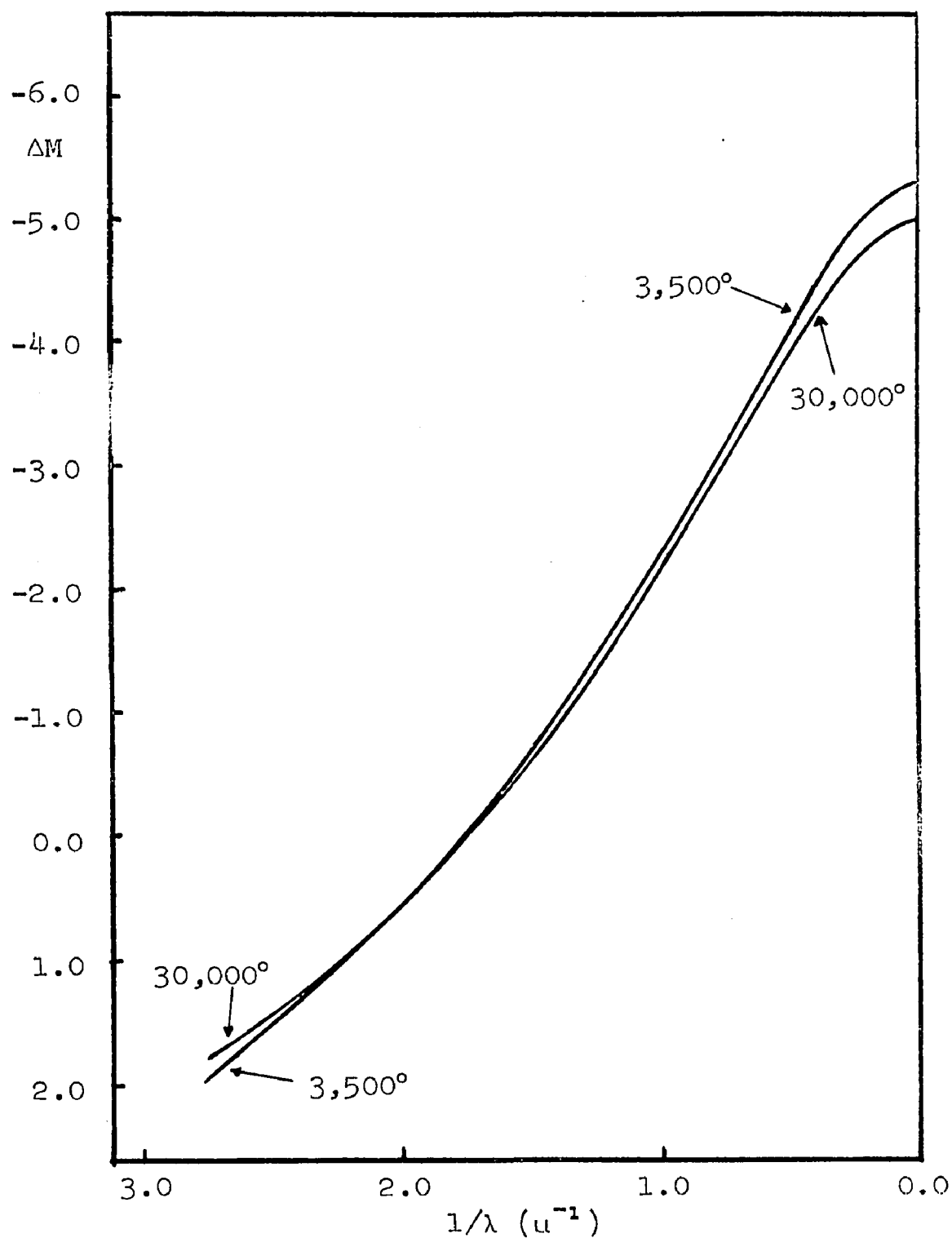


FIGURE 22

Normalized Extinction Curves for Two Stars whose Color Temperatures are 3,500 and 30,000 Degrees

C. Regional Monochromatic Curves

The monochromatic extinction laws for the various regions of the I Orion association are shown in Figures 23 to 30, and the data are summarized in Table 14. The figures show the extinction efficiency plotted as a function of frequency, but the positions of the photometric filters at $\nu_0 = c/\lambda_0$ are also indicated. The efficiency factors, $E(\nu)$, have been normalized so that $E(\nu) = 2.0$ for $\nu = 0.684 \times 10^{15}$ cps ($\nu = 0.684 \times 10^{15}$ cps is the frequency midpoint of the B filter). The curves will require a rescaling if they are to be fit to any theoretically determined monochromatic laws. Also, the curves given in Figures 23-30 are valid only in the interval from $\nu = 0.09 \times 10^{15}$ to 0.90×10^{15} cps since this is the approximate spectral range covered by the observations. A constant added to all the $E(\nu)$ within this interval would not change the normalized extinction curve observed from $\lambda = 0.36$ to 3.4μ with UBVRIJKL data, but would change the curve beyond $\lambda = 3.4 \mu$ and also the ratio of total to selective absorption. Therefore, the method adopted here to determine the monochromatic law corresponding to a given heterochromatic relation yields no new information regarding the true ratio of total to selective absorption other than that seen originally from the heterochromatic curve. The monochromatic laws given in Figures

Table 14

Normalized Monochromatic Extinction Data

Extinction Efficiency Factors-- $E(\nu)$

Region	$\nu =$.05	.10	.15	.20	.25	.30	.35	.40	.45	.50	.55	.60	.65	.70	.75	.80	.85	.90	.95	1.00	$\times 10^{15}$ cps
East 'Belt'		.12	.45	.76	.84	.92	1.04	1.18	1.33	1.47	1.61	1.72	1.83	1.93	2.03	2.10	2.17	2.22	2.25	2.29	2.30	
NGC 2024 No. 1		.13	.29	.45	.59	.72	.83	.99	1.21	1.39	1.56	1.71	1.84	1.94	2.02	2.09	2.15	2.20	2.24	2.27	2.28	
Northwestern		.09	.24	.41	.54	.65	.75	.85	1.04	1.22	1.40	1.58	1.75	1.91	2.04	2.15	2.26	2.35	2.42	2.46	2.47	
M78		.04	.11	.21	.36	.51	.62	.74	.96	1.19	1.38	1.59	1.77	1.91	2.03	2.13	2.22	2.32	2.38	2.42	2.44	
Outer 'Sword'		.05	.11	.18	.26	.37	.50	.64	.80	1.08	1.31	1.52	1.70	1.89	2.06	2.19	2.28	2.35	2.39	2.42	2.42	
HD 37061		.07	.21	.42	.59	.73	.85	1.02	1.21	1.38	1.54	1.69	1.82	1.93	2.03	2.11	2.18	2.24	2.29	2.33	2.35	
Trapezium (Exact)		.05	.29	.63	.84	.97	1.05	1.17	1.39	1.54	1.67	1.78	1.87	1.96	2.02	2.08	2.12	2.17	2.20	2.22	2.22	
Trapezium (Smoothed)		.15	.37	.61	.80	.95	1.08	1.22	1.39	1.54	1.67	1.78	1.87	1.96	2.02	2.08	2.12	2.17	2.20	2.22	2.72	
'Normal'		.03	.09	.16	.27	.40	.55	.71	.90	1.11	1.34	1.54	1.72	1.89	2.03	2.17	2.29	2.36	2.43	2.47	2.48	

Figure 23. Normalized Monochromatic Extinction Law for the East 'Belt' Region

The extinction efficiency is plotted against frequency. The frequency midpoints of the photometric filters are also shown. The curves are normalized so that the extinction efficiency equals 2.0 at the midpoint of the B filter. Comparison with the 'normal' law, the dashed curve, must be made for equal extinction in the B filter, since different scale factors are implicit in the 'normal' and regional curves. Monochromatic laws for the other regions in Orion are given in Figures 24 - 30.

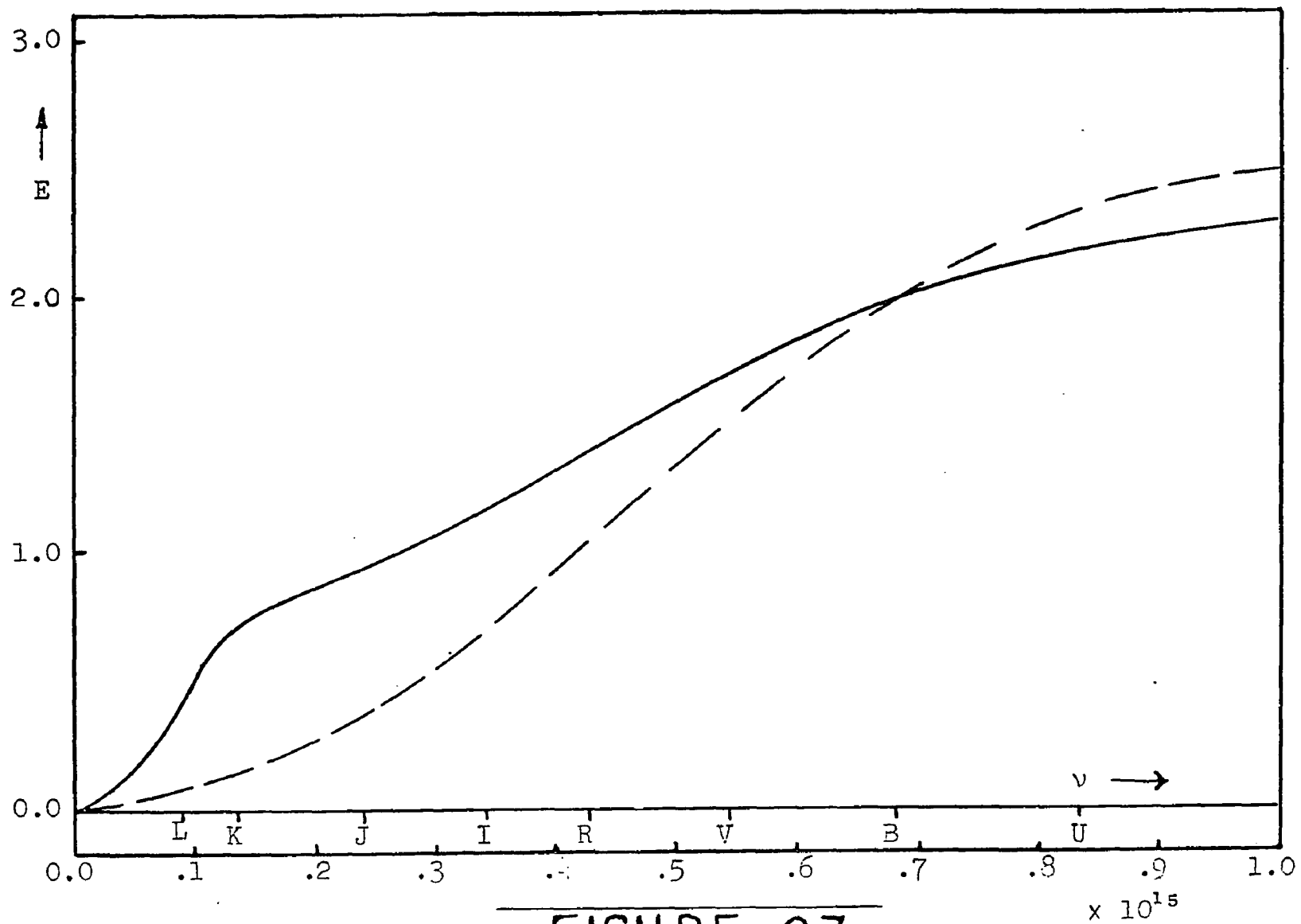


FIGURE 23

Normalized Monochromatic Extinction Law for the East 'Belt' Region

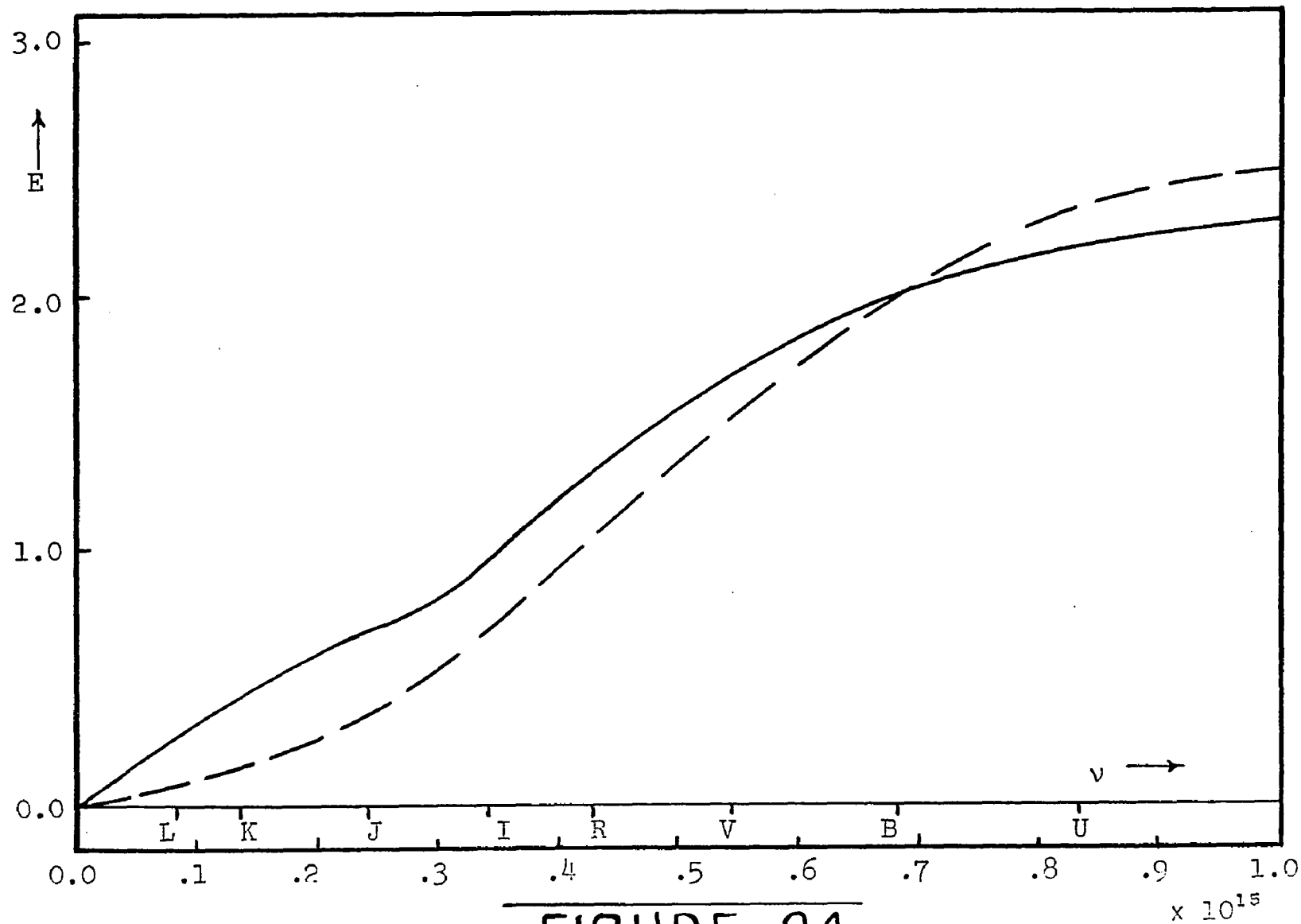


FIGURE 24

Normalized Monochromatic Extinction Law for NGC 2024 No. 1

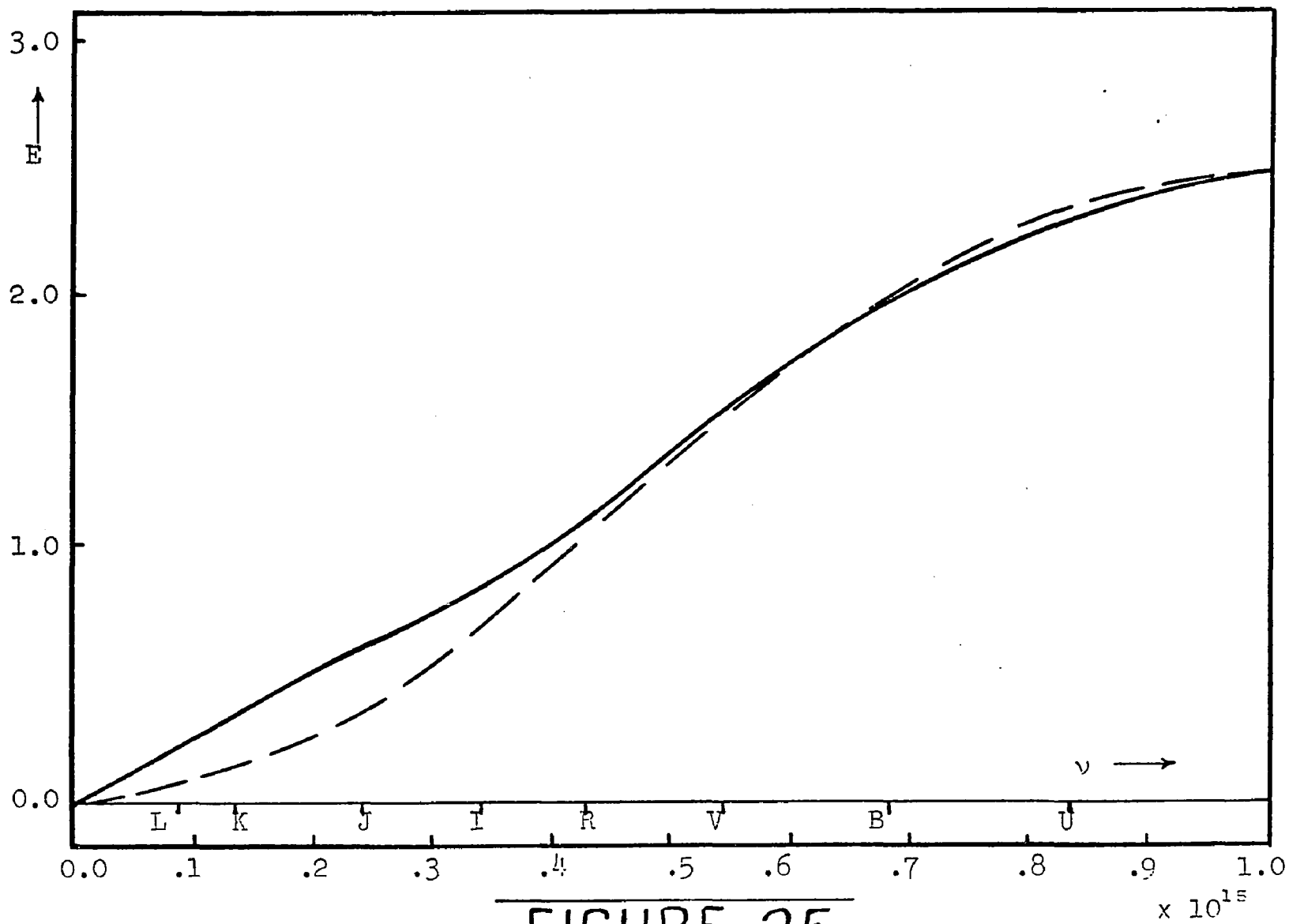


FIGURE 25

Normalized Monochromatic Extinction Law for the Northwestern Region

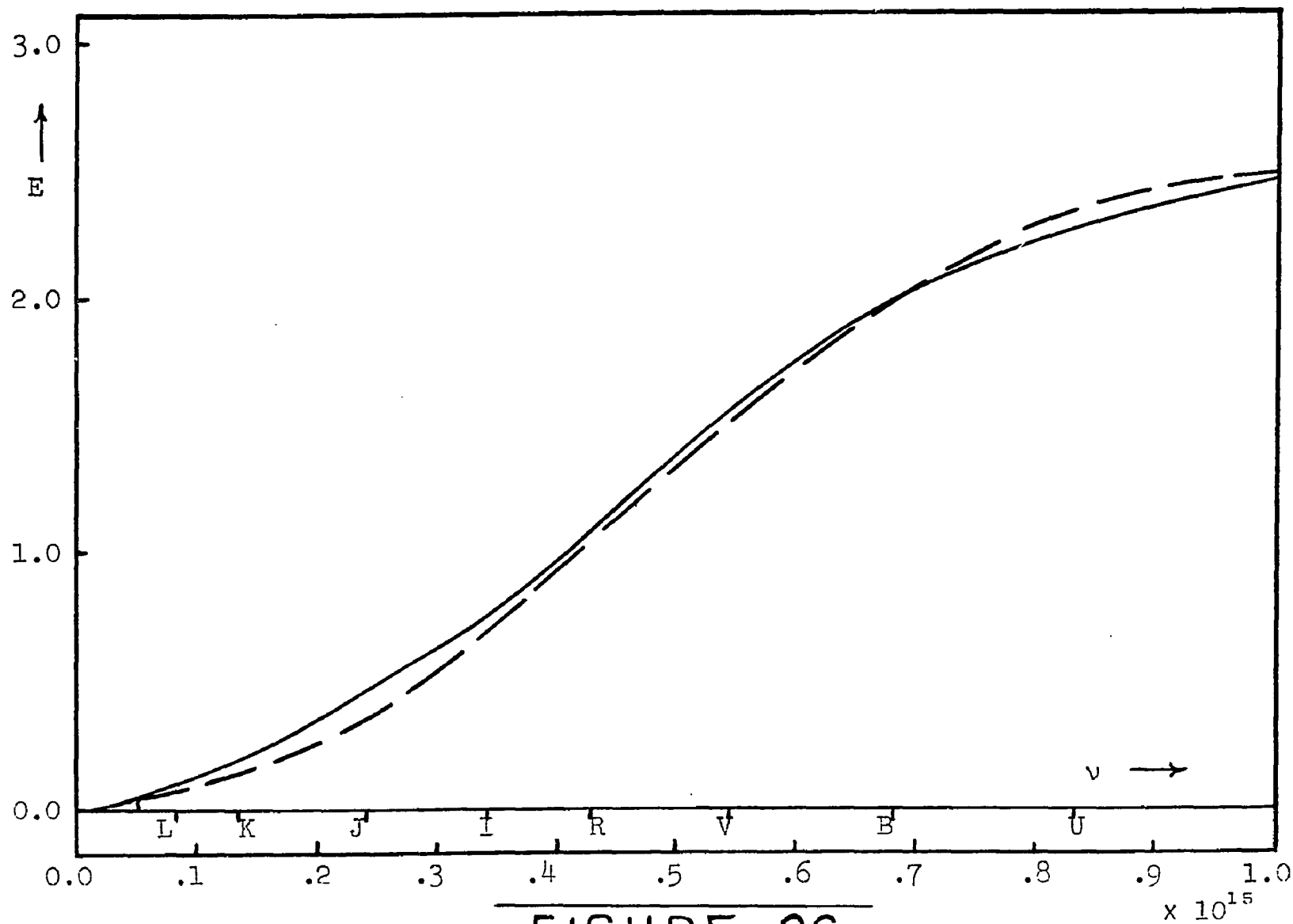


FIGURE 26

Normalized Monochromatic Extinction Law for M 78 A, B

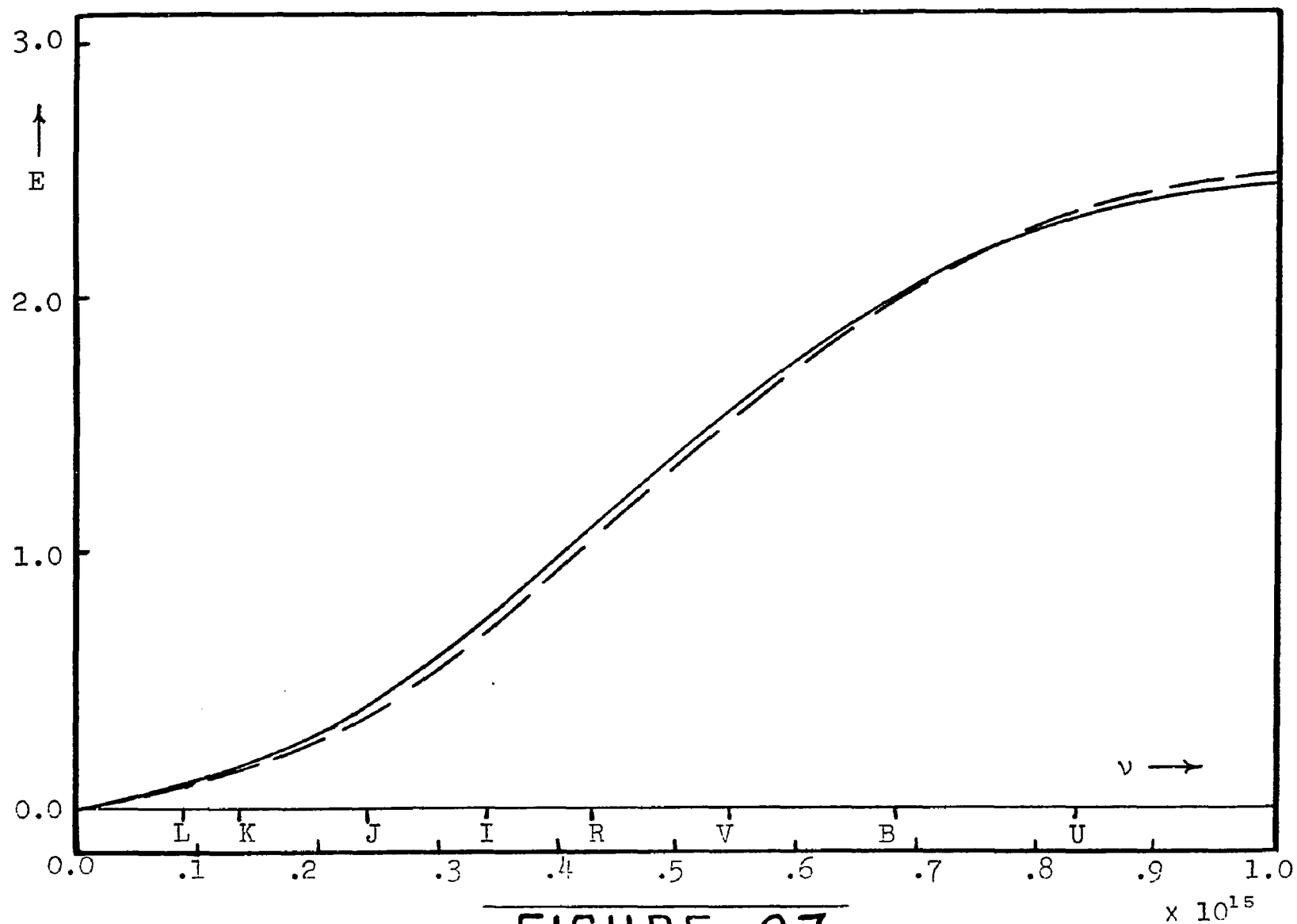


FIGURE 27

Normalized Monochromatic Extinction Law for the Outer 'Sword' Region

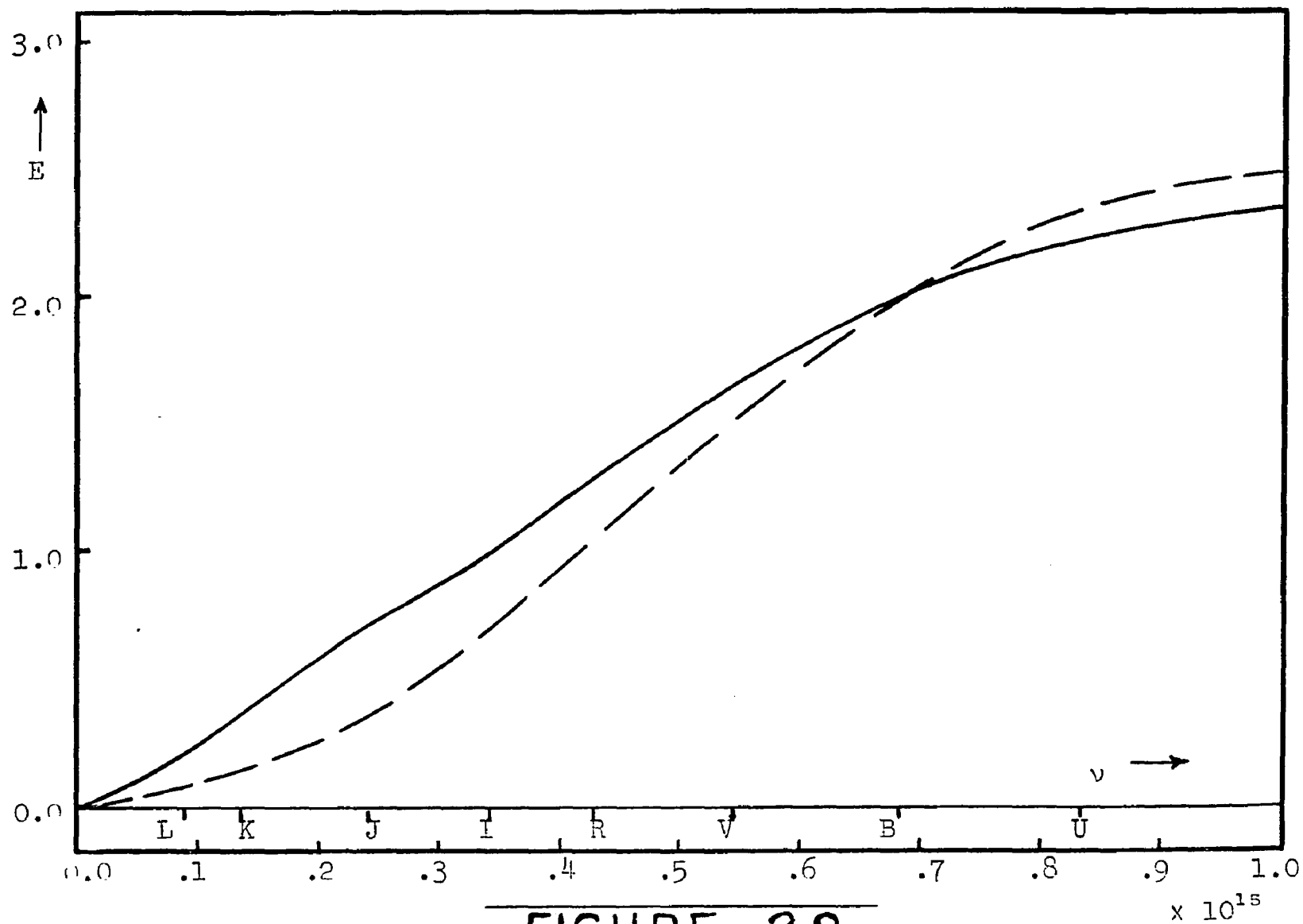


FIGURE 28

Normalized Monochromatic Extinction Law for HD 37061

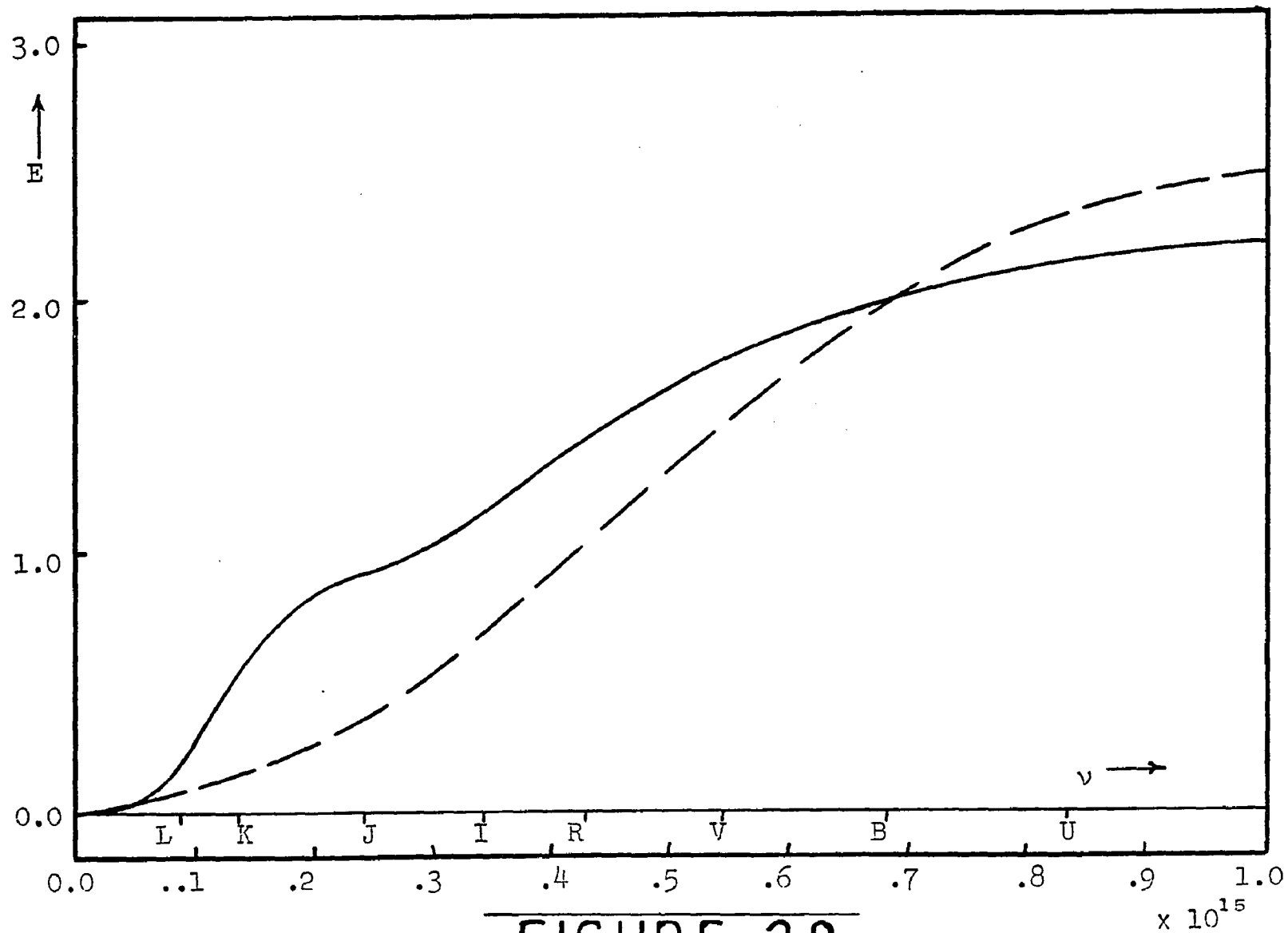


FIGURE 29

Normalized Monochromatic Extinction Law for the Trapezium Region (exact fit)

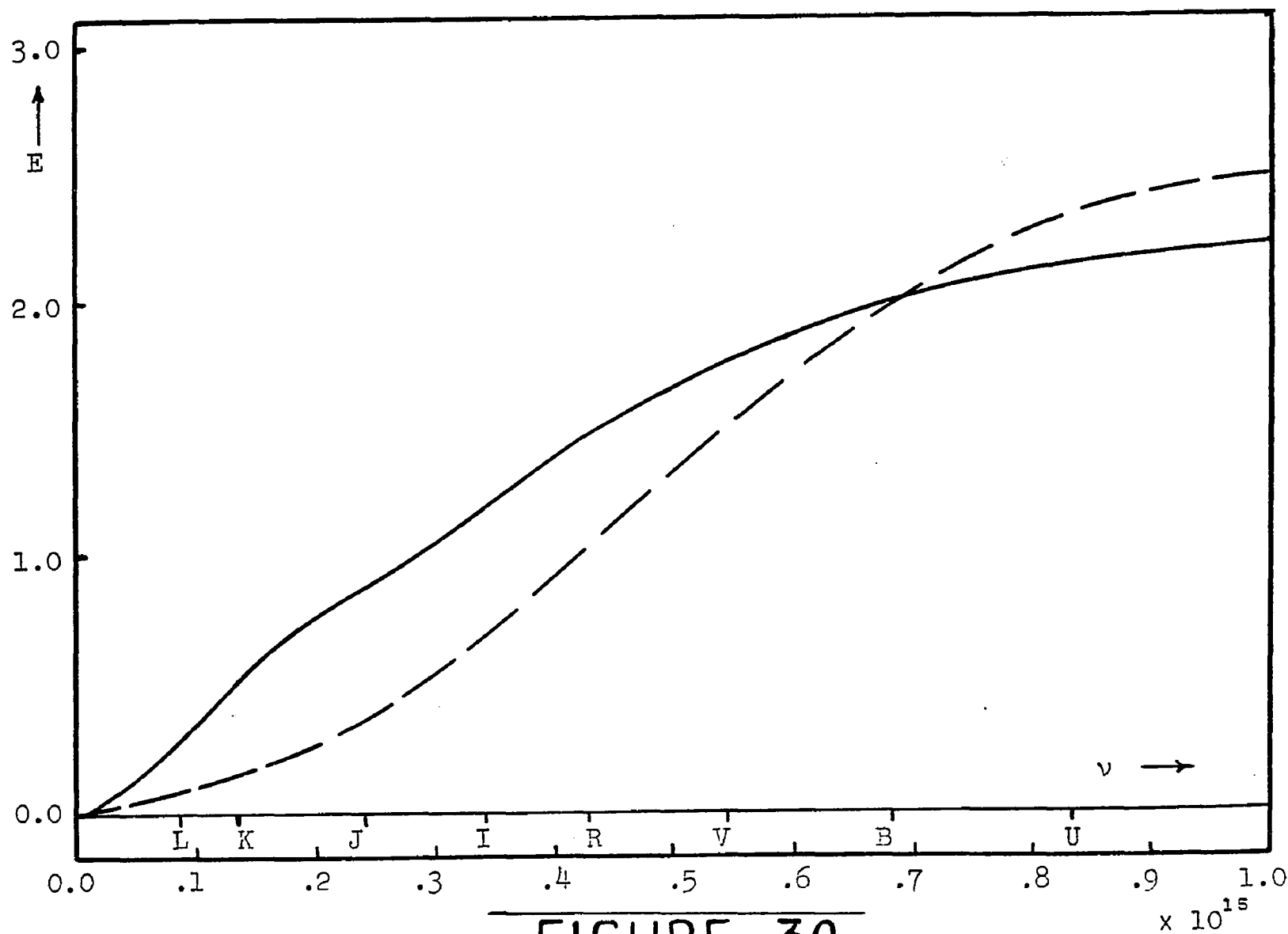


FIGURE 30

Normalized Monochromatic Extinction Law for the Trapezium Region (smoothed)

23 - 30 produce values of R which are in good agreement with those obtained by extrapolating the observational curves to $1/\lambda = 0$, but little more can be said regarding the accuracy of these values. As was mentioned previously, all monochromatic laws given here are characterized by the condition $E(0) = 0$, and thus, no component of the total extinction will be completely neutral with respect to wavelength. Finally, the dashed curve drawn in each of the figures represents the 'normal' extinction law for $\lambda > 3,500 \text{ \AA}$ and is included for comparative purposes only.

D. Properties of the Monochromatic Laws

The monochromatic extinction laws for the various regions will now be discussed. The values of the observed excess ratios and those resulting from the adopted monochromatic law for each region are listed in Table 15.

East 'Belt' Region

The excess ratios resulting from the monochromatic routine were fitted to the observed values at $E_{B-V} = +0.^m18$ and $T_c = 30,000^\circ$. The monochromatic law, shown in Figure 23, exhibits a very rapid rise in the infrared. For equal extinction in the blue filter, the efficiency factors in the K filter, near $\nu = 0.14 \times 10^{15}$ cps, are nearly five times those of the 'normal' law. The steep slope at $\nu = 0.1 \times 10^{15}$ cps reflects the high E_{V-L}/E_{V-K} ratio of 1.37 for this

Table 15

Observed and Monochromatic Color
Excess Ratios

	$\frac{E_{U-V}}{E_{B-V}}$	$\frac{E_{B-V}}{E_{B-V}}$	$\frac{E_{V-R}}{E_{B-V}}$	$\frac{E_{V-I}}{E_{B-V}}$	$\frac{E_{V-J}}{E_{B-V}}$	$\frac{E_{V-K}}{E_{B-V}}$	$\frac{E_{V-L}}{E_{B-V}}$	R
<u>East 'Belt' Region</u>								
Observed	1.72	1.00	0.80	1.78	2.65	3.39	4.64	5-6
Mono.	1.73	1.00	0.83	1.78	2.67	3.36	4.63	5.84
<u>NGC 2024 No. 1</u>								
Observed	1.83	1.00	1.13	2.28	3.21	4.17	4.71	5.5
Mono.	1.79	1.00	1.17	2.29	3.20	4.17	4.70	5.54
<u>North-western Region</u>								
Observed	1.72	1.00	0.81	1.58	2.05	2.68	3.08	3.5
Mono.	1.74	1.00	0.79	1.57	2.07	2.70	3.10	3.56
<u>M78 A, B (NGC 2068)</u>								
Observed	1.76	1.00	0.97	1.94	2.56	3.30	3.54	~4
Mono.	1.76	1.00	1.00	1.93	2.54	3.29	3.54	3.74
<u>Orion 'Sword' (outer part)</u>								
Observed (Smoothed)	1.71	1.00	0.87	1.68	2.27	2.68	2.82	~3
Mono.	1.68	1.00	0.85	1.70	2.27	2.70	2.84	3.02
<u>HD 37061</u>								
Observed	1.74	1.00	0.91	1.96	2.84	3.91	4.49	~5
Mono.	1.73	1.00	0.91	1.94	2.85	3.89	4.51	5.05
<u>Trapezium Region</u>								
Observed	1.70	1.00	1.00	2.47	3.51	5.14	6.76	~7
Mono. (Exact)	1.71	1.00	1.03	2.45	3.51	5.17	6.77	7.64
" (Smooth)	1.71	1.00	1.00	2.28	3.59	5.23	6.28	7.64

region; the 'normal' value is 1.06. The 'non-normal' character of the observed extinction law (Figure 9) is seen to be just as evident in the monochromatic relation.⁵

NGC 2024 No. 1

The monochromatic law for NGC 2024 No. 1, shown in Figure 24, was fitted at $E_{B-V} = +1^m.73$ and $T_c = 30,000^\circ$. The curve shows a steady increase in the extinction from the far infrared, but not the sudden rise seen in Figure 23. The slight dip in the curve at the position of the I filter produces the rise seen at this point in the corresponding curve in Figure 9. The fact that this star is located only 8' from ζ Orionis, in the center of the east 'Belt' region, yet exhibits a significantly different extinction law, will be discussed further in the following chapter.

Northwestern Region

The monochromatic law for this region is shown in Figure 25. The excess ratios were matched for $E_{B-V} = 0^m.16$ and $T_c = 20,000^\circ$ K. For equal extinction in the B filter,

5. At this point, one should note that the differences in the slopes in the UBV spectral range of the 'normal' and various regional monochromatic extinction laws in Figures 23 - 30 do not produce corresponding differences in the observed UBV reddening, but do indicate a difference in the ratio of total to selective absorption. For example, the E_{U-V}/E_{B-V} ratios for the two curves in Figure 23 are identical, but the values of R are 5.84 and 3.08. The fact that a small slope at these frequencies indicates a high value for R is actually the result of the normalization method adopted here.

the extinction here is again seen to be greater than 'normal' in the infrared with an undulation near the position of the I filter.

M 78 A, B (NGC 2068)

The fitting procedure for these two stars was done at $E_{B-V} = 1.^m04$ and $T_c = 20,000^\circ$ K. The curve, shown in Figure 26, closely resembles the 'normal' law save for the depression at $\nu = 0.35 \times 10^{15}$ cps and a slightly higher ratio of total to selective absorption.

Orion 'Sword' (Outer Part)

The fitting conditions used to obtain the monochromatic law for this region are $E_{B-V} = +0.^m20$ and $T_c = 20,000^\circ$ K. The curve is given in Figure 27. We note here with some nostalgia that apparently the 'normal' law has not lost all of its erstwhile domain.

HD 37061

The monochromatic extinction law for HD 37061 is given in Figure 28. The excess ratios were matched for $E_{B-V} = +0.^m55$ and $T_c = 30,000^\circ$ K. For equal extinction in the B filter, the efficiency factors for HD 37061, when compared to the 'normal' law, are higher in the infrared and lower in the ultraviolet, with a smaller slope seen throughout the blue region.

Trapezium Region

Two monochromatic extinction laws have been derived for this interesting region. The mean reddening here is

$E_{B-V} = +0.^m30$, and the intensity distribution used was the $30,000^\circ$ K black-body. The first monochromatic law, shown in Figure 29, represents a nearly exact fit to the observations. The salient features of this law are the rapid rise in the infrared near $\nu = 0.1 \times 10^{15}$ cps and the dip at the center of the I filter. The second curve, plotted in Figure 30 produces a smoothed observational law, the points of which all lie within the 91% error bars shown on Figure 11. This monochromatic law was calculated to determine to what degree the undulations present in Figure 29 could be removed and still obtain reasonable accord with the observations. The smoothness of the curve in Figure 30 shows that this can be accomplished, but since the values of E_{V-I}/E_{B-V} and E_{V-L}/E_{B-V} resulting from this law differ from the observed mean values by more than twice the probable errors, the probability of the smoothed curve--based solely on the data and excluding any errors in the interpretation--must be less than 5% that of the exact fit.

VIII

Discussion

A. Regions of 'Normal' Extinction

From the data and interpretation given in the earlier parts of this study, we have found considerable evidence for real variations of the interstellar extinction law within the I Orion association. The observational extinction curves shown in Figures 9, 10, and 11 suggest, however, that in a large portion of the association the law is essentially 'normal.' When the errors are considered, one notices that the curves for the outer 'Sword' and north-western regions are very similar. The apparent value of the ratio of total to selective absorption in these two regions is approximately 3.5. These areas of 'normal' extinction are characterized by a comparatively open, sparsely populated star distribution, low reddening, and a general absence of bright nebulosity. The average reddening here is only $0^m.09$ (E_{B-V}), but north and east of θ^1 Orionis it is somewhat higher. The higher extinction found for some areas near the Trapezium is caused by obscuring matter that is a part of the main body of nebular material centered at θ^1 Orionis, whereas the low extinction seen in the western and

southwestern 'Sword' regions and in the northwestern part of the association is most probably due to absorbing material that is not confined to the association but that is uniformly distributed between these stars and the sun. Blaauw (1964) suggests that the northwestern region is the oldest part of the association; the lower stellar density and scarcity of interstellar matter is consistent with an older population.

B. Regions of 'Anomalous' Extinction

This investigation has found two regions where the interstellar extinction law is decidedly 'non-normal.' These are the eastern part of the 'Belt' and the area of the 'Sword' immediately adjacent to θ^1 Orionis. The deviations from normal extinction found for these two regions are of the same form: a rapid increase in the extinction from the infrared to the visual spectral regions and, therefore, a higher ratio of total to selective absorption. Both regions are rich in nebulous material. NGC 1982 and, of course, NGC 1976 completely engulf the Trapezium region, while NGC 2023 and NGC 2024 are found in the east 'Belt' area. The extinction in the east 'Belt' region near ζ Orionis varies considerably from location to location and is very high, with $E_{B-V} > 1.0$, for some stars. Near the Trapezium the reddening is lower, but still appreciable, with a mean E_{B-V} of 0.3.

The density of association members is greater in these regions than in those where more normal extinction is observed.

Figure 31 shows the E_{V-I}/E_{B-V} ratio for stars in the 'Sword' region as a function of the distance from θ^1 Orionis. The vertical arrows represent the probable errors of the mean ratio for stars in each 15' annulus. The number of stars, n , is also given for each region. The dependence of E_{V-I}/E_{B-V} on distance from θ^1 Orionis seen here is in agreement with the extinction curves given in Figure 11, and moreover, Figure 31 indicates that the anomalous extinction is confined to within 15' of the Trapezium. The intermediate shape of the extinction law for HD 37061 indicates that the most significant anomalies are strongly concentrated in the very center of the nebula. Stars located north and south of NGC 1976 in the nebular regions of NGC 1973, NGC 1975, and NGC 1980 do not exhibit these 'abnormal' extinction characteristics.

The morphological situation for the east 'Belt' region is somewhat different. This area is a sizable one extending over approximately eight square degrees. Admittedly, the reddened stars in this region are fainter, and the observational data are somewhat more uncertain than for the Trapezium region. Yet, a ratio of total to selective absorption of 5.0 or greater is certainly implied for the

Figure 31. E_{V-I}/E_{B-V} versus Distance from θ^1 Orionis

The weighted mean value of E_{V-I}/E_{B-V} is shown for stars in 15' annuli centered on θ^1 Orionis. The number of stars in each annulus, n , is also given. The errors shown are the probable errors of the mean. Within 15' of the Trapezium, the ratio is abnormally high, while at other distances no meaningful variations are seen.

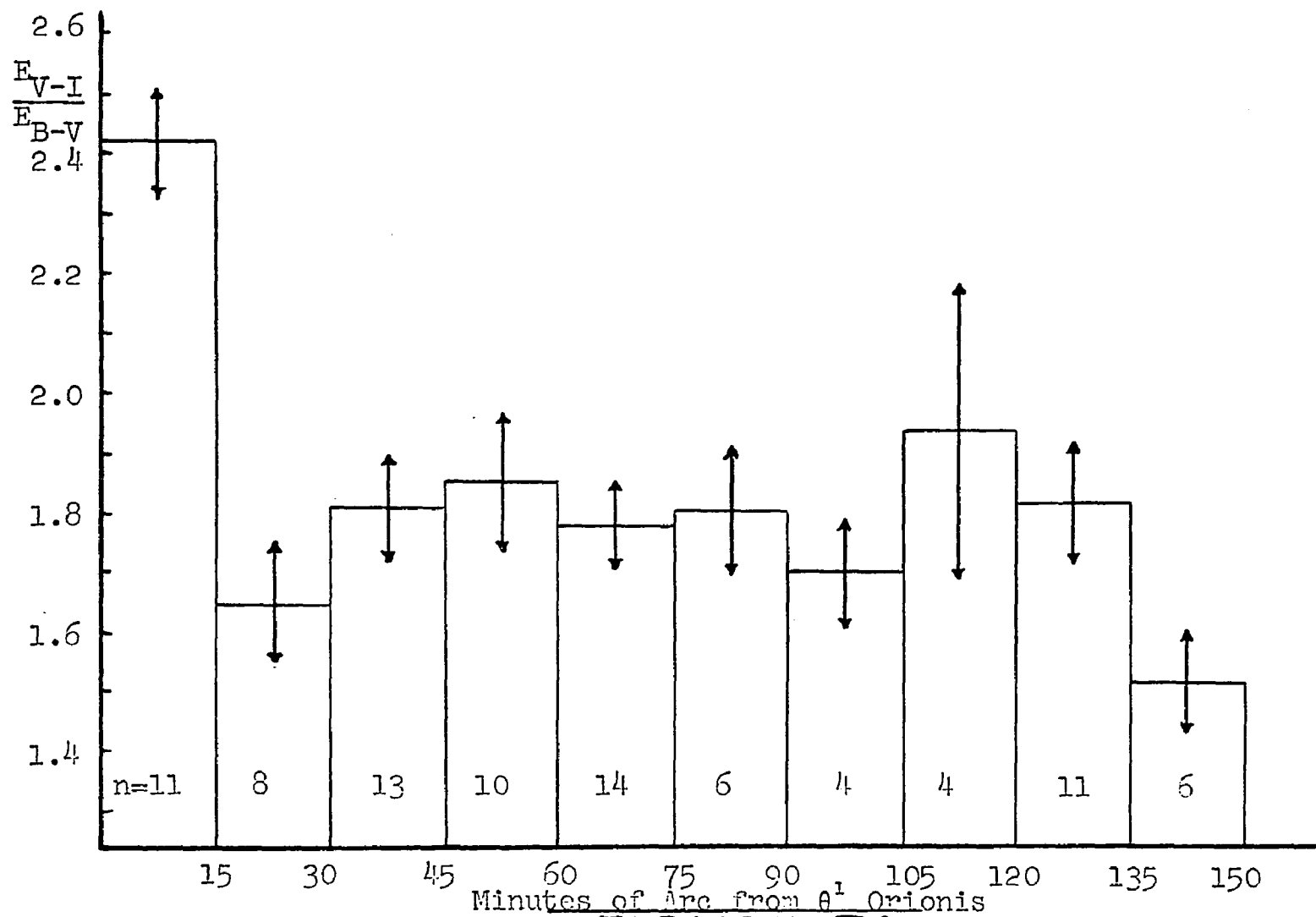


FIGURE 31

$\frac{E_{V-I}}{E_{B-V}}$ versus Distance from θ^1 Orionis

stars in this area for which JKL photometry has been obtained. The bright nebulosity in this region is not as conspicuous or as widespread as it is near the Trapezium. NGC 2024 No. 1 is deeply imbedded in a sizable nebula, but the Palomar blue plate shows only small, localized patches of nebulosity around HD 37140 and HD 37903.

The differences in the derived extinction laws for NGC 2024 No. 1 and the other east 'Belt' stars are indeed curious. These differences are not due to bandwidth effects resulting from the great variation in the amount of extinction in this region since the monochromatic laws, given in Figures 23 and 24, show similar discordances. NGC 2024 No. 1 is very highly reddened, and the infrared brightness is such that the extinction law for this star should be well determined. A similar degree of accuracy does not apply to the weighted mean curve for the east 'Belt' region. The most striking characteristic of this extinction law is the sharp turn up from the K to L points. The E_{V-L}/E_{V-K} ratio here is 1.37, while near θ^1 Orionis it is 1.32. The ratio for NGC 2024 No. 1 is only 1.13. I believe that the computed errors for the east 'Belt' law, shown on Figure 9, may be somewhat too modest and that the uncertainty of the L point may be considerably larger--perhaps by a factor of two. The true value of E_{V-L}/E_{B-V} may be somewhat lower than the weighted mean value. In any case, the differences between

the NGC 2024 No. 1 and east 'Belt' curves at the I, J, and K points cannot arise from observational uncertainties.

Therefore the assumption that a mean extinction law will be applicable for all stars in a given region, which is a premise for this analysis, is not valid in this area. No similar situation was found elsewhere in the association.

C. Extinction and Nebulosity

Without exception, all of the moderately reddened stars in the Orion association that exhibit highly 'non-normal' extinction laws are closely associated with bright nebulosity. Hallam (1959), from observations in the $0.29\ \mu$ to $1.1\ \mu$ region, as well as Johnson and Borgman (1963) found evidence for a similar correlation. The present study allows a more precise specification of this relationship.

Not all of the stars in nebular regions exhibit 'non-normal' extinction laws. The stars south of θ^1 Orionis near λ Orionis in NGC 1980 illustrate this point, as the extinction law here appears 'normal.' The two stars in M 78 are additional examples. These heavily reddened stars are located in the central part of a dense reflection nebula. The spectral types are in the B 2 - B 5 range (Sharpless, 1952; Chapman and Stockton, 1966). The source of the illumination for the nebula is most probably M 78 B (Elvius and Hall, 1966). The surrounding nebulosity notwithstanding,

the mean extinction law for these two stars, shown in Figure 10, is not significantly peculiar. The infrared indices are slightly larger than 'normal,' but the ratio of total to selective absorption is no larger than 4.0. Such a value is in good agreement with an earlier estimate made by Sharpless (1952). Therefore, the same physical parameters that characterize the absorbing material near the Trapezium are not present in M 78.

The extinction laws for HD 37061 and the Trapezium region, given in Figure 11, indicate that the deviations from 'normal' extinction found in nebulous regions are not always of the same magnitude.⁶ Additional evidence to this effect has been recently discovered by Johnson (1966c) for NGC 6530. One star in this nebula (M 8) exhibits an extinction law that is nearly identical to that of the Trapezium region, while the law for another star nearby is intermediate, similar to that of HD 37061. This work also indicates that the Orion Nebula is not the only region where the observed extinction law is highly 'abnormal.'

The theory of the scattering properties of interstellar grains (van de Hulst, 1949; Krishna Swamy, 1965; Wickramasinghe, Dharmawardhana, and Wild, 1966) indicates

6. We must recall at this point, however, the previously discussed uncertainty concerning the exact nature of the Trapezium region extinction law.

that when a particle distribution is modified by increasing the number of larger size particles, the extinction in the infrared spectral region increases. A possible explanation for the extinction phenomenon seen in some emission nebulae, therefore, may be found in the sizes of the interstellar grains. Baade and Minkowski (1937b) were the first to suggest that radiation pressure of early-type stars would tend to change a given grain size distribution near hot stars by driving away the smaller particles. Details of this mechanism were first treated by Greenstein (1951), who calculated the momentum transferred to grains that scatter and absorb starlight. The ratio of this momentum transfer to the gravitational attractive force between the particle and the star, P/G , is the parameter that determines the motion of the particle. Due to the distance inverse square dependence of both forces, P/G is independent of the distance between the star and the particle. The calculations show that particles smaller than a certain critical radius, which is a function of the mass and luminosity of the star, will be repelled by the star. For particles near the Orion Trapezium which are responsible for the extinction in the visual region, the P/G ratio would be nearly 10^4 . O'Dell and Hubbard (1965) recently improved this theory by including the effect of the viscous drag produced by

collisions of the accelerated grain with gas particles. Since momentum must be conserved, the accretion and subsequent isotropic evaporation of volatile hydrogen and helium atoms result in a net deceleration of the grain. The balancing of the radiation pressure acceleration and the drag deceleration sets an upper limit to the maximum velocity the grain can attain; this maximum velocity is independent of the grain size but does vary with distance from the star. The velocities are much smaller than those found when the drag force is neglected.

This mechanism is in reasonable accord with the extinction data of this study. If we assume that the major source of radiation pressure in the Orion Nebula is θ^1 Orionis, then the time scales are such that in the estimated lifetime of the nebula, 2×10^4 years (Vandervoort, 1964), the small grains near the Trapezium will have moved considerably outward, whereas some 15' - 20' away from θ^1 Orionis, about 10^5 years are required before the same grains are accelerated to their maximum velocity (O'Dell and Hubbard, 1965). Therefore, the original particle distribution should still be well preserved 20' from θ^1 Orionis but would have changed appreciably in the inner regions of the nebula. We recall again that the anomalous extinction for the Orion nebula area is confined to within 15' of the

Trapezium.⁷ The recent work of Whiteoak (1966), which suggests that the ultraviolet extinction in the Orion Nebula is slightly less than that in 'normal' regions, is consistent with a depletion of the number of smaller grains near the stars, since these particles produce most of the extinction in the blue and ultraviolet spectral region. A similar effect is seen in Johnson's (1966c) data for NGC 6530. The later spectral types and the high density of the interstellar matter for the stars in M 78 could account for the near 'normal' extinction observed here since both of these conditions would retard the net outward acceleration suffered by small particles surrounding the stars.

The modification of the size distribution of interstellar particles near hot, young stars by radiation pressure can, therefore, account qualitatively for the extinction 'anomalies' observed in Orion and in other areas. Varying degrees of 'non-normal' extinction laws, depending on the stellar spectral type and the proximity and density of the obscuring medium, may be expected. The effect of the

7. O'Dell and Hubbard (1965) find that radiation pressure is unable to account for a sharp decrease in the effective gas to dust ratio with increasing distance from the Trapezium. Their calculations, however, have assumed an extinction law similar to that shown in Figure 12 for the Trapezium region. This assumption is certainly questionable for the outer two regions (IV and V) investigated by these authors since they are approximately 13' and 18' from θ^1 Orionis. Therefore, the results of this work, especially for the outer regions, may be suspect.

ultraviolet radiation field on small particles is another factor that could account for modified size distributions. Due to poorly known cosmic abundances and chemical reaction rates at low temperatures, this mechanism is difficult to treat quantitatively. In any case, if either of these explanations is valid, we may suspect that the high ratio of total to selective absorption found in the east 'Belt' region may not be applicable for all the stars found here, since the two stars whose excess ratios are most heavily weighted in the calculation of the mean law, HD 37903 and HD 37140, are both visibly associated with bright nebulosity, while many of the other stars found here are not. The infrared excess ratios for the other three stars are larger than 'normal,' yet these values, when taken separately, are uncertain due to the small reddening. The mean E_{V-I}/E_{B-V} ratio of eight additional stars having UBVRI observations agrees well with the weighted mean, but this agreement is not meaningful since the weighted mean value differs only slightly from that of the 'normal' law.

D. Monochromatic Extinction Laws

Several of the mean extinction curves found in the Orion area exhibit a curious feature that has yet to be discussed. This peculiarity, an undulation at the position of the I filter, is most conspicuous in the monochromatic

laws, and thus the following discussion will refer to these curves--in particular those given in Figures 24, 25, 26 and 29. The depression seen near $\nu = 0.35 \times 10^{15}$ cps indicates that the extinction efficiency increases more rapidly between the R and I filters than it does in adjacent spectral regions. The 'non-normal' wavelength dependence observed for those regions where $R > 5.0$ (Figures 9 and 11) is first noticed at the I filter, and becomes more conspicuous with increasing wavelength.

This dip at the I band of the monochromatic curves could be caused by an error in the V-I intrinsic colors of the early-type stars. The assumed colors would have to be too blue and the color excesses too large. This does not seem likely since there is no dependence of this feature on color excess. Such a dependence would be expected since a given error in the color excess would cause an error in the excess ratio which would be small for highly reddened stars and large for stars that are only slightly reddened. Yet the heavily reddened stars in M 78 and NGC 2024 No. 1 clearly show this feature, while the slightly reddened region of the outer 'Sword' does not.

A more plausible explanation may be that this peculiarity is truly an extinction characteristic. This possibility was investigated by analyzing the theoretical extinction resulting from combinations of particle size

distributions according to the theory of van de Hulst (1949). Four of the theoretical extinction curves obtained in this analysis are shown in Figures 32a and 32b. The curves are not normalized and simply show the extinction efficiency, E , plotted against ρ_1 , where $\rho_1 = 4\pi r_1(m-1)/\lambda$, m = index of refraction, r_1 = size scaling parameter. The abscissa, therefore, is just an unspecified frequency scale that is directly comparable to that of Figures 23 - 30. For each of the curves, the particle distributions $F_1(u)$ and $F_2(u)$ ($u = r/r_1$ and r/r_2 = dimensionless particle size), the relative number of particles, n_1/n_2 , and the relative size of the particles, r_2/r_1 , are given. We see that varying degrees of depressions and undulations are readily obtainable, and that only a very small number of larger particles are required to produce these effects. The bimodal size distributions similar to those used here may indicate the presence of an accelerated mode of crystal or grain formation.⁸ The

8. Some recent polarization work is of considerable interest in this regard. Visvanathan (1965) found from studies of the southern hemisphere that the wavelength dependence of polarization in the UVB region is reasonably constant over the sky, but that this dependence in the infrared varies significantly from place to place. This variation is very similar to that shown by the wavelength dependence of interstellar extinction, and suggests that the large particle component of the absorbing medium varies from region to region, while the distribution of small particles remains essentially the same. Moreover, at $\lambda = 8722 \text{ \AA}$, the mean polarization in H II regions was found to be 10% larger than that outside of H II regions. Also, Gehrels and Silvester (1966) recently determined the polarization for HD 37041 (θ^2 Orionis) and found it to be highly atypical--increasing steadily with increasing wavelength out to $\lambda \approx 1 \mu$.

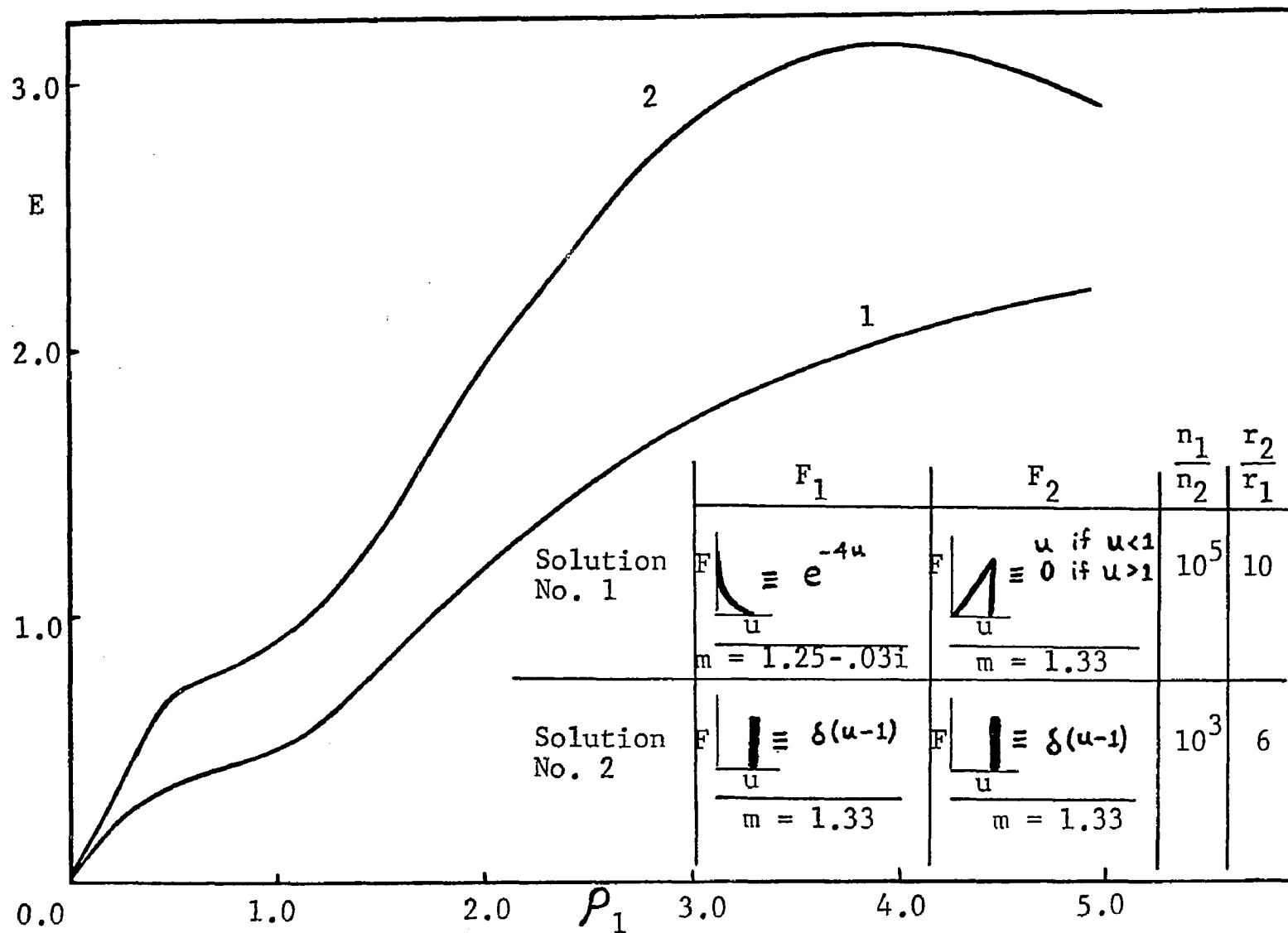


FIGURE 32a

Extinction from Combined Distributions of Particle Sizes

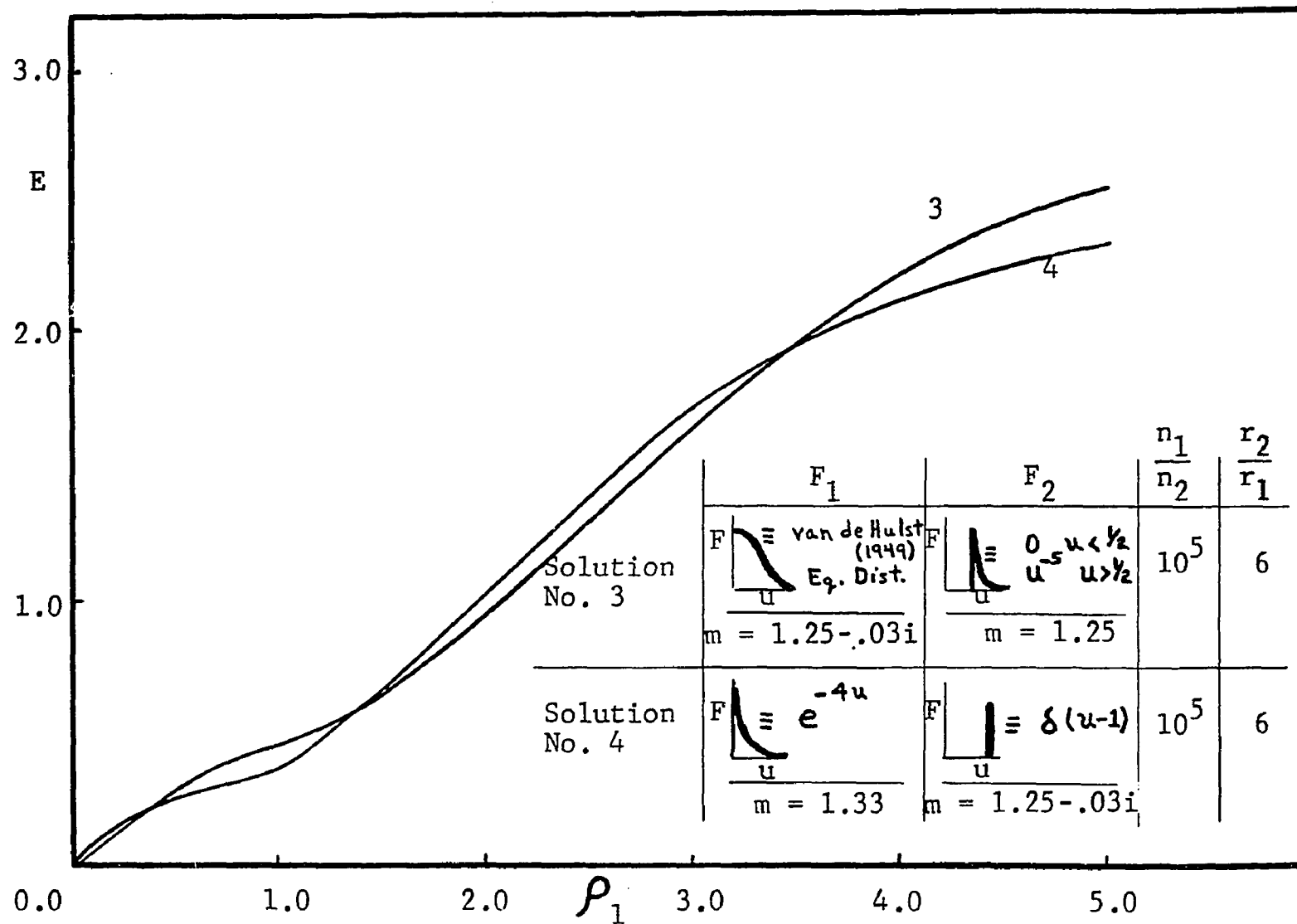


FIGURE 32b

Extinction from Combined Distributions of Particle Sizes

number of large particles with the $F_2(u)$ distribution is small, and hence this mechanism could be a very subtle one.

Unfortunately, more detailed fitting of the smoothed monochromatic laws of Figures 23 - 30 to theoretically determined extinction curves is not possible at this juncture. Adequate knowledge of the ultraviolet part of the extinction law is the obstacle in this respect. An analysis of some preliminary ultraviolet rocket observations by Boggess and Borgman (1964) indicated that the 'normal' extinction law may show a steady increase in the extinction from 3000 Å to 2200 Å. Such a wavelength dependence is definitely contrary to that of van de Hulst's (1949) curve no. 15, although this particular theoretical law adequately represents the 'normal' extinction phenomenon in the visual and infrared regions. Efforts to fit the entire 'normal' law, including the ultraviolet region, to theoretical solutions have been only partially successful (Krishna Swamy, 1965; Schalen, 1965), although Schalen (1965) found some agreement using either graphite-ice particles or small iron spheres. Unfortunately, no ultraviolet data are available for stars in Orion and, moreover, the ultraviolet part of the monochromatic laws of Figures 23 - 30 is highly uncertain past $\lambda = 3,500$ Å. Since the ultraviolet wavelength dependence of the theoretical extinction laws varies tremendously for different types and sizes of particles, more accurate

determinations of the observed extinction curves at these wavelengths are required before meaningful comparisons with the theory can be realized. We can safely assume, however, that regions exhibiting a very high ratio of total to selective absorption are characterized by larger interstellar particles and, to a lesser degree, that the major depressions and undulations seen in some of the regional curves are the result of two or more distributions of particles of significantly different sizes.

IX

CONCLUSIONS

The primary conclusions of this investigation are summarized below:

1. The wavelength dependence of interstellar extinction is reasonably 'normal' in a large fraction of the I Orion association, but is definitely 'non-normal' in two regions: a small area of 15' radius centered on θ^1 Orionis, and a larger area in the eastern part of the 'Belt,' including ζ Orionis. The anomalies in the latter region may apply only to the stars that are closely associated with bright nebulosity. The 'non-normal' extinction characteristics common to these two regions are a steep extinction gradient in the infrared and a large ratio of total to selective absorption.

2. The extreme anomalies are not found for any stars whose spectral types are later than B 2 or that are not intimately associated with nebulosity.

3. The proximity of star and obscuring cloud is an important factor in determining the wavelength dependence of the extinction phenomenon. The modifying effect of the radiation pressure of hot stars on the size distribution of

particles near the stars is consistent with the observations of this study and others.

4. The mean size of the interstellar grains near a star that exhibits a high ratio of total to selective absorption is larger than that in more 'normal' regions; other peculiar features seen in some extinction curves can result from composite distribution of particles of different characteristic sizes.

5. Additional observations of stars imbedded in nebulous matter will be required before these results can be generalized and more definitely established. Infrared polarization data will be particularly valuable in this respect. Until this information is obtained, however, we must realize that the results of this study follow from an interpretation that, at present, appears logical and self-consistent. The actual validity of the assumptions implicit in this interpretation will be amply tested in the near future.

APPENDIX A

Probable Errors of Color Excess Ratios

Star	E_{B-V}	$\sigma(R_R)$	$\sigma(R_I)$	$\sigma(R_J)$	$\sigma(R_K)$	$\sigma(R_L)$
HD 30836	+ .07	.346	.585	.852	1.230	1.339
34748	+ .12	.254	.376	.513	.659	.992
34989	+ .14	.218	.355	.501	.569	.850
35039	+ .08	.321	.488	.918	1.078	1.439
35079	+ .13	.210	.345	.542	.696	1.038
35149	+ .13	.201	.311	.578	.617	.888
35411	+ .11	.236	.346	.594	.760	.858
35502	+ .14	.207	.321	.486	.628	.986
35673	+ .08	.392	.611	.860	1.036	---
35910	+ .06	.461	.734	1.024	1.784	---
36351	+ .07	.386	.587	.830	1.201	1.728
36486	+ .08	.321	.620	.892	1.013	1.252
36629	+ .26	.111	.184	.268	.353	---
36646	+ .10	.305	.384	.641	.820	---
36695	+ .09	.295	.471	.715	.911	1.101
36781	+ .14	.219	.355	.706	.950	---
36811	+ .17	.171	.269	.480	.569	.863
36822	+ .15	.195	.309	.445	.539	.662
36824	+ .07	.451	.663	.861	1.170	1.879
36861	+ .12	.238	.430	.629	.729	---
37020-3	+ .36	.092	.173	.223	.312	.397
37022	+ .32	.102	.193	.308	.398	.486
37025	+ .05	.610	1.090	1.984	2.432	---
-5° 1318	+ .46	.067	.129	.219	.322	.478
37041	+ .21	.145	.273	.370	.505	.764
37042	+ .21	.133	.231	.389	.484	.722
37043	+ .05	.596	1.180	1.627	1.904	2.252
37061	+ .57	.053	.096	.131	.166	.216
37128	+ .09	.269	.499	.747	.901	1.129
37140	+ .27	.112	.178	.333	.447	.721
37428	+ .20	.156	.266	.505	.666	1.073
37468	+ .05	.568	.912	1.502	1.988	2.410
37490	+ .10	.306	.496	.697	.908	1.068
-0° 1050	+ .70	.042	.067	.161	.223	---
37742	+ .06	.415	.770	1.170	1.454	1.900
NGC 2024 No. 1	+1.72	.020	.033	.051	.061	.082
37903	+ .36	.079	.134	.198	.254	.362
38051	+ .55	.052	.084	.139	.176	---
38563 A	+ .76	.039	.067	.132	.182	.300
38563 B	+1.32	.023	.038	.056	.067	.094
38771	+ .07	.404	.661	.813	.982	1.172
41117	+ .46	.061	.099	.131	.160	.193

APPENDIX A--Continued

Weights for Color Excess Ratios

Star	E_{B-V}	$\frac{E_{V-R}}{E_{B-V}}$	$\frac{E_{V-I}}{E_{B-V}}$	$\frac{E_{V-J}}{E_{B-V}}$	$\frac{E_{V-K}}{E_{B-V}}$	$\frac{E_{V-L}}{E_{B-V}}$
30836	+ .07	8.35	2.92	1.38	0.66	0.56
34748	+ .12	15.50	7.08	3.80	2.30	1.02
34989	+ .14	21.04	8.51	3.98	3.09	1.38
35039	+ .08	9.70	4.20	1.19	0.86	0.48
35079	+ .13	22.68	8.40	3.40	2.06	0.93
35149	+ .13	24.75	10.37	2.99	2.63	1.27
35411	+ .11	17.95	8.35	2.84	1.73	1.36
35502	+ .14	23.34	9.70	4.24	2.53	1.03
35673	+ .08	6.51	2.68	1.35	0.93	--
35910	+ .06	4.70	1.86	0.95	0.31	--
36351	+ .07	6.71	2.90	1.45	0.69	0.34
36486	+ .08	9.70	2.60	1.26	0.97	0.64
36629	+ .26	81.18	29.54	13.92	8.03	--
36646	+ .10	10.75	6.78	2.43	1.49	--
36695	+ .09	11.49	4.51	1.96	1.21	0.82
36781	+ .14	20.85	7.94	2.01	1.11	--
36811	+ .17	34.20	13.82	4.34	3.09	1.34
36822	+ .15	26.30	10.47	5.05	3.44	2.28
36824	+ .07	4.92	2.27	1.35	0.73	0.28
36861	+ .12	17.66	5.41	2.53	1.88	--
37020-3	+ .36	118.14	33.41	20.11	10.27	6.35
37022	+ .32	96.12	26.84	10.54	6.31	4.24
37025	+ .05	2.69	0.84	0.25	0.17	--
-5° 1318	+ .46	222.76	60.09	20.85	7.65	4.38
37041	+ .21	47.55	13.42	7.31	3.92	1.71
37042	+ .21	56.53	18.74	6.61	4.27	1.92
37043	+ .05	2.82	0.72	0.38	0.28	0.20
37061	+ .57	355.96	123.45	58.28	36.29	21.44
37128	+ .09	13.79	4.02	1.79	1.23	0.78
37140	+ .27	79.71	31.56	9.02	5.00	1.92
37428	+ .20	41.09	14.13	3.92	2.26	0.87
37468	+ .05	3.10	1.20	0.44	0.25	0.17
37490	+ .10	10.68	4.06	2.06	1.21	0.88
-0° 1050	+ .70	566.87	222.76	38.58	20.11	--
37742	+ .06	5.81	1.69	0.73	0.47	0.28
NGC 2024 No. 1	+1.72	2500.0	918.3	384.5	268.7	148.7
37903	+ .36	160.22	55.70	25.50	15.50	7.63
38051	+ .55	369.83	141.73	51.75	32.29	--
38563 A	+ .76	657.41	222.76	57.40	30.18	11.12
38563 B	+1.32	1890.3	692.48	318.91	222.76	113.17
38771	+ .07	6.13	2.29	1.51	1.04	0.73
41117	+ .46	268.73	102.03	58.28	39.06	26.84

APPENDIX B
Wideband Extinction Law Calculations

T = 30000 DEGREES - BLACK BODY INTENSITY DISTRIBUTION

MONOCHROMATIC EXTINCTION INPUT

1/LAMDA = 2.86	2.27	1.75	1.47	1.15	0.84	0.47	0.29	0.20	0.11
E-FACTORS 1.35	1.14	0.82	0.62	0.40	0.23	0.08	0.04	0.02	0.01

WIDE BAND EXTINCTION IN MAGNITUDES

K	U	B	V	R	I	J	K	L	M	N	A(V)/E(B-V)
0.10	0.147	0.125	0.094	0.071	0.046	0.025	0.009	0.004	0.002	0.001	3.077
0.20	0.293	0.250	0.189	0.141	0.092	0.051	0.019	0.008	0.004	0.002	3.077
0.30	0.440	0.375	0.283	0.211	0.138	0.076	0.028	0.013	0.007	0.002	3.077
0.40	0.586	0.499	0.377	0.281	0.183	0.101	0.037	0.017	0.009	0.003	3.078
0.50	0.732	0.624	0.471	0.351	0.229	0.127	0.046	0.021	0.011	0.004	3.078
0.60	0.879	0.749	0.565	0.421	0.275	0.152	0.056	0.025	0.013	0.005	3.078
0.70	1.025	0.873	0.659	0.491	0.320	0.177	0.065	0.030	0.015	0.006	3.078
0.80	1.172	0.997	0.753	0.560	0.366	0.202	0.074	0.034	0.018	0.006	3.079
0.90	1.318	1.122	0.847	0.630	0.412	0.227	0.084	0.038	0.020	0.007	3.079
1.00	1.465	1.246	0.941	0.699	0.457	0.253	0.093	0.042	0.022	0.008	3.079
1.10	1.611	1.370	1.034	0.768	0.503	0.278	0.102	0.046	0.024	0.009	3.079
1.20	1.757	1.494	1.128	0.837	0.548	0.303	0.111	0.051	0.027	0.010	3.080
1.30	1.904	1.618	1.221	0.906	0.593	0.328	0.121	0.055	0.029	0.011	3.080
1.40	2.050	1.742	1.315	0.975	0.639	0.353	0.130	0.059	0.031	0.011	3.080
1.50	2.196	1.866	1.408	1.043	0.684	0.379	0.139	0.063	0.033	0.012	3.081
1.60	2.343	1.989	1.502	1.112	0.729	0.404	0.149	0.068	0.035	0.013	3.081
1.70	2.489	2.113	1.595	1.180	0.774	0.429	0.158	0.072	0.038	0.014	3.081
1.80	2.635	2.236	1.688	1.249	0.819	0.454	0.167	0.076	0.040	0.015	3.081
1.90	2.782	2.360	1.782	1.317	0.864	0.479	0.176	0.080	0.042	0.015	3.082
2.00	2.928	2.483	1.875	1.385	0.909	0.504	0.186	0.084	0.044	0.016	3.082
2.10	3.074	2.606	1.968	1.452	0.954	0.529	0.195	0.089	0.046	0.017	3.082
2.20	3.220	2.729	2.061	1.520	0.999	0.554	0.204	0.093	0.049	0.018	3.082
2.30	3.367	2.852	2.154	1.588	1.044	0.579	0.213	0.097	0.051	0.019	3.083
2.40	3.513	2.975	2.247	1.655	1.089	0.604	0.223	0.101	0.053	0.019	3.083
2.50	3.659	3.098	2.339	1.722	1.134	0.629	0.232	0.105	0.055	0.020	3.083
2.60	3.805	3.221	2.432	1.790	1.178	0.654	0.241	0.110	0.057	0.021	3.084
2.70	3.951	3.344	2.525	1.857	1.223	0.679	0.250	0.114	0.060	0.022	3.084
2.80	4.098	3.466	2.617	1.924	1.267	0.704	0.260	0.118	0.062	0.023	3.084
2.90	4.244	3.589	2.710	1.990	1.312	0.729	0.269	0.122	0.064	0.023	3.084
3.00	4.390	3.711	2.802	2.057	1.357	0.754	0.278	0.127	0.066	0.024	3.085
3.10	4.536	3.833	2.895	2.124	1.401	0.779	0.287	0.131	0.068	0.025	3.085
3.20	4.682	3.955	2.987	2.190	1.445	0.804	0.297	0.135	0.071	0.026	3.085
3.30	4.828	4.078	3.079	2.256	1.490	0.829	0.306	0.139	0.073	0.027	3.086
3.40	4.974	4.200	3.172	2.322	1.534	0.854	0.315	0.143	0.075	0.027	3.086
3.50	5.120	4.321	3.264	2.388	1.578	0.879	0.324	0.148	0.077	0.028	3.086
3.60	5.266	4.443	3.356	2.454	1.622	0.904	0.334	0.152	0.079	0.029	3.086
3.70	5.413	4.565	3.448	2.520	1.667	0.929	0.343	0.156	0.082	0.030	3.087
3.80	5.559	4.686	3.540	2.586	1.711	0.954	0.352	0.160	0.084	0.031	3.087
3.90	5.705	4.808	3.632	2.651	1.755	0.978	0.361	0.164	0.086	0.031	3.087
4.00	5.851	4.929	3.723	2.717	1.799	1.003	0.370	0.169	0.088	0.032	3.087
4.50	6.580	5.535	4.181	3.041	2.018	1.127	0.417	0.190	0.099	0.036	3.089
5.00	7.310	6.138	4.637	3.363	2.236	1.251	0.463	0.211	0.110	0.040	3.090
5.50	8.039	6.738	5.091	3.682	2.453	1.374	0.509	0.232	0.121	0.044	3.091
6.00	8.768	7.336	5.544	3.998	2.669	1.497	0.555	0.253	0.132	0.048	3.092
6.50	9.496	7.931	5.994	4.310	2.883	1.620	0.601	0.274	0.143	0.052	3.093
7.00	10.224	8.524	6.442	4.620	3.096	1.743	0.647	0.295	0.154	0.056	3.094
7.50	10.952	9.114	6.889	4.927	3.308	1.865	0.692	0.316	0.165	0.060	3.095
8.00	11.679	9.702	7.333	5.232	3.519	1.986	0.738	0.337	0.176	0.064	3.096

T = 30000 DEGREES - BLACK BODY INTENSITY DISTRIBUTION

K	A(V)	E(B-V)	U-V	B-V	V-R	V-I	V-J	V-K	V-L	V-M	V-N	A(V)/E(B-V)
0.10	0.094	0.031	1.703	1.000	0.777	1.579	2.251	2.774	2.939	3.005	3.050	3.077
0.20	0.189	0.061	1.704	1.000	0.779	1.579	2.251	2.774	2.939	3.005	3.051	3.077
0.30	0.283	0.092	1.705	1.000	0.780	1.580	2.251	2.774	2.939	3.005	3.051	3.077
0.40	0.377	0.122	1.707	1.000	0.782	1.580	2.251	2.774	2.940	3.005	3.051	3.078
0.50	0.471	0.153	1.708	1.000	0.783	1.580	2.251	2.774	2.940	3.006	3.051	3.078
0.60	0.565	0.184	1.710	1.000	0.785	1.581	2.251	2.774	2.940	3.006	3.052	3.078
0.70	0.659	0.214	1.711	1.000	0.786	1.581	2.251	2.775	2.940	3.006	3.052	3.078
0.80	0.753	0.245	1.713	1.000	0.788	1.582	2.252	2.775	2.941	3.006	3.052	3.079
0.90	0.847	0.275	1.714	1.000	0.789	1.582	2.252	2.775	2.941	3.007	3.052	3.079
1.00	0.941	0.305	1.716	1.000	0.791	1.583	2.252	2.775	2.941	3.007	3.053	3.079
1.10	1.034	0.336	1.717	1.000	0.792	1.583	2.252	2.775	2.941	3.007	3.053	3.079
1.20	1.128	0.366	1.719	1.000	0.794	1.584	2.252	2.775	2.941	3.007	3.053	3.080
1.30	1.221	0.397	1.720	1.000	0.795	1.584	2.252	2.776	2.942	3.008	3.053	3.080
1.40	1.315	0.427	1.722	1.000	0.797	1.585	2.252	2.776	2.942	3.008	3.054	3.080
1.50	1.408	0.457	1.723	1.000	0.798	1.585	2.253	2.776	2.942	3.008	3.054	3.081
1.60	1.502	0.487	1.725	1.000	0.800	1.585	2.253	2.776	2.942	3.008	3.054	3.081
1.70	1.595	0.518	1.727	1.000	0.801	1.586	2.253	2.776	2.942	3.009	3.055	3.081
1.80	1.688	0.548	1.728	1.000	0.803	1.586	2.253	2.777	2.943	3.009	3.055	3.081
1.90	1.782	0.578	1.730	1.000	0.804	1.587	2.253	2.777	2.943	3.009	3.055	3.082
2.00	1.875	0.608	1.731	1.000	0.806	1.587	2.253	2.777	2.943	3.009	3.055	3.082
2.10	1.968	0.638	1.733	1.000	0.807	1.588	2.253	2.777	2.943	3.010	3.056	3.082
2.20	2.061	0.669	1.734	1.000	0.809	1.588	2.253	2.777	2.944	3.010	3.056	3.082
2.30	2.154	0.699	1.736	1.000	0.810	1.589	2.254	2.777	2.944	3.010	3.056	3.083
2.40	2.247	0.729	1.738	1.000	0.812	1.589	2.254	2.778	2.944	3.010	3.056	3.083
2.50	2.339	0.759	1.739	1.000	0.813	1.589	2.254	2.778	2.944	3.011	3.057	3.083
2.60	2.432	0.789	1.741	1.000	0.815	1.590	2.254	2.778	2.945	3.011	3.057	3.084
2.70	2.525	0.819	1.742	1.000	0.816	1.590	2.254	2.778	2.945	3.011	3.057	3.084
2.80	2.617	0.849	1.744	1.000	0.818	1.591	2.254	2.778	2.945	3.011	3.058	3.084
2.90	2.710	0.879	1.746	1.000	0.819	1.591	2.254	2.778	2.945	3.012	3.058	3.084
3.00	2.802	0.909	1.747	1.000	0.821	1.592	2.254	2.779	2.945	3.012	3.058	3.085
3.10	2.895	0.938	1.749	1.000	0.822	1.592	2.255	2.779	2.946	3.012	3.058	3.085
3.20	2.987	0.968	1.751	1.000	0.823	1.592	2.255	2.779	2.946	3.012	3.059	3.085
3.30	3.079	0.998	1.752	1.000	0.825	1.593	2.255	2.779	2.946	3.013	3.059	3.086
3.40	3.172	1.028	1.754	1.000	0.826	1.593	2.255	2.779	2.946	3.013	3.059	3.086
3.50	3.264	1.058	1.756	1.000	0.828	1.594	2.255	2.779	2.947	3.013	3.059	3.086
3.60	3.356	1.087	1.757	1.000	0.829	1.594	2.255	2.780	2.947	3.013	3.060	3.086
3.70	3.448	1.117	1.759	1.000	0.831	1.595	2.255	2.780	2.947	3.014	3.060	3.087
3.80	3.540	1.147	1.761	1.000	0.832	1.595	2.255	2.780	2.947	3.014	3.060	3.087
3.90	3.632	1.176	1.762	1.000	0.833	1.595	2.255	2.780	2.947	3.014	3.060	3.087
4.00	3.723	1.206	1.764	1.000	0.835	1.596	2.256	2.780	2.948	3.014	3.061	3.087
4.50	4.181	1.354	1.772	1.000	0.842	1.598	2.256	2.781	2.949	3.015	3.062	3.089
5.00	4.637	1.501	1.781	1.000	0.849	1.600	2.256	2.782	2.950	3.017	3.063	3.090
5.50	5.091	1.647	1.790	1.000	0.856	1.602	2.257	2.782	2.951	3.018	3.064	3.091
6.00	5.544	1.793	1.799	1.000	0.862	1.604	2.257	2.783	2.951	3.019	3.066	3.092
6.50	5.994	1.938	1.808	1.000	0.869	1.606	2.257	2.784	2.952	3.020	3.067	3.093
7.00	6.442	2.082	1.817	1.000	0.875	1.607	2.257	2.784	2.953	3.020	3.067	3.094
7.50	6.889	2.226	1.826	1.000	0.881	1.609	2.257	2.784	2.953	3.021	3.068	3.095
8.00	7.333	2.369	1.835	1.000	0.887	1.610	2.257	2.784	2.954	3.022	3.069	3.096

EXTINCTION LAW CALCULATION

150

T = 20000 DEGREES - BLACK BODY INTENSITY DISTRIBUTION

MONOCHROMATIC EXTINCTION INPUT

1/LAMDA = 2.86	2.27	1.75	1.47	1.15	0.84	0.47	0.29	0.20	0.11
E-FACTORS 1.35	1.14	0.82	0.62	0.40	0.23	0.08	0.04	0.02	0.01

WIDE BAND EXTINCTION IN MAGNITUDES

K	U	B	V	R	I	J	K	L	M	N	A(V)/E(B-V)
0.10	0.146	0.125	0.094	0.070	0.046	0.025	0.009	0.004	0.002	0.001	3.086
0.20	0.293	0.249	0.188	0.140	0.092	0.051	0.019	0.008	0.004	0.002	3.087
0.30	0.439	0.374	0.282	0.210	0.137	0.076	0.028	0.013	0.007	0.002	3.087
0.40	0.586	0.498	0.376	0.280	0.183	0.101	0.037	0.017	0.009	0.003	3.087
0.50	0.732	0.623	0.470	0.350	0.229	0.126	0.046	0.021	0.011	0.004	3.088
0.60	0.878	0.747	0.564	0.419	0.274	0.152	0.056	0.025	0.013	0.005	3.088
0.70	1.025	0.871	0.658	0.489	0.320	0.177	0.065	0.030	0.015	0.006	3.088
0.80	1.171	0.995	0.752	0.558	0.365	0.202	0.074	0.034	0.018	0.006	3.088
0.90	1.317	1.119	0.845	0.627	0.411	0.227	0.084	0.038	0.020	0.007	3.089
1.00	1.463	1.243	0.939	0.696	0.456	0.252	0.093	0.042	0.022	0.008	3.089
1.10	1.610	1.367	1.033	0.765	0.501	0.277	0.102	0.046	0.024	0.009	3.089
1.20	1.756	1.491	1.126	0.834	0.547	0.303	0.111	0.051	0.026	0.010	3.090
1.30	1.902	1.614	1.220	0.902	0.592	0.328	0.121	0.055	0.029	0.011	3.090
1.40	2.048	1.738	1.313	0.971	0.637	0.353	0.130	0.059	0.031	0.011	3.090
1.50	2.195	1.861	1.406	1.039	0.682	0.378	0.139	0.063	0.033	0.012	3.090
1.60	2.341	1.985	1.499	1.107	0.727	0.403	0.148	0.068	0.035	0.013	3.091
1.70	2.487	2.108	1.593	1.175	0.772	0.428	0.158	0.072	0.038	0.014	3.091
1.80	2.633	2.231	1.686	1.243	0.817	0.453	0.167	0.076	0.040	0.015	3.091
1.90	2.779	2.354	1.779	1.311	0.862	0.478	0.176	0.080	0.042	0.015	3.092
2.00	2.926	2.477	1.872	1.379	0.907	0.503	0.185	0.084	0.044	0.016	3.092
2.10	3.072	2.600	1.965	1.446	0.952	0.528	0.195	0.089	0.046	0.017	3.092
2.20	3.218	2.723	2.058	1.514	0.997	0.553	0.204	0.093	0.049	0.018	3.092
2.30	3.364	2.846	2.150	1.581	1.041	0.578	0.213	0.097	0.051	0.019	3.093
2.40	3.510	2.968	2.243	1.648	1.086	0.603	0.222	0.101	0.053	0.019	3.093
2.50	3.656	3.091	2.336	1.715	1.131	0.628	0.232	0.105	0.055	0.020	3.093
2.60	3.802	3.213	2.428	1.782	1.175	0.653	0.241	0.110	0.057	0.021	3.094
2.70	3.948	3.336	2.521	1.849	1.220	0.678	0.250	0.114	0.060	0.022	3.094
2.80	4.094	3.458	2.613	1.915	1.264	0.703	0.259	0.118	0.062	0.023	3.094
2.90	4.240	3.580	2.706	1.982	1.309	0.728	0.269	0.122	0.064	0.023	3.094
3.00	4.386	3.702	2.798	2.048	1.353	0.753	0.278	0.126	0.066	0.024	3.095
3.10	4.532	3.824	2.890	2.114	1.397	0.778	0.287	0.131	0.068	0.025	3.095
3.20	4.678	3.946	2.982	2.181	1.442	0.803	0.296	0.135	0.071	0.026	3.095
3.30	4.824	4.068	3.074	2.247	1.486	0.828	0.306	0.139	0.073	0.027	3.096
3.40	4.970	4.189	3.166	2.312	1.530	0.853	0.315	0.143	0.075	0.027	3.096
3.50	5.116	4.311	3.258	2.378	1.574	0.878	0.324	0.148	0.077	0.028	3.096
3.60	5.262	4.432	3.350	2.444	1.618	0.902	0.333	0.152	0.079	0.029	3.096
3.70	5.408	4.554	3.442	2.509	1.662	0.927	0.343	0.156	0.082	0.030	3.097
3.80	5.554	4.675	3.534	2.575	1.706	0.952	0.352	0.160	0.084	0.031	3.097
3.90	5.700	4.796	3.626	2.640	1.750	0.977	0.361	0.164	0.086	0.031	3.097
4.00	5.846	4.917	3.717	2.705	1.794	1.002	0.370	0.169	0.088	0.032	3.098
4.50	6.575	5.521	4.174	3.028	2.013	1.126	0.416	0.190	0.099	0.036	3.099
5.00	7.304	6.122	4.629	3.349	2.230	1.249	0.462	0.211	0.110	0.040	3.100
5.50	8.032	6.721	5.082	3.666	2.447	1.372	0.508	0.232	0.121	0.044	3.101
6.00	8.761	7.317	5.534	3.981	2.662	1.495	0.554	0.253	0.132	0.048	3.103
6.50	9.488	7.911	5.983	4.292	2.875	1.618	0.600	0.274	0.143	0.052	3.104
7.00	10.216	8.502	6.431	4.601	3.088	1.740	0.646	0.295	0.154	0.056	3.105
7.50	10.943	9.091	6.876	4.906	3.300	1.862	0.692	0.316	0.165	0.060	3.105
8.00	11.670	9.676	7.320	5.209	3.510	1.983	0.738	0.337	0.176	0.064	3.106

T = 20000 DEGREES - BLACK BODY INTENSITY DISTRIBUTION

K	A(V)	E(B-V)	U-V	B-V	V-R	V-I	V-J	V-K	V-L	V-M	V-N	A(V)/E(B-V)
0.10	0.094	0.031	1.711	1.000	0.786	1.585	2.258	2.782	2.948	3.014	3.060	3.086
0.20	0.188	0.061	1.713	1.000	0.787	1.586	2.258	2.782	2.948	3.014	3.060	3.087
0.30	0.282	0.091	1.714	1.000	0.789	1.586	2.258	2.782	2.949	3.015	3.060	3.087
0.40	0.376	0.122	1.716	1.000	0.790	1.586	2.258	2.783	2.949	3.015	3.061	3.087
0.50	0.470	0.152	1.717	1.000	0.792	1.587	2.258	2.783	2.949	3.015	3.061	3.088
0.60	0.564	0.183	1.719	1.000	0.793	1.587	2.258	2.783	2.949	3.015	3.061	3.088
0.70	0.658	0.213	1.720	1.000	0.795	1.588	2.259	2.783	2.949	3.016	3.062	3.088
0.80	0.752	0.243	1.722	1.000	0.796	1.588	2.259	2.783	2.950	3.016	3.062	3.088
0.90	0.845	0.274	1.723	1.000	0.798	1.589	2.259	2.784	2.950	3.016	3.062	3.089
1.00	0.939	0.304	1.725	1.000	0.799	1.589	2.259	2.784	2.950	3.016	3.062	3.089
1.10	1.033	0.334	1.727	1.000	0.801	1.590	2.259	2.784	2.950	3.017	3.063	3.089
1.20	1.126	0.364	1.728	1.000	0.803	1.590	2.259	2.784	2.951	3.017	3.063	3.090
1.30	1.220	0.395	1.730	1.000	0.804	1.591	2.259	2.784	2.951	3.017	3.063	3.090
1.40	1.313	0.425	1.731	1.000	0.806	1.591	2.260	2.784	2.951	3.017	3.063	3.090
1.50	1.406	0.455	1.733	1.000	0.807	1.592	2.260	2.785	2.951	3.018	3.064	3.090
1.60	1.499	0.485	1.734	1.000	0.809	1.592	2.260	2.785	2.952	3.018	3.064	3.091
1.70	1.593	0.515	1.736	1.000	0.810	1.592	2.260	2.785	2.952	3.018	3.064	3.091
1.80	1.686	0.545	1.738	1.000	0.812	1.593	2.260	2.785	2.952	3.018	3.065	3.091
1.90	1.779	0.575	1.739	1.000	0.813	1.593	2.260	2.785	2.952	3.019	3.065	3.092
2.00	1.872	0.605	1.741	1.000	0.815	1.594	2.260	2.786	2.953	3.019	3.065	3.092
2.10	1.965	0.635	1.742	1.000	0.816	1.594	2.261	2.786	2.953	3.019	3.065	3.092
2.20	2.058	0.665	1.744	1.000	0.817	1.595	2.261	2.786	2.953	3.019	3.066	3.092
2.30	2.150	0.695	1.746	1.000	0.819	1.595	2.261	2.786	2.953	3.020	3.066	3.093
2.40	2.243	0.725	1.747	1.000	0.820	1.596	2.261	2.786	2.953	3.020	3.066	3.093
2.50	2.336	0.755	1.749	1.000	0.822	1.596	2.261	2.786	2.954	3.020	3.067	3.093
2.60	2.428	0.785	1.750	1.000	0.823	1.596	2.261	2.787	2.954	3.021	3.067	3.094
2.70	2.521	0.815	1.752	1.000	0.825	1.597	2.261	2.787	2.954	3.021	3.067	3.094
2.80	2.613	0.845	1.754	1.000	0.826	1.597	2.261	2.787	2.954	3.021	3.067	3.094
2.90	2.706	0.874	1.755	1.000	0.828	1.598	2.262	2.787	2.955	3.021	3.068	3.094
3.00	2.798	0.904	1.757	1.000	0.829	1.598	2.262	2.787	2.955	3.022	3.068	3.095
3.10	2.890	0.934	1.759	1.000	0.831	1.599	2.262	2.788	2.955	3.022	3.068	3.095
3.20	2.982	0.963	1.760	1.000	0.832	1.599	2.262	2.788	2.955	3.022	3.069	3.095
3.30	3.074	0.993	1.762	1.000	0.834	1.600	2.262	2.788	2.956	3.022	3.069	3.096
3.40	3.166	1.023	1.764	1.000	0.835	1.600	2.262	2.788	2.956	3.023	3.069	3.096
3.50	3.258	1.052	1.765	1.000	0.836	1.600	2.262	2.788	2.956	3.023	3.069	3.096
3.60	3.350	1.082	1.767	1.000	0.838	1.601	2.262	2.788	2.956	3.023	3.070	3.096
3.70	3.442	1.112	1.769	1.000	0.839	1.601	2.263	2.789	2.956	3.023	3.070	3.097
3.80	3.534	1.141	1.770	1.000	0.841	1.602	2.263	2.789	2.957	3.024	3.070	3.097
3.90	3.626	1.171	1.772	1.000	0.842	1.602	2.263	2.789	2.957	3.024	3.070	3.097
4.00	3.717	1.200	1.774	1.000	0.844	1.603	2.263	2.789	2.957	3.024	3.071	3.098
4.50	4.174	1.347	1.783	1.000	0.851	1.605	2.263	2.790	2.958	3.025	3.072	3.099
5.00	4.629	1.493	1.791	1.000	0.858	1.607	2.264	2.791	2.959	3.026	3.073	3.100
5.50	5.082	1.639	1.800	1.000	0.864	1.608	2.264	2.791	2.960	3.027	3.074	3.101
6.00	5.534	1.784	1.809	1.000	0.871	1.610	2.264	2.792	2.961	3.028	3.076	3.103
6.50	5.983	1.928	1.818	1.000	0.877	1.612	2.265	2.792	2.962	3.029	3.077	3.104
7.00	6.431	2.071	1.827	1.000	0.884	1.614	2.265	2.793	2.962	3.030	3.077	3.105
7.50	6.876	2.214	1.836	1.000	0.890	1.615	2.265	2.793	2.963	3.031	3.078	3.105
8.00	7.320	2.357	1.846	1.000	0.895	1.617	2.264	2.793	2.963	3.031	3.079	3.106

EXTINCTION LAW CALCULATION

152

T = 10000 DEGREES - BLACK BODY INTENSITY DISTRIBUTION

MONOCHROMATIC EXTINCTION INPUT

1/LAMDA = 2.86	2.27	1.75	1.47	1.15	0.84	0.47	0.29	0.20	0.11
E-FACTORS 1.35	1.14	0.82	0.62	0.40	0.23	0.08	0.04	0.02	0.01

WIDE BAND EXTINCTION IN MAGNITUDES

K	U	B	V	R	I	J	K	L	M	N	A(V)/E(B-V)
0.10	0.146	0.124	0.094	0.069	0.045	0.025	0.009	0.004	0.002	0.001	3.122
0.20	0.292	0.247	0.187	0.138	0.091	0.050	0.019	0.008	0.004	0.002	3.123
0.30	0.438	0.371	0.281	0.207	0.136	0.075	0.028	0.013	0.007	0.002	3.123
0.40	0.584	0.494	0.374	0.276	0.181	0.101	0.037	0.017	0.009	0.003	3.123
0.50	0.730	0.617	0.468	0.345	0.227	0.126	0.046	0.021	0.011	0.004	3.124
0.60	0.876	0.741	0.561	0.413	0.272	0.151	0.056	0.025	0.013	0.005	3.124
0.70	1.022	0.864	0.654	0.481	0.317	0.176	0.065	0.030	0.015	0.006	3.124
0.80	1.168	0.987	0.748	0.550	0.362	0.201	0.074	0.034	0.018	0.006	3.125
0.90	1.314	1.110	0.841	0.618	0.407	0.226	0.083	0.038	0.020	0.007	3.125
1.00	1.459	1.233	0.934	0.686	0.452	0.251	0.093	0.042	0.022	0.008	3.125
1.10	1.605	1.355	1.027	0.754	0.497	0.276	0.102	0.046	0.024	0.009	3.126
1.20	1.751	1.478	1.120	0.821	0.542	0.301	0.111	0.051	0.026	0.010	3.126
1.30	1.897	1.601	1.213	0.889	0.587	0.326	0.120	0.055	0.029	0.010	3.126
1.40	2.043	1.723	1.306	0.956	0.631	0.351	0.130	0.059	0.031	0.011	3.127
1.50	2.189	1.846	1.398	1.024	0.676	0.376	0.139	0.063	0.033	0.012	3.127
1.60	2.334	1.968	1.491	1.091	0.721	0.401	0.148	0.067	0.035	0.013	3.127
1.70	2.480	2.090	1.584	1.158	0.765	0.426	0.157	0.072	0.037	0.014	3.128
1.80	2.626	2.212	1.676	1.225	0.810	0.451	0.167	0.076	0.040	0.014	3.128
1.90	2.772	2.334	1.769	1.292	0.854	0.476	0.176	0.080	0.042	0.015	3.128
2.00	2.917	2.456	1.861	1.358	0.899	0.501	0.185	0.084	0.044	0.016	3.129
2.10	3.063	2.578	1.954	1.425	0.943	0.526	0.194	0.088	0.046	0.017	3.129
2.20	3.209	2.700	2.046	1.491	0.988	0.551	0.204	0.093	0.049	0.018	3.129
2.30	3.355	2.821	2.138	1.558	1.032	0.575	0.213	0.097	0.051	0.019	3.130
2.40	3.500	2.943	2.230	1.624	1.076	0.600	0.222	0.101	0.053	0.019	3.130
2.50	3.646	3.064	2.322	1.690	1.121	0.625	0.231	0.105	0.055	0.020	3.130
2.60	3.792	3.185	2.414	1.756	1.165	0.650	0.240	0.110	0.057	0.021	3.131
2.70	3.937	3.307	2.506	1.821	1.209	0.675	0.250	0.114	0.060	0.022	3.131
2.80	4.083	3.428	2.598	1.887	1.253	0.700	0.259	0.118	0.062	0.023	3.131
2.90	4.229	3.549	2.690	1.952	1.297	0.725	0.268	0.122	0.064	0.023	3.131
3.00	4.374	3.670	2.782	2.018	1.341	0.749	0.277	0.126	0.066	0.024	3.132
3.10	4.520	3.791	2.873	2.083	1.385	0.774	0.287	0.131	0.068	0.025	3.132
3.20	4.665	3.911	2.965	2.148	1.429	0.799	0.296	0.135	0.071	0.026	3.132
3.30	4.811	4.032	3.056	2.213	1.473	0.824	0.305	0.139	0.073	0.027	3.133
3.40	4.956	4.153	3.148	2.278	1.516	0.848	0.314	0.143	0.075	0.027	3.133
3.50	5.102	4.273	3.239	2.343	1.560	0.873	0.323	0.147	0.077	0.028	3.133
3.60	5.247	4.393	3.331	2.407	1.604	0.898	0.333	0.152	0.079	0.029	3.134
3.70	5.393	4.514	3.422	2.472	1.648	0.923	0.342	0.156	0.082	0.030	3.134
3.80	5.539	4.634	3.513	2.536	1.691	0.947	0.351	0.160	0.084	0.031	3.134
3.90	5.684	4.754	3.604	2.601	1.735	0.972	0.360	0.164	0.086	0.031	3.134
4.00	5.829	4.874	3.695	2.665	1.778	0.997	0.369	0.168	0.088	0.032	3.135
4.50	6.557	5.472	4.149	2.984	1.995	1.120	0.415	0.189	0.099	0.036	3.136
5.00	7.283	6.068	4.601	3.299	2.210	1.243	0.461	0.210	0.110	0.040	3.137
5.50	8.010	6.661	5.051	3.612	2.425	1.365	0.507	0.231	0.121	0.044	3.138
6.00	8.736	7.251	5.499	3.922	2.638	1.487	0.553	0.252	0.132	0.048	3.139
6.50	9.462	7.839	5.946	4.229	2.850	1.609	0.599	0.273	0.143	0.052	3.140
7.00	10.187	8.424	6.390	4.533	3.060	1.731	0.645	0.294	0.154	0.056	3.141
7.50	10.912	9.007	6.832	4.835	3.270	1.852	0.690	0.315	0.165	0.060	3.141
8.00	11.636	9.587	7.272	5.134	3.478	1.973	0.736	0.336	0.176	0.064	3.141

T = 10000 DEGREES - BLACK BODY INTENSITY DISTRIBUTION

K	A(V)	E(B-V)	U-V	B-V	V-R	V-I	V-J	V-K	V-L	V-M	V-N	A(V)/E(B-V)
0.10	0.094	0.030	1.744	1.000	0.817	1.608	2.284	2.813	2.982	3.049	3.095	3.122
0.20	0.187	0.060	1.746	1.000	0.818	1.609	2.284	2.813	2.982	3.049	3.096	3.123
0.30	0.281	0.090	1.747	1.000	0.820	1.609	2.284	2.814	2.982	3.049	3.096	3.123
0.40	0.374	0.120	1.749	1.000	0.821	1.610	2.284	2.814	2.982	3.050	3.096	3.123
0.50	0.468	0.150	1.751	1.000	0.823	1.610	2.284	2.814	2.983	3.050	3.097	3.124
0.60	0.561	0.180	1.752	1.000	0.824	1.611	2.284	2.814	2.983	3.050	3.097	3.124
0.70	0.654	0.209	1.754	1.000	0.826	1.611	2.285	2.815	2.983	3.050	3.097	3.124
0.80	0.748	0.239	1.756	1.000	0.827	1.612	2.285	2.815	2.984	3.051	3.098	3.125
0.90	0.841	0.269	1.757	1.000	0.829	1.612	2.285	2.815	2.984	3.051	3.098	3.125
1.00	0.934	0.299	1.759	1.000	0.830	1.613	2.285	2.815	2.984	3.051	3.098	3.125
1.10	1.027	0.329	1.760	1.000	0.832	1.613	2.285	2.816	2.984	3.052	3.099	3.126
1.20	1.120	0.358	1.762	1.000	0.833	1.614	2.285	2.816	2.985	3.052	3.099	3.126
1.30	1.213	0.388	1.764	1.000	0.835	1.614	2.286	2.816	2.985	3.052	3.099	3.126
1.40	1.306	0.418	1.765	1.000	0.836	1.615	2.286	2.816	2.985	3.053	3.100	3.127
1.50	1.398	0.447	1.767	1.000	0.838	1.615	2.286	2.816	2.986	3.053	3.100	3.127
1.60	1.491	0.477	1.769	1.000	0.839	1.616	2.286	2.817	2.986	3.053	3.100	3.127
1.70	1.584	0.506	1.771	1.000	0.841	1.616	2.286	2.817	2.986	3.054	3.101	3.128
1.80	1.676	0.536	1.772	1.000	0.842	1.616	2.286	2.817	2.986	3.054	3.101	3.128
1.90	1.769	0.565	1.774	1.000	0.844	1.617	2.287	2.817	2.987	3.054	3.101	3.128
2.00	1.861	0.595	1.776	1.000	0.845	1.617	2.287	2.818	2.987	3.054	3.101	3.129
2.10	1.954	0.624	1.777	1.000	0.847	1.618	2.287	2.818	2.987	3.055	3.102	3.129
2.20	2.046	0.654	1.779	1.000	0.848	1.618	2.287	2.818	2.987	3.055	3.102	3.129
2.30	2.138	0.683	1.781	1.000	0.850	1.619	2.287	2.818	2.988	3.055	3.102	3.130
2.40	2.230	0.713	1.783	1.000	0.851	1.619	2.287	2.818	2.988	3.056	3.103	3.130
2.50	2.322	0.742	1.784	1.000	0.853	1.620	2.287	2.819	2.988	3.056	3.103	3.130
2.60	2.414	0.771	1.786	1.000	0.854	1.620	2.288	2.819	2.988	3.056	3.103	3.131
2.70	2.506	0.800	1.788	1.000	0.856	1.621	2.288	2.819	2.989	3.056	3.104	3.131
2.80	2.598	0.830	1.789	1.000	0.857	1.621	2.288	2.819	2.989	3.057	3.104	3.131
2.90	2.690	0.859	1.791	1.000	0.858	1.621	2.288	2.819	2.989	3.057	3.104	3.131
3.00	2.782	0.888	1.793	1.000	0.860	1.622	2.288	2.820	2.989	3.057	3.105	3.132
3.10	2.873	0.917	1.795	1.000	0.861	1.622	2.288	2.820	2.990	3.058	3.105	3.132
3.20	2.965	0.947	1.797	1.000	0.863	1.623	2.288	2.820	2.990	3.058	3.105	3.132
3.30	3.056	0.976	1.798	1.000	0.864	1.623	2.288	2.820	2.990	3.058	3.105	3.133
3.40	3.148	1.005	1.800	1.000	0.866	1.624	2.289	2.820	2.990	3.058	3.106	3.133
3.50	3.239	1.034	1.802	1.000	0.867	1.624	2.289	2.820	2.991	3.059	3.106	3.133
3.60	3.331	1.063	1.804	1.000	0.868	1.624	2.289	2.821	2.991	3.059	3.106	3.134
3.70	3.422	1.092	1.805	1.000	0.870	1.625	2.289	2.821	2.991	3.059	3.107	3.134
3.80	3.513	1.121	1.807	1.000	0.871	1.625	2.289	2.821	2.991	3.059	3.107	3.134
3.90	3.604	1.150	1.809	1.000	0.873	1.626	2.289	2.821	2.992	3.060	3.107	3.134
4.00	3.695	1.179	1.811	1.000	0.874	1.626	2.289	2.821	2.992	3.060	3.107	3.135
4.50	4.149	1.323	1.820	1.000	0.881	1.628	2.290	2.822	2.993	3.061	3.109	3.136
5.00	4.601	1.467	1.829	1.000	0.888	1.630	2.290	2.823	2.994	3.062	3.110	3.137
5.50	5.051	1.610	1.838	1.000	0.894	1.632	2.290	2.823	2.995	3.063	3.111	3.138
6.00	5.499	1.752	1.848	1.000	0.900	1.633	2.290	2.824	2.995	3.064	3.112	3.139
6.50	5.946	1.893	1.857	1.000	0.906	1.635	2.290	2.824	2.996	3.064	3.113	3.140
7.00	6.390	2.035	1.866	1.000	0.912	1.636	2.290	2.824	2.996	3.065	3.113	3.141
7.50	6.832	2.175	1.876	1.000	0.918	1.638	2.290	2.824	2.996	3.065	3.113	3.141
8.00	7.272	2.315	1.885	1.000	0.924	1.639	2.289	2.823	2.996	3.065	3.114	3.141

EXTINCTION LAW CALCULATION

154

T = 3500 DEGREES - BLACK BODY INTENSITY DISTRIBUTION

MONOCHROMATIC EXTINCTION INPUT

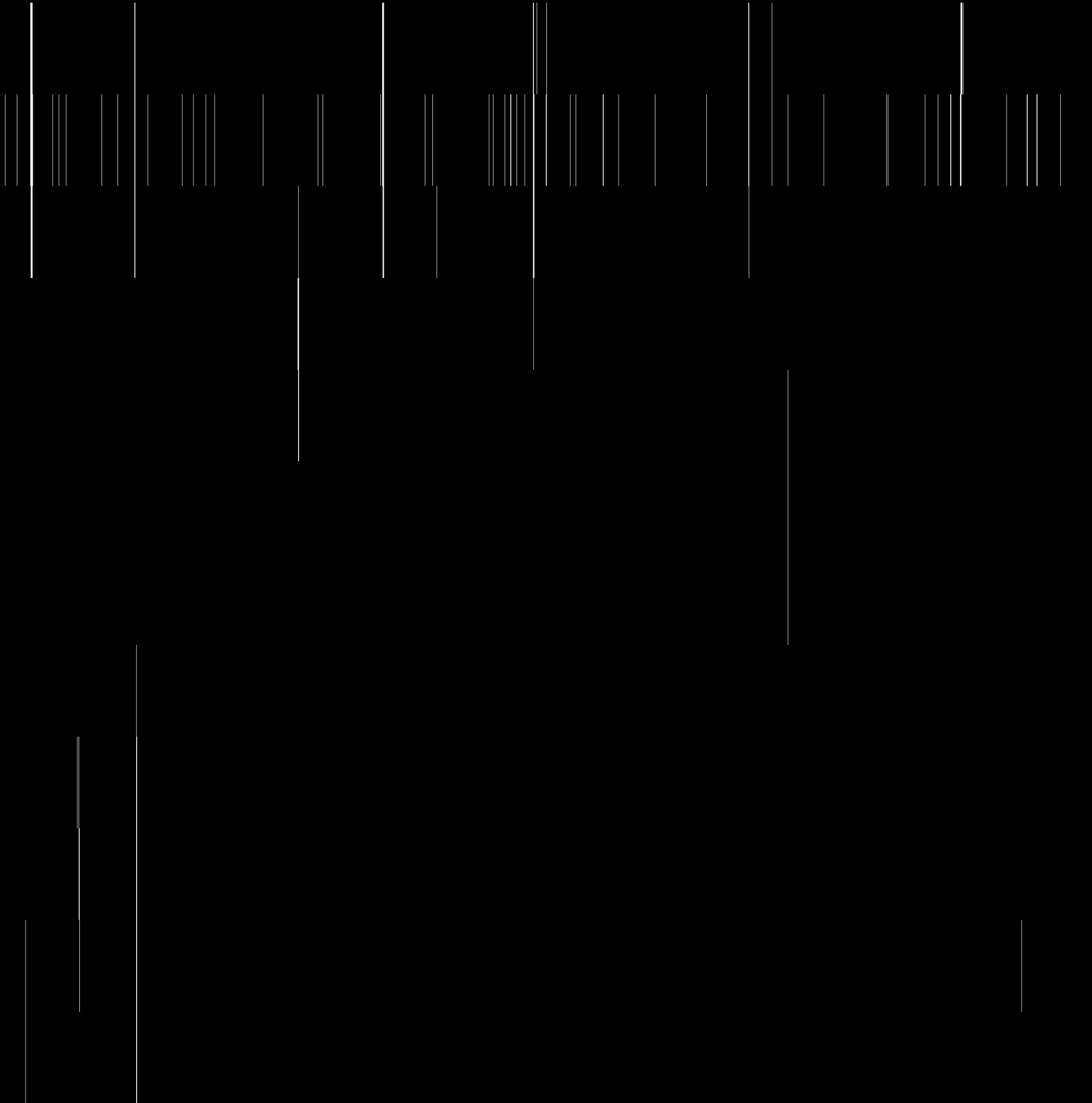
1/LAMDA = 2.86	2.27	1.75	1.47	1.15	0.84	0.47	0.29	0.20	0.11
E-FACTORS 1.35	1.14	0.82	0.62	0.40	0.23	0.08	0.04	0.02	0.01

WIDE BAND EXTINCTION IN MAGNITUDES

K	U	B	V	R	I	J	K	L	M	N	A(V)/E(B-V)
0.10	0.144	0.119	0.091	0.065	0.044	0.025	0.009	0.004	0.002	0.001	3.277
0.20	0.289	0.238	0.182	0.129	0.087	0.049	0.018	0.008	0.004	0.002	3.277
0.30	0.433	0.357	0.273	0.193	0.130	0.074	0.028	0.013	0.007	0.002	3.277
0.40	0.577	0.475	0.364	0.257	0.174	0.098	0.037	0.017	0.009	0.003	3.277
0.50	0.722	0.594	0.455	0.321	0.217	0.123	0.046	0.021	0.011	0.004	3.277
0.60	0.866	0.712	0.546	0.385	0.260	0.147	0.055	0.025	0.013	0.005	3.278
0.70	1.010	0.831	0.636	0.449	0.304	0.172	0.064	0.029	0.015	0.006	3.278
0.80	1.154	0.949	0.727	0.513	0.347	0.196	0.073	0.034	0.018	0.006	3.278
0.90	1.299	1.067	0.818	0.576	0.390	0.220	0.083	0.038	0.020	0.007	3.278
1.00	1.443	1.185	0.908	0.640	0.433	0.245	0.092	0.042	0.022	0.008	3.278
1.10	1.587	1.303	0.999	0.703	0.476	0.269	0.101	0.046	0.024	0.009	3.278
1.20	1.731	1.421	1.089	0.766	0.519	0.294	0.110	0.050	0.026	0.010	3.278
1.30	1.876	1.539	1.179	0.829	0.562	0.318	0.119	0.055	0.029	0.010	3.279
1.40	2.020	1.656	1.269	0.892	0.605	0.343	0.128	0.059	0.031	0.011	3.279
1.50	2.164	1.774	1.359	0.955	0.648	0.367	0.138	0.063	0.033	0.012	3.279
1.60	2.308	1.891	1.449	1.018	0.690	0.391	0.147	0.067	0.035	0.013	3.279
1.70	2.452	2.009	1.539	1.081	0.733	0.416	0.156	0.071	0.037	0.014	3.279
1.80	2.596	2.126	1.629	1.143	0.776	0.440	0.165	0.076	0.040	0.014	3.279
1.90	2.740	2.243	1.719	1.205	0.819	0.464	0.174	0.080	0.042	0.015	3.279
2.00	2.885	2.360	1.809	1.268	0.861	0.489	0.183	0.084	0.044	0.016	3.279
2.10	3.029	2.477	1.898	1.330	0.904	0.513	0.192	0.088	0.046	0.017	3.279
2.20	3.173	2.594	1.988	1.392	0.946	0.537	0.202	0.092	0.048	0.018	3.279
2.30	3.317	2.711	2.077	1.454	0.989	0.561	0.211	0.096	0.051	0.018	3.279
2.40	3.461	2.828	2.167	1.516	1.031	0.586	0.220	0.101	0.053	0.019	3.279
2.50	3.605	2.944	2.256	1.577	1.073	0.610	0.229	0.105	0.055	0.020	3.279
2.60	3.749	3.061	2.345	1.639	1.116	0.634	0.238	0.109	0.057	0.021	3.279
2.70	3.893	3.177	2.435	1.700	1.158	0.658	0.247	0.113	0.059	0.021	3.279
2.80	4.037	3.293	2.524	1.762	1.200	0.683	0.256	0.117	0.062	0.022	3.279
2.90	4.181	3.410	2.613	1.823	1.242	0.707	0.266	0.122	0.064	0.023	3.279
3.00	4.325	3.526	2.702	1.884	1.284	0.731	0.275	0.126	0.066	0.024	3.279
3.10	4.469	3.642	2.791	1.945	1.326	0.755	0.284	0.130	0.068	0.025	3.278
3.20	4.613	3.758	2.879	2.006	1.368	0.779	0.293	0.134	0.070	0.025	3.278
3.30	4.757	3.873	2.968	2.067	1.410	0.803	0.302	0.138	0.073	0.026	3.278
3.40	4.901	3.989	3.057	2.127	1.452	0.828	0.311	0.143	0.075	0.027	3.278
3.50	5.044	4.105	3.145	2.188	1.494	0.852	0.320	0.147	0.077	0.028	3.278
3.60	5.188	4.220	3.234	2.248	1.536	0.876	0.329	0.151	0.079	0.029	3.278
3.70	5.332	4.336	3.322	2.309	1.578	0.900	0.339	0.155	0.081	0.029	3.277
3.80	5.476	4.451	3.410	2.369	1.620	0.924	0.348	0.159	0.083	0.030	3.277
3.90	5.620	4.566	3.498	2.429	1.661	0.948	0.357	0.163	0.086	0.031	3.277
4.00	5.764	4.681	3.587	2.489	1.703	0.972	0.366	0.168	0.088	0.032	3.277
4.50	6.483	5.255	4.026	2.788	1.910	1.092	0.411	0.189	0.099	0.036	3.275
5.00	7.201	5.827	4.463	3.084	2.117	1.212	0.457	0.209	0.110	0.040	3.274
5.50	7.919	6.396	4.899	3.377	2.322	1.332	0.502	0.230	0.121	0.044	3.271
6.00	8.637	6.963	5.332	3.668	2.526	1.451	0.548	0.251	0.132	0.048	3.269
6.50	9.354	7.527	5.763	3.957	2.728	1.570	0.593	0.272	0.143	0.051	3.266
7.00	10.072	8.089	6.192	4.243	2.930	1.688	0.638	0.293	0.154	0.055	3.263
7.50	10.788	8.649	6.618	4.527	3.131	1.806	0.684	0.314	0.165	0.059	3.259
8.00	11.505	9.207	7.043	4.809	3.330	1.924	0.729	0.335	0.176	0.063	3.255

T = 3500 DEGREES - BLACK BODY INTENSITY DISTRIBUTION

K	A(V)	E(B-V)	U-V	B-V	V-R	V-I	V-J	V-K	V-L	V-M	V-N	A(V)/E(B-V)
0.10	0.091	0.028	1.913	1.000	0.956	1.712	2.394	2.947	3.126	3.198	3.248	3.277
0.20	0.182	0.056	1.915	1.000	0.958	1.712	2.394	2.947	3.126	3.198	3.248	3.277
0.30	0.273	0.083	1.917	1.000	0.959	1.713	2.394	2.947	3.126	3.198	3.248	3.277
0.40	0.364	0.111	1.919	1.000	0.961	1.713	2.394	2.947	3.126	3.198	3.249	3.277
0.50	0.455	0.139	1.921	1.000	0.962	1.713	2.394	2.947	3.126	3.198	3.249	3.277
0.60	0.546	0.167	1.923	1.000	0.963	1.714	2.394	2.947	3.126	3.198	3.249	3.278
0.70	0.636	0.194	1.925	1.000	0.965	1.714	2.394	2.947	3.127	3.199	3.249	3.278
0.80	0.727	0.222	1.927	1.000	0.966	1.714	2.394	2.947	3.127	3.199	3.249	3.278
0.90	0.818	0.249	1.929	1.000	0.967	1.715	2.394	2.947	3.127	3.199	3.249	3.278
1.00	0.908	0.277	1.931	1.000	0.968	1.715	2.394	2.947	3.127	3.199	3.249	3.278
1.10	0.999	0.305	1.933	1.000	0.970	1.715	2.394	2.947	3.127	3.199	3.250	3.278
1.20	1.089	0.332	1.935	1.000	0.971	1.716	2.394	2.947	3.127	3.199	3.250	3.278
1.30	1.179	0.360	1.937	1.000	0.972	1.716	2.394	2.947	3.127	3.199	3.250	3.279
1.40	1.269	0.387	1.939	1.000	0.974	1.716	2.394	2.947	3.127	3.199	3.250	3.279
1.50	1.359	0.415	1.941	1.000	0.975	1.717	2.394	2.947	3.127	3.199	3.250	3.279
1.60	1.449	0.442	1.942	1.000	0.976	1.717	2.394	2.947	3.127	3.199	3.250	3.279
1.70	1.539	0.469	1.944	1.000	0.977	1.717	2.394	2.947	3.127	3.199	3.250	3.279
1.80	1.629	0.497	1.946	1.000	0.978	1.717	2.393	2.947	3.127	3.199	3.250	3.279
1.90	1.719	0.524	1.948	1.000	0.980	1.718	2.393	2.947	3.127	3.199	3.250	3.279
2.00	1.809	0.552	1.950	1.000	0.981	1.718	2.393	2.947	3.127	3.199	3.250	3.279
2.10	1.898	0.579	1.952	1.000	0.982	1.718	2.393	2.947	3.127	3.199	3.250	3.279
2.20	1.988	0.606	1.954	1.000	0.983	1.718	2.393	2.947	3.127	3.199	3.250	3.279
2.30	2.077	0.634	1.956	1.000	0.984	1.719	2.393	2.946	3.127	3.199	3.250	3.279
2.40	2.167	0.661	1.958	1.000	0.986	1.719	2.393	2.946	3.127	3.199	3.250	3.279
2.50	2.256	0.688	1.960	1.000	0.987	1.719	2.392	2.946	3.127	3.199	3.250	3.279
2.60	2.345	0.715	1.962	1.000	0.988	1.719	2.392	2.946	3.126	3.199	3.250	3.279
2.70	2.435	0.743	1.964	1.000	0.989	1.719	2.392	2.946	3.126	3.199	3.250	3.279
2.80	2.524	0.770	1.966	1.000	0.990	1.720	2.392	2.946	3.126	3.199	3.250	3.279
2.90	2.613	0.797	1.968	1.000	0.991	1.720	2.392	2.945	3.126	3.199	3.250	3.279
3.00	2.702	0.824	1.970	1.000	0.992	1.720	2.391	2.945	3.126	3.199	3.250	3.279
3.10	2.791	0.851	1.972	1.000	0.993	1.720	2.391	2.945	3.126	3.198	3.250	3.278
3.20	2.879	0.878	1.974	1.000	0.995	1.720	2.391	2.945	3.126	3.198	3.249	3.278
3.30	2.968	0.905	1.976	1.000	0.996	1.720	2.391	2.945	3.125	3.198	3.249	3.278
3.40	3.057	0.932	1.977	1.000	0.997	1.721	2.390	2.944	3.125	3.198	3.249	3.278
3.50	3.145	0.960	1.979	1.000	0.998	1.721	2.390	2.944	3.125	3.198	3.249	3.278
3.60	3.234	0.987	1.981	1.000	0.999	1.721	2.390	2.944	3.125	3.198	3.249	3.278
3.70	3.322	1.014	1.983	1.000	1.000	1.721	2.390	2.944	3.124	3.197	3.249	3.277
3.80	3.410	1.041	1.985	1.000	1.001	1.721	2.389	2.943	3.124	3.197	3.248	3.277
3.90	3.498	1.068	1.987	1.000	1.002	1.721	2.389	2.943	3.124	3.197	3.248	3.277
4.00	3.587	1.095	1.989	1.000	1.003	1.721	2.389	2.943	3.124	3.197	3.248	3.277
4.50	4.026	1.229	1.998	1.000	1.007	1.721	2.387	2.941	3.122	3.195	3.246	3.275
5.00	4.463	1.363	2.008	1.000	1.012	1.721	2.385	2.939	3.120	3.193	3.245	3.274
5.50	4.899	1.497	2.017	1.000	1.016	1.721	2.382	2.936	3.118	3.191	3.242	3.271
6.00	5.332	1.631	2.026	1.000	1.020	1.720	2.379	2.933	3.115	3.188	3.240	3.269
6.50	5.763	1.764	2.036	1.000	1.023	1.720	2.376	2.930	3.112	3.185	3.237	3.266
7.00	6.192	1.898	2.045	1.000	1.027	1.719	2.373	2.926	3.108	3.182	3.233	3.263
7.50	6.618	2.031	2.053	1.000	1.030	1.717	2.369	2.922	3.104	3.178	3.230	3.259
8.00	7.043	2.164	2.062	1.000	1.032	1.716	2.365	2.918	3.100	3.173	3.225	3.255



EXTINCTION LAW CALCULATION

156

T = 30000 DEGREES - BLACK BODY INTENSITY DISTRIBUTION

MONOCHROMATIC EXTINCTION INPUT

1/LAMDA = 2.86	2.27	1.75	1.47	1.15	0.84	0.47	0.29	0.20	0.11
E-FACTORS 2.13	1.96	1.65	1.42	1.08	0.74	0.33	0.18	0.11	0.06

WIDE BAND EXTINCTION IN MAGNITUDES

K	U	B	V	R	I	J	K	L	M	N	A(V)/E(B-V)
0.10	0.231	0.214	0.186	0.157	0.121	0.080	0.036	0.020	0.013	0.006	6.657
0.20	0.462	0.427	0.372	0.314	0.243	0.160	0.072	0.039	0.025	0.013	6.653
0.30	0.692	0.641	0.557	0.471	0.364	0.241	0.108	0.059	0.038	0.019	6.649
0.40	0.923	0.855	0.743	0.628	0.485	0.321	0.144	0.079	0.051	0.026	6.646
0.50	1.154	1.068	0.928	0.784	0.605	0.401	0.181	0.099	0.063	0.032	6.642
0.60	1.385	1.282	1.114	0.940	0.726	0.481	0.217	0.118	0.076	0.039	6.638
0.70	1.615	1.495	1.299	1.096	0.846	0.560	0.253	0.138	0.089	0.045	6.634
0.80	1.846	1.708	1.485	1.251	0.967	0.640	0.289	0.158	0.102	0.052	6.631
0.90	2.077	1.922	1.670	1.407	1.087	0.720	0.325	0.177	0.114	0.058	6.627
1.00	2.307	2.135	1.855	1.562	1.207	0.799	0.361	0.197	0.127	0.065	6.623
1.10	2.538	2.348	2.040	1.717	1.327	0.879	0.397	0.217	0.140	0.071	6.619
1.20	2.769	2.561	2.225	1.872	1.446	0.958	0.433	0.236	0.152	0.078	6.615
1.30	2.999	2.774	2.410	2.026	1.566	1.037	0.469	0.256	0.165	0.084	6.612
1.40	3.230	2.987	2.595	2.180	1.685	1.117	0.505	0.276	0.178	0.091	6.608
1.50	3.461	3.200	2.779	2.334	1.805	1.196	0.541	0.295	0.190	0.097	6.604
1.60	3.691	3.413	2.964	2.488	1.924	1.275	0.577	0.315	0.203	0.104	6.600
1.70	3.922	3.626	3.149	2.641	2.043	1.354	0.612	0.335	0.216	0.110	6.596
1.80	4.152	3.839	3.333	2.795	2.162	1.433	0.648	0.354	0.228	0.117	6.592
1.90	4.383	4.052	3.518	2.948	2.280	1.512	0.684	0.374	0.241	0.123	6.588
2.00	4.613	4.264	3.702	3.100	2.399	1.591	0.720	0.394	0.254	0.129	6.584
2.10	4.844	4.477	3.886	3.253	2.517	1.669	0.756	0.413	0.266	0.136	6.581
2.20	5.074	4.689	4.071	3.405	2.635	1.748	0.792	0.433	0.279	0.142	6.577
2.30	5.305	4.902	4.255	3.557	2.753	1.826	0.828	0.453	0.292	0.149	6.573
2.40	5.535	5.114	4.439	3.709	2.871	1.905	0.864	0.472	0.304	0.155	6.569
2.50	5.766	5.327	4.623	3.861	2.989	1.983	0.899	0.492	0.317	0.162	6.565
2.60	5.996	5.539	4.806	4.012	3.106	2.061	0.935	0.512	0.330	0.168	6.561
2.70	6.227	5.751	4.990	4.163	3.224	2.140	0.971	0.531	0.342	0.175	6.557
2.80	6.457	5.964	5.174	4.314	3.341	2.218	1.007	0.551	0.355	0.181	6.553
2.90	6.688	6.176	5.358	4.465	3.458	2.296	1.042	0.571	0.368	0.188	6.549
3.00	6.918	6.388	5.541	4.615	3.575	2.374	1.078	0.590	0.380	0.194	6.545

T = 30000 DEGREES - BLACK BODY INTENSITY DISTRIBUTION

K	A(V)	E(B-V)	U-V	B-V	V-R	V-I	V-J	V-K	V-L	V-M	V-N	A(V)/E(B-V)
0.10	0.186	0.028	1.611	1.000	1.024	2.309	3.781	5.362	5.951	6.202	6.424	6.657
0.20	0.372	0.056	1.612	1.000	1.026	2.310	3.780	5.359	5.947	6.198	6.421	6.653
0.30	0.557	0.084	1.612	1.000	1.029	2.310	3.778	5.356	5.944	6.195	6.417	6.649
0.40	0.743	0.112	1.613	1.000	1.031	2.311	3.777	5.353	5.941	6.191	6.414	6.646
0.50	0.928	0.140	1.613	1.000	1.033	2.311	3.776	5.350	5.937	6.188	6.410	6.642
0.60	1.114	0.168	1.614	1.000	1.036	2.312	3.774	5.347	5.934	6.184	6.406	6.638
0.70	1.299	0.196	1.614	1.000	1.038	2.312	3.773	5.344	5.930	6.181	6.403	6.634
0.80	1.485	0.224	1.615	1.000	1.041	2.313	3.772	5.341	5.927	6.177	6.399	6.631
0.90	1.670	0.252	1.615	1.000	1.043	2.313	3.770	5.338	5.923	6.173	6.395	6.627
1.00	1.855	0.280	1.616	1.000	1.046	2.314	3.769	5.335	5.920	6.170	6.392	6.623
1.10	2.040	0.308	1.616	1.000	1.048	2.314	3.768	5.332	5.916	6.166	6.388	6.619
1.20	2.225	0.336	1.617	1.000	1.051	2.315	3.766	5.329	5.913	6.163	6.384	6.615
1.30	2.410	0.364	1.617	1.000	1.053	2.315	3.765	5.326	5.909	6.159	6.380	6.612
1.40	2.595	0.393	1.618	1.000	1.055	2.316	3.764	5.322	5.906	6.155	6.377	6.608
1.50	2.779	0.421	1.618	1.000	1.058	2.316	3.762	5.319	5.902	6.152	6.373	6.604
1.60	2.964	0.449	1.619	1.000	1.060	2.316	3.761	5.316	5.898	6.148	6.369	6.600
1.70	3.149	0.477	1.619	1.000	1.063	2.317	3.760	5.313	5.895	6.144	6.366	6.596
1.80	3.333	0.506	1.620	1.000	1.065	2.317	3.758	5.310	5.891	6.141	6.362	6.592
1.90	3.518	0.534	1.620	1.000	1.068	2.318	3.757	5.307	5.888	6.137	6.358	6.588
2.00	3.702	0.562	1.621	1.000	1.070	2.318	3.756	5.304	5.884	6.133	6.354	6.584
2.10	3.886	0.591	1.622	1.000	1.072	2.319	3.754	5.300	5.881	6.130	6.350	6.581
2.20	4.071	0.619	1.622	1.000	1.075	2.319	3.753	5.297	5.877	6.126	6.347	6.577
2.30	4.255	0.647	1.623	1.000	1.077	2.320	3.751	5.294	5.873	6.122	6.343	6.573
2.40	4.439	0.676	1.623	1.000	1.080	2.320	3.750	5.291	5.870	6.118	6.339	6.569
2.50	4.623	0.704	1.624	1.000	1.082	2.320	3.749	5.288	5.866	6.115	6.335	6.565
2.60	4.806	0.733	1.624	1.000	1.084	2.321	3.747	5.285	5.862	6.111	6.331	6.561
2.70	4.990	0.761	1.625	1.000	1.087	2.321	3.746	5.281	5.859	6.107	6.328	6.557
2.80	5.174	0.790	1.625	1.000	1.089	2.322	3.744	5.278	5.855	6.103	6.324	6.553
2.90	5.358	0.818	1.626	1.000	1.092	2.322	3.743	5.275	5.851	6.100	6.320	6.549
3.00	5.541	0.847	1.626	1.000	1.094	2.322	3.741	5.272	5.848	6.096	6.316	6.545
3.10	5.725	0.875	1.627	1.000	1.096	2.323	3.740	5.268	5.844	6.092	6.312	6.541
3.20	5.908	0.904	1.628	1.000	1.099	2.323	3.738	5.265	5.840	6.088	6.308	6.537
3.30	6.091	0.932	1.628	1.000	1.101	2.323	3.737	5.262	5.837	6.085	6.304	6.533
3.40	6.274	0.961	1.629	1.000	1.103	2.324	3.736	5.259	5.833	6.081	6.300	6.529
3.50	6.458	0.990	1.629	1.000	1.106	2.324	3.734	5.255	5.829	6.077	6.296	6.525
3.60	6.641	1.018	1.630	1.000	1.108	2.325	3.733	5.252	5.826	6.073	6.293	6.521
3.70	6.823	1.047	1.630	1.000	1.110	2.325	3.731	5.249	5.822	6.069	6.289	6.517
3.80	7.006	1.076	1.631	1.000	1.113	2.325	3.730	5.245	5.818	6.065	6.285	6.513
3.90	7.189	1.105	1.632	1.000	1.115	2.326	3.728	5.242	5.814	6.062	6.281	6.509
4.00	7.372	1.133	1.632	1.000	1.117	2.326	3.727	5.239	5.811	6.058	6.277	6.505
4.50	8.284	1.278	1.635	1.000	1.129	2.328	3.719	5.222	5.792	6.038	6.257	6.484
5.00	9.193	1.422	1.638	1.000	1.140	2.329	3.711	5.205	5.772	6.018	6.237	6.463
5.50	10.101	1.568	1.641	1.000	1.150	2.330	3.703	5.188	5.753	5.998	6.216	6.442
6.00	11.006	1.714	1.644	1.000	1.161	2.331	3.694	5.170	5.733	5.978	6.195	6.421
6.50	11.908	1.861	1.647	1.000	1.171	2.332	3.686	5.152	5.713	5.958	6.174	6.399
7.00	12.808	2.008	1.651	1.000	1.181	2.333	3.677	5.135	5.693	5.937	6.153	6.377
7.50	13.706	2.157	1.654	1.000	1.190	2.333	3.668	5.116	5.672	5.916	6.131	6.355
8.00	14.601	2.306	1.657	1.000	1.199	2.333	3.659	5.098	5.652	5.895	6.110	6.333

T = 20000 DEGREES - BLACK BODY INTENSITY DISTRIBUTION

MONOCHROMATIC EXTINCTION INPUT

1/LAMDA = 2.86 2.27 1.75 1.47 1.15 0.84 0.47 0.29 0.20 0.11
 E-FACTORS 2.13 1.96 1.65 1.42 1.08 0.74 0.33 0.18 0.11 0.06

WIDE BAND EXTINCTION IN MAGNITUDES

K	U	B	V	R	I	J	K	L	M	N	A(V)/E(B-V)
0.10	0.231	0.214	0.186	0.157	0.121	0.080	0.036	0.020	0.013	0.006	6.667
0.20	0.461	0.427	0.371	0.313	0.242	0.160	0.072	0.039	0.025	0.013	6.663
0.30	0.692	0.640	0.557	0.470	0.363	0.240	0.108	0.059	0.038	0.019	6.660
0.40	0.923	0.854	0.742	0.626	0.484	0.320	0.144	0.079	0.051	0.026	6.656
0.50	1.153	1.067	0.928	0.782	0.604	0.400	0.180	0.098	0.063	0.032	6.652
0.60	1.384	1.280	1.113	0.938	0.725	0.480	0.217	0.118	0.076	0.039	6.648
0.70	1.614	1.493	1.298	1.093	0.845	0.560	0.253	0.138	0.089	0.045	6.644
0.80	1.845	1.707	1.483	1.248	0.965	0.639	0.289	0.158	0.102	0.052	6.641
0.90	2.076	1.920	1.668	1.403	1.085	0.719	0.325	0.177	0.114	0.058	6.637
1.00	2.306	2.133	1.853	1.558	1.205	0.798	0.361	0.197	0.127	0.065	6.633
1.10	2.537	2.346	2.038	1.713	1.325	0.878	0.397	0.217	0.140	0.071	6.629
1.20	2.767	2.559	2.223	1.867	1.444	0.957	0.433	0.236	0.152	0.078	6.625
1.30	2.998	2.771	2.408	2.021	1.563	1.036	0.468	0.256	0.165	0.084	6.622
1.40	3.228	2.984	2.592	2.175	1.683	1.115	0.504	0.276	0.178	0.091	6.618
1.50	3.459	3.197	2.777	2.328	1.802	1.194	0.540	0.295	0.190	0.097	6.614
1.60	3.689	3.410	2.962	2.482	1.921	1.273	0.576	0.315	0.203	0.104	6.610
1.70	3.920	3.622	3.146	2.635	2.039	1.352	0.612	0.335	0.216	0.110	6.606
1.80	4.150	3.835	3.330	2.788	2.158	1.431	0.648	0.354	0.228	0.116	6.602
1.90	4.381	4.047	3.515	2.940	2.276	1.510	0.684	0.374	0.241	0.123	6.598
2.00	4.611	4.260	3.699	3.093	2.395	1.589	0.720	0.394	0.254	0.129	6.595
2.10	4.842	4.472	3.883	3.245	2.513	1.667	0.756	0.413	0.266	0.136	6.591
2.20	5.072	4.684	4.067	3.397	2.631	1.746	0.791	0.433	0.279	0.142	6.587
2.30	5.302	4.897	4.251	3.548	2.748	1.824	0.827	0.453	0.292	0.149	6.583
2.40	5.533	5.109	4.435	3.700	2.866	1.902	0.863	0.472	0.304	0.155	6.579
2.50	5.763	5.321	4.618	3.851	2.984	1.981	0.899	0.492	0.317	0.162	6.575
2.60	5.993	5.533	4.802	4.002	3.101	2.059	0.935	0.512	0.330	0.168	6.571
2.70	6.224	5.745	4.986	4.152	3.218	2.137	0.970	0.531	0.342	0.175	6.567
2.80	6.454	5.957	5.169	4.303	3.335	2.215	1.006	0.551	0.355	0.181	6.563
2.90	6.684	6.169	5.353	4.453	3.452	2.293	1.042	0.571	0.368	0.187	6.559
3.00	6.915	6.381	5.536	4.603	3.569	2.371	1.078	0.590	0.380	0.194	6.555
3.10	7.145	6.592	5.719	4.753	3.685	2.448	1.113	0.610	0.393	0.200	6.551
3.20	7.375	6.804	5.902	4.902	3.802	2.526	1.149	0.630	0.405	0.207	6.547
3.30	7.605	7.016	6.086	5.052	3.918	2.604	1.185	0.649	0.418	0.213	6.543
3.40	7.836	7.227	6.269	5.201	4.034	2.681	1.220	0.669	0.431	0.220	6.539
3.50	8.066	7.439	6.451	5.349	4.150	2.759	1.256	0.688	0.443	0.226	6.535
3.60	8.296	7.650	6.634	5.498	4.266	2.836	1.292	0.708	0.456	0.233	6.531
3.70	8.526	7.862	6.817	5.646	4.381	2.913	1.327	0.728	0.469	0.239	6.527
3.80	8.756	8.073	7.000	5.794	4.497	2.990	1.363	0.747	0.481	0.245	6.523
3.90	8.987	8.284	7.182	5.942	4.612	3.067	1.398	0.767	0.494	0.252	6.519
4.00	9.217	8.495	7.365	6.090	4.727	3.144	1.434	0.787	0.506	0.258	6.514
4.50	10.367	9.550	8.276	6.824	5.301	3.528	1.612	0.885	0.570	0.290	6.494
5.00	11.518	10.603	9.184	7.553	5.870	3.910	1.789	0.983	0.633	0.322	6.473
5.50	12.667	11.655	10.091	8.276	6.436	4.290	1.966	1.081	0.696	0.355	6.452
6.00	13.817	12.705	10.995	8.993	6.997	4.667	2.143	1.179	0.759	0.387	6.430
6.50	14.966	13.753	11.896	9.704	7.555	5.043	2.319	1.277	0.822	0.419	6.409
7.00	16.115	14.799	12.795	10.410	8.109	5.416	2.495	1.374	0.884	0.451	6.386
7.50	17.263	15.843	13.692	11.111	8.659	5.788	2.670	1.472	0.947	0.482	6.364
8.00	18.412	16.886	14.586	11.807	9.206	6.158	2.846	1.570	1.010	0.514	6.341

T = 20000 DEGREES - BLACK BODY INTENSITY DISTRIBUTION

K	A(V)	E(B-V)	U-V	B-V	V-R	V-I	V-J	V-K	V-L	V-M	V-N	A(V)/E(B-V)
0.10	0.186	0.028	1.616	1.000	1.034	2.316	3.788	5.370	5.959	6.211	6.434	6.667
0.20	0.371	0.056	1.617	1.000	1.037	2.317	3.786	5.367	5.956	6.208	6.431	6.663
0.30	0.557	0.084	1.618	1.000	1.039	2.317	3.785	5.364	5.953	6.204	6.427	6.660
0.40	0.742	0.112	1.618	1.000	1.042	2.318	3.784	5.361	5.949	6.200	6.423	6.656
0.50	0.928	0.139	1.619	1.000	1.044	2.318	3.783	5.358	5.946	6.197	6.420	6.652
0.60	1.113	0.167	1.619	1.000	1.047	2.319	3.781	5.355	5.942	6.193	6.416	6.648
0.70	1.298	0.195	1.620	1.000	1.049	2.319	3.780	5.352	5.939	6.190	6.412	6.644
0.80	1.483	0.223	1.620	1.000	1.052	2.320	3.779	5.349	5.935	6.186	6.409	6.641
0.90	1.668	0.251	1.621	1.000	1.054	2.320	3.777	5.346	5.932	6.183	6.405	6.637
1.00	1.853	0.279	1.621	1.000	1.056	2.321	3.776	5.343	5.928	6.179	6.401	6.633
1.10	2.038	0.307	1.622	1.000	1.059	2.321	3.775	5.339	5.925	6.175	6.398	6.629
1.20	2.223	0.336	1.622	1.000	1.061	2.322	3.773	5.336	5.921	6.172	6.394	6.625
1.30	2.408	0.364	1.623	1.000	1.064	2.322	3.772	5.333	5.918	6.168	6.390	6.622
1.40	2.592	0.392	1.623	1.000	1.066	2.323	3.771	5.330	5.914	6.164	6.386	6.618
1.50	2.777	0.420	1.624	1.000	1.069	2.323	3.769	5.327	5.911	6.161	6.383	6.614
1.60	2.962	0.448	1.624	1.000	1.071	2.324	3.768	5.324	5.907	6.157	6.379	6.610
1.70	3.146	0.476	1.625	1.000	1.073	2.324	3.766	5.321	5.903	6.153	6.375	6.606
1.80	3.330	0.504	1.626	1.000	1.076	2.324	3.765	5.318	5.900	6.150	6.371	6.602
1.90	3.515	0.533	1.626	1.000	1.078	2.325	3.764	5.314	5.896	6.146	6.368	6.598
2.00	3.699	0.561	1.627	1.000	1.081	2.325	3.762	5.311	5.893	6.142	6.364	6.595
2.10	3.883	0.589	1.627	1.000	1.083	2.326	3.761	5.308	5.889	6.139	6.360	6.591
2.20	4.067	0.617	1.628	1.000	1.086	2.326	3.759	5.305	5.885	6.135	6.356	6.587
2.30	4.251	0.646	1.628	1.000	1.088	2.327	3.758	5.302	5.882	6.131	6.352	6.583
2.40	4.435	0.674	1.629	1.000	1.090	2.327	3.757	5.299	5.878	6.128	6.349	6.579
2.50	4.618	0.702	1.629	1.000	1.093	2.327	3.755	5.295	5.875	6.124	6.345	6.575
2.60	4.802	0.731	1.630	1.000	1.095	2.328	3.754	5.292	5.871	6.120	6.341	6.571
2.70	4.986	0.759	1.631	1.000	1.098	2.328	3.752	5.289	5.867	6.116	6.337	6.567
2.80	5.169	0.788	1.631	1.000	1.100	2.329	3.751	5.286	5.864	6.112	6.333	6.563
2.90	5.353	0.816	1.632	1.000	1.102	2.329	3.749	5.282	5.860	6.109	6.329	6.559
3.00	5.536	0.845	1.632	1.000	1.105	2.329	3.748	5.279	5.856	6.105	6.325	6.555
3.10	5.719	0.873	1.633	1.000	1.107	2.330	3.747	5.276	5.852	6.101	6.322	6.551
3.20	5.902	0.902	1.633	1.000	1.109	2.330	3.745	5.273	5.849	6.097	6.318	6.547
3.30	6.086	0.930	1.634	1.000	1.112	2.330	3.744	5.269	5.845	6.093	6.314	6.543
3.40	6.269	0.959	1.635	1.000	1.114	2.331	3.742	5.266	5.841	6.090	6.310	6.539
3.50	6.451	0.987	1.635	1.000	1.116	2.331	3.741	5.263	5.838	6.086	6.306	6.535
3.60	6.634	1.016	1.636	1.000	1.119	2.332	3.739	5.259	5.834	6.082	6.302	6.531
3.70	6.817	1.044	1.636	1.000	1.121	2.332	3.738	5.256	5.830	6.078	6.298	6.527
3.80	7.000	1.073	1.637	1.000	1.123	2.332	3.736	5.253	5.826	6.074	6.294	6.523
3.90	7.182	1.102	1.638	1.000	1.126	2.333	3.735	5.249	5.823	6.070	6.290	6.519
4.00	7.365	1.131	1.638	1.000	1.128	2.333	3.733	5.246	5.819	6.066	6.286	6.514
4.50	8.276	1.274	1.641	1.000	1.139	2.334	3.725	5.229	5.800	6.047	6.266	6.494
5.00	9.184	1.419	1.644	1.000	1.150	2.336	3.717	5.212	5.780	6.027	6.246	6.473
5.50	10.091	1.564	1.647	1.000	1.161	2.337	3.709	5.195	5.761	6.007	6.225	6.452
6.00	10.995	1.710	1.651	1.000	1.171	2.338	3.701	5.177	5.741	5.987	6.204	6.430
6.50	11.896	1.856	1.654	1.000	1.181	2.339	3.692	5.159	5.721	5.966	6.183	6.409
7.00	12.795	2.004	1.657	1.000	1.190	2.339	3.683	5.141	5.700	5.945	6.162	6.386
7.50	13.692	2.151	1.660	1.000	1.199	2.339	3.674	5.123	5.680	5.924	6.140	6.364
8.00	14.586	2.300	1.663	1.000	1.208	2.339	3.664	5.104	5.659	5.902	6.118	6.341

T = 10000 DEGREES - BLACK BODY INTENSITY DISTRIBUTION

MONOCHROMATIC EXTINCTION INPUT

1/LAMDA = 2.86 2.27 1.75 1.47 1.15 0.84 0.47 0.29 0.20 0.11
 E-FACTORS 2.13 1.96 1.65 1.42 1.08 0.74 0.33 0.18 0.11 0.06

WIDE BAND EXTINCTION IN MAGNITUDES

K	U	B	V	R	I	J	K	L	M	N	A(V)/E(B-V)
0.10	0.230	0.213	0.185	0.156	0.120	0.080	0.036	0.020	0.013	0.006	6.706
0.20	0.461	0.425	0.370	0.311	0.241	0.160	0.072	0.039	0.025	0.013	6.702
0.30	0.691	0.638	0.555	0.466	0.361	0.239	0.108	0.059	0.038	0.019	6.699
0.40	0.921	0.850	0.740	0.621	0.481	0.319	0.144	0.079	0.051	0.026	6.695
0.50	1.151	1.063	0.925	0.775	0.601	0.399	0.180	0.098	0.063	0.032	6.691
0.60	1.381	1.275	1.109	0.930	0.721	0.478	0.216	0.118	0.076	0.039	6.687
0.70	1.612	1.488	1.294	1.084	0.840	0.557	0.252	0.138	0.089	0.045	6.683
0.80	1.842	1.700	1.479	1.237	0.960	0.637	0.288	0.157	0.101	0.052	6.680
0.90	2.072	1.912	1.663	1.391	1.079	0.716	0.324	0.177	0.114	0.058	6.676
1.00	2.302	2.124	1.847	1.544	1.198	0.795	0.360	0.197	0.127	0.065	6.672
1.10	2.532	2.336	2.032	1.698	1.317	0.874	0.396	0.217	0.139	0.071	6.668
1.20	2.762	2.549	2.216	1.851	1.436	0.953	0.432	0.236	0.152	0.078	6.664
1.30	2.993	2.761	2.400	2.003	1.554	1.032	0.468	0.256	0.165	0.084	6.660
1.40	3.223	2.972	2.584	2.156	1.673	1.111	0.504	0.276	0.177	0.091	6.656
1.50	3.453	3.184	2.768	2.308	1.791	1.190	0.539	0.295	0.190	0.097	6.653
1.60	3.683	3.396	2.952	2.460	1.909	1.268	0.575	0.315	0.203	0.103	6.649
1.70	3.913	3.608	3.136	2.612	2.027	1.347	0.611	0.334	0.215	0.110	6.645
1.80	4.143	3.820	3.320	2.763	2.145	1.425	0.647	0.354	0.228	0.116	6.641
1.90	4.373	4.031	3.503	2.914	2.263	1.504	0.683	0.374	0.241	0.123	6.637
2.00	4.603	4.243	3.687	3.065	2.381	1.582	0.719	0.393	0.253	0.129	6.633
2.10	4.833	4.454	3.870	3.216	2.498	1.660	0.754	0.413	0.266	0.136	6.629
2.20	5.063	4.666	4.054	3.367	2.615	1.738	0.790	0.433	0.279	0.142	6.625
2.30	5.293	4.877	4.237	3.517	2.732	1.816	0.826	0.452	0.291	0.149	6.621
2.40	5.523	5.088	4.420	3.667	2.849	1.894	0.862	0.472	0.304	0.155	6.617
2.50	5.753	5.300	4.603	3.817	2.966	1.972	0.897	0.492	0.317	0.162	6.613
2.60	5.983	5.511	4.787	3.966	3.083	2.050	0.933	0.511	0.329	0.168	6.609
2.70	6.213	5.722	4.970	4.116	3.199	2.128	0.969	0.531	0.342	0.174	6.605
2.80	6.443	5.933	5.152	4.265	3.315	2.206	1.004	0.551	0.355	0.181	6.601
2.90	6.672	6.144	5.335	4.414	3.432	2.283	1.040	0.570	0.367	0.187	6.597
3.00	6.902	6.355	5.518	4.562	3.548	2.361	1.076	0.590	0.380	0.194	6.593
3.10	7.132	6.566	5.701	4.711	3.663	2.438	1.111	0.610	0.393	0.200	6.589
3.20	7.362	6.777	5.883	4.859	3.779	2.516	1.147	0.629	0.405	0.207	6.584
3.30	7.592	6.987	6.065	5.007	3.895	2.593	1.183	0.649	0.418	0.213	6.580
3.40	7.822	7.198	6.248	5.155	4.010	2.670	1.218	0.668	0.430	0.219	6.576
3.50	8.051	7.408	6.430	5.302	4.125	2.747	1.254	0.688	0.443	0.226	6.572
3.60	8.281	7.619	6.612	5.449	4.240	2.824	1.289	0.708	0.456	0.232	6.568
3.70	8.511	7.829	6.794	5.596	4.355	2.901	1.325	0.727	0.468	0.239	6.564
3.80	8.741	8.040	6.976	5.743	4.470	2.978	1.361	0.747	0.481	0.245	6.560
3.90	8.971	8.250	7.158	5.889	4.585	3.055	1.396	0.767	0.494	0.252	6.556
4.00	9.200	8.460	7.340	6.036	4.699	3.131	1.432	0.786	0.506	0.258	6.551
4.50	10.349	9.511	8.248	6.764	5.269	3.513	1.609	0.884	0.569	0.290	6.530
5.00	11.497	10.559	9.153	7.486	5.835	3.893	1.786	0.982	0.632	0.322	6.509
5.50	12.645	11.606	10.056	8.203	6.397	4.271	1.963	1.080	0.695	0.354	6.487
6.00	13.792	12.651	10.956	8.914	6.955	4.647	2.139	1.178	0.758	0.386	6.465
6.50	14.939	13.694	11.854	9.620	7.509	5.021	2.315	1.276	0.821	0.418	6.442
7.00	16.086	14.735	12.749	10.320	8.060	5.393	2.491	1.374	0.884	0.450	6.420
7.50	17.232	15.775	13.642	11.015	8.606	5.763	2.666	1.471	0.947	0.482	6.396
8.00	18.379	16.812	14.532	11.706	9.149	6.131	2.841	1.569	1.009	0.514	6.373

T = 10000 DEGREES - BLACK BODY INTENSITY DISTRIBUTION

K	A(V)	E(B-V)	U-V	B-V	V-R	V-I	V-J	V-K	V-L	V-M	V-N	A(V)/E(B-V)
0.10	0.185	0.028	1.637	1.000	1.072	2.342	3.813	5.400	5.993	6.246	6.471	6.706
0.20	0.370	0.055	1.637	1.000	1.075	2.342	3.811	5.397	5.989	6.243	6.468	6.702
0.30	0.555	0.083	1.638	1.000	1.077	2.343	3.810	5.394	5.986	6.239	6.464	6.699
0.40	0.740	0.111	1.638	1.000	1.080	2.343	3.809	5.390	5.982	6.236	6.460	6.695
0.50	0.925	0.138	1.639	1.000	1.082	2.344	3.807	5.387	5.979	6.232	6.457	6.691
0.60	1.109	0.166	1.640	1.000	1.084	2.344	3.806	5.384	5.975	6.228	6.453	6.687
0.70	1.294	0.194	1.640	1.000	1.087	2.345	3.805	5.381	5.972	6.225	6.449	6.683
0.80	1.479	0.221	1.641	1.000	1.089	2.345	3.803	5.378	5.968	6.221	6.446	6.680
0.90	1.663	0.249	1.641	1.000	1.092	2.345	3.802	5.375	5.965	6.218	6.442	6.676
1.00	1.847	0.277	1.642	1.000	1.094	2.346	3.801	5.372	5.961	6.214	6.438	6.672
1.10	2.032	0.305	1.642	1.000	1.097	2.346	3.799	5.369	5.958	6.210	6.434	6.668
1.20	2.216	0.333	1.643	1.000	1.099	2.347	3.798	5.366	5.954	6.207	6.431	6.664
1.30	2.400	0.360	1.644	1.000	1.101	2.347	3.797	5.362	5.950	6.203	6.427	6.660
1.40	2.584	0.388	1.644	1.000	1.104	2.348	3.795	5.359	5.947	6.199	6.423	6.656
1.50	2.768	0.416	1.645	1.000	1.106	2.348	3.794	5.356	5.943	6.196	6.419	6.653
1.60	2.952	0.444	1.645	1.000	1.109	2.349	3.792	5.353	5.940	6.192	6.416	6.649
1.70	3.136	0.472	1.646	1.000	1.111	2.349	3.791	5.350	5.936	6.188	6.412	6.645
1.80	3.320	0.500	1.647	1.000	1.114	2.349	3.790	5.347	5.932	6.184	6.408	6.641
1.90	3.503	0.528	1.647	1.000	1.116	2.350	3.788	5.343	5.929	6.181	6.404	6.637
2.00	3.687	0.556	1.648	1.000	1.118	2.350	3.787	5.340	5.925	6.177	6.400	6.633
2.10	3.870	0.584	1.648	1.000	1.121	2.351	3.785	5.337	5.921	6.173	6.396	6.629
2.20	4.054	0.612	1.649	1.000	1.123	2.351	3.784	5.334	5.918	6.169	6.393	6.625
2.30	4.237	0.640	1.650	1.000	1.125	2.351	3.782	5.330	5.914	6.166	6.389	6.621
2.40	4.420	0.668	1.650	1.000	1.128	2.352	3.781	5.327	5.910	6.162	6.385	6.617
2.50	4.603	0.696	1.651	1.000	1.130	2.352	3.780	5.324	5.907	6.158	6.381	6.613
2.60	4.787	0.724	1.652	1.000	1.132	2.353	3.778	5.321	5.903	6.154	6.377	6.609
2.70	4.970	0.752	1.652	1.000	1.135	2.353	3.777	5.317	5.899	6.150	6.373	6.605
2.80	5.152	0.781	1.653	1.000	1.137	2.353	3.775	5.314	5.895	6.146	6.369	6.601
2.90	5.335	0.809	1.653	1.000	1.139	2.354	3.774	5.311	5.892	6.143	6.365	6.597
3.00	5.518	0.837	1.654	1.000	1.142	2.354	3.772	5.307	5.888	6.139	6.361	6.593
3.10	5.701	0.865	1.655	1.000	1.144	2.354	3.771	5.304	5.884	6.135	6.357	6.589
3.20	5.883	0.893	1.655	1.000	1.146	2.355	3.769	5.301	5.880	6.131	6.353	6.584
3.30	6.065	0.922	1.656	1.000	1.149	2.355	3.768	5.297	5.877	6.127	6.349	6.580
3.40	6.248	0.950	1.657	1.000	1.151	2.355	3.766	5.294	5.873	6.123	6.345	6.576
3.50	6.430	0.978	1.657	1.000	1.153	2.356	3.764	5.291	5.869	6.119	6.341	6.572
3.60	6.612	1.007	1.658	1.000	1.155	2.356	3.763	5.287	5.865	6.115	6.337	6.568
3.70	6.794	1.035	1.658	1.000	1.157	2.356	3.761	5.284	5.861	6.111	6.333	6.564
3.80	6.976	1.064	1.659	1.000	1.160	2.357	3.760	5.280	5.857	6.108	6.329	6.560
3.90	7.158	1.092	1.660	1.000	1.162	2.357	3.758	5.277	5.854	6.104	6.325	6.556
4.00	7.340	1.120	1.660	1.000	1.164	2.357	3.757	5.274	5.850	6.100	6.321	6.551
4.50	8.248	1.263	1.664	1.000	1.175	2.359	3.748	5.256	5.830	6.080	6.301	6.530
5.00	9.153	1.406	1.667	1.000	1.185	2.360	3.740	5.239	5.810	6.059	6.280	6.509
5.50	10.056	1.550	1.670	1.000	1.195	2.360	3.731	5.221	5.790	6.039	6.259	6.487
6.00	10.956	1.695	1.673	1.000	1.205	2.361	3.723	5.203	5.770	6.018	6.237	6.465
6.50	11.854	1.840	1.677	1.000	1.214	2.361	3.713	5.184	5.749	5.996	6.215	6.442
7.00	12.749	1.986	1.680	1.000	1.223	2.361	3.704	5.166	5.728	5.975	6.193	6.420
7.50	13.642	2.133	1.684	1.000	1.232	2.361	3.694	5.146	5.707	5.953	6.170	6.396
8.00	14.532	2.280	1.687	1.000	1.239	2.361	3.684	5.127	5.685	5.930	6.147	6.373

T = 3500 DEGREES - BLACK BODY INTENSITY DISTRIBUTION

MONOCHROMATIC EXTINCTION INPUT

1/LAMDA = 2.86	2.27	1.75	1.47	1.15	0.84	0.47	0.29	0.20	0.11
E-FACTORS 2.13	1.96	1.65	1.42	1.08	0.74	0.33	0.18	0.11	0.06

WIDE BAND EXTINCTION IN MAGNITUDES

K	U	B	V	R	I	J	K	L	M	N	A(V)/E(B-V)
0.10	0.229	0.209	0.182	0.149	0.117	0.078	0.036	0.020	0.013	0.006	6.858
0.20	0.457	0.418	0.365	0.298	0.234	0.157	0.072	0.039	0.025	0.013	6.854
0.30	0.686	0.626	0.547	0.447	0.351	0.235	0.107	0.059	0.038	0.019	6.849
0.40	0.914	0.835	0.729	0.596	0.468	0.313	0.143	0.079	0.051	0.026	6.845
0.50	1.143	1.044	0.911	0.744	0.584	0.391	0.179	0.098	0.063	0.032	6.840
0.60	1.372	1.252	1.092	0.892	0.701	0.469	0.215	0.118	0.076	0.039	6.836
0.70	1.600	1.461	1.274	1.040	0.817	0.547	0.250	0.137	0.089	0.045	6.831
0.80	1.829	1.669	1.456	1.188	0.933	0.624	0.286	0.157	0.101	0.052	6.827
0.90	2.057	1.878	1.637	1.335	1.049	0.702	0.322	0.177	0.114	0.058	6.822
1.00	2.286	2.086	1.819	1.483	1.164	0.780	0.357	0.196	0.126	0.064	6.817
1.10	2.514	2.294	2.000	1.630	1.280	0.857	0.393	0.216	0.139	0.071	6.813
1.20	2.743	2.502	2.182	1.777	1.395	0.934	0.429	0.236	0.152	0.077	6.808
1.30	2.971	2.710	2.363	1.923	1.511	1.012	0.464	0.255	0.164	0.084	6.803
1.40	3.200	2.918	2.544	2.069	1.626	1.089	0.500	0.275	0.177	0.090	6.799
1.50	3.428	3.126	2.725	2.216	1.741	1.166	0.535	0.294	0.190	0.097	6.794
1.60	3.656	3.334	2.906	2.361	1.856	1.243	0.571	0.314	0.202	0.103	6.789
1.70	3.885	3.542	3.087	2.507	1.970	1.320	0.607	0.334	0.215	0.109	6.784
1.80	4.113	3.749	3.268	2.653	2.085	1.397	0.642	0.353	0.227	0.116	6.780
1.90	4.342	3.957	3.448	2.798	2.199	1.474	0.678	0.373	0.240	0.122	6.775
2.00	4.570	4.165	3.629	2.943	2.313	1.551	0.713	0.393	0.253	0.129	6.770
2.10	4.798	4.372	3.809	3.088	2.427	1.627	0.749	0.412	0.265	0.135	6.765
2.20	5.027	4.580	3.990	3.232	2.541	1.704	0.784	0.432	0.278	0.142	6.760
2.30	5.255	4.787	4.170	3.376	2.655	1.781	0.820	0.451	0.291	0.148	6.755
2.40	5.484	4.994	4.350	3.521	2.769	1.857	0.855	0.471	0.303	0.154	6.750
2.50	5.712	5.202	4.530	3.664	2.882	1.933	0.891	0.491	0.316	0.161	6.745
2.60	5.940	5.409	4.710	3.808	2.995	2.010	0.926	0.510	0.328	0.167	6.740
2.70	6.168	5.616	4.890	3.952	3.108	2.086	0.962	0.530	0.341	0.174	6.736
2.80	6.397	5.823	5.070	4.095	3.221	2.162	0.997	0.549	0.354	0.180	6.730
2.90	6.625	6.030	5.249	4.238	3.334	2.238	1.032	0.569	0.366	0.186	6.725
3.00	6.853	6.237	5.429	4.381	3.447	2.314	1.068	0.588	0.379	0.193	6.720
3.10	7.081	6.443	5.608	4.523	3.559	2.390	1.103	0.608	0.391	0.199	6.715
3.20	7.310	6.650	5.788	4.666	3.671	2.465	1.138	0.628	0.404	0.206	6.710
3.30	7.538	6.857	5.967	4.808	3.784	2.541	1.174	0.647	0.417	0.212	6.705
3.40	7.766	7.063	6.146	4.950	3.896	2.617	1.209	0.667	0.429	0.218	6.700
3.50	7.994	7.270	6.325	5.092	4.007	2.692	1.244	0.686	0.442	0.225	6.695
3.60	8.222	7.476	6.504	5.233	4.119	2.768	1.280	0.706	0.454	0.231	6.690
3.70	8.451	7.683	6.683	5.374	4.231	2.843	1.315	0.726	0.467	0.238	6.684
3.80	8.679	7.889	6.862	5.516	4.342	2.918	1.350	0.745	0.480	0.244	6.679
3.90	8.907	8.095	7.040	5.656	4.453	2.994	1.386	0.765	0.492	0.250	6.674
4.00	9.135	8.301	7.219	5.797	4.564	3.069	1.421	0.784	0.505	0.257	6.669
4.50	10.276	9.331	8.110	6.498	5.118	3.443	1.597	0.882	0.568	0.289	6.642
5.00	11.416	10.359	8.999	7.193	5.667	3.816	1.773	0.980	0.630	0.321	6.614
5.50	12.555	11.385	9.884	7.884	6.213	4.186	1.948	1.078	0.693	0.353	6.587
6.00	13.695	12.409	10.767	8.570	6.755	4.554	2.123	1.175	0.756	0.384	6.558
6.50	14.834	13.432	11.648	9.251	7.293	4.921	2.298	1.273	0.819	0.416	6.529
7.00	15.973	14.452	12.525	9.928	7.828	5.285	2.472	1.370	0.881	0.448	6.499
7.50	17.112	15.471	13.400	10.600	8.359	5.648	2.646	1.468	0.944	0.480	6.468
8.00	18.250	16.488	14.271	11.268	8.887	6.009	2.820	1.565	1.006	0.512	6.437

T = 3500 DEGREES - BLACK BODY INTENSITY DISTRIBUTION

K	A(V)	E(B-V)	U-V	B-V	V-R	V-I	V-J	V-K	V-L	V-M	V-N	A(V)/E(B-V)
0.10	0.182	0.027	1.743	1.000	1.242	2.451	3.912	5.512	6.119	6.382	6.616	6.858
0.20	0.365	0.053	1.743	1.000	1.244	2.452	3.910	5.508	6.115	6.378	6.611	6.854
0.30	0.547	0.080	1.744	1.000	1.246	2.452	3.908	5.505	6.111	6.374	6.607	6.849
0.40	0.729	0.106	1.745	1.000	1.248	2.452	3.907	5.501	6.107	6.370	6.603	6.845
0.50	0.911	0.133	1.746	1.000	1.250	2.452	3.905	5.497	6.103	6.365	6.598	6.840
0.60	1.092	0.160	1.746	1.000	1.252	2.452	3.903	5.493	6.098	6.361	6.594	6.836
0.70	1.274	0.187	1.747	1.000	1.254	2.453	3.901	5.490	6.094	6.357	6.589	6.831
0.80	1.456	0.213	1.748	1.000	1.256	2.453	3.900	5.486	6.090	6.352	6.585	6.827
0.90	1.637	0.240	1.749	1.000	1.258	2.453	3.898	5.482	6.086	6.348	6.580	6.822
1.00	1.819	0.267	1.749	1.000	1.260	2.453	3.896	5.478	6.081	6.344	6.576	6.817
1.10	2.000	0.294	1.750	1.000	1.262	2.453	3.894	5.475	6.077	6.339	6.571	6.813
1.20	2.182	0.320	1.751	1.000	1.264	2.453	3.892	5.471	6.073	6.335	6.567	6.808
1.30	2.363	0.347	1.751	1.000	1.266	2.454	3.890	5.467	6.069	6.330	6.562	6.803
1.40	2.544	0.374	1.752	1.000	1.268	2.454	3.888	5.463	6.064	6.326	6.558	6.799
1.50	2.725	0.401	1.753	1.000	1.270	2.454	3.886	5.459	6.060	6.321	6.553	6.794
1.60	2.906	0.428	1.753	1.000	1.272	2.454	3.885	5.455	6.055	6.317	6.549	6.789
1.70	3.087	0.455	1.754	1.000	1.274	2.454	3.883	5.451	6.051	6.312	6.544	6.784
1.80	3.268	0.482	1.755	1.000	1.276	2.454	3.881	5.447	6.047	6.308	6.539	6.780
1.90	3.448	0.509	1.756	1.000	1.278	2.454	3.879	5.443	6.042	6.303	6.535	6.775
2.00	3.629	0.536	1.756	1.000	1.280	2.454	3.877	5.439	6.038	6.299	6.530	6.770
2.10	3.809	0.563	1.757	1.000	1.282	2.454	3.875	5.435	6.033	6.294	6.525	6.765
2.20	3.990	0.590	1.758	1.000	1.284	2.454	3.873	5.431	6.029	6.289	6.520	6.760
2.30	4.170	0.617	1.758	1.000	1.285	2.454	3.871	5.427	6.024	6.285	6.516	6.755
2.40	4.350	0.644	1.759	1.000	1.287	2.454	3.869	5.423	6.020	6.280	6.511	6.750
2.50	4.530	0.672	1.760	1.000	1.289	2.454	3.867	5.419	6.015	6.275	6.506	6.745
2.60	4.710	0.699	1.761	1.000	1.291	2.454	3.865	5.415	6.010	6.271	6.501	6.740
2.70	4.890	0.726	1.761	1.000	1.292	2.454	3.862	5.411	6.006	6.266	6.496	6.736
2.80	5.070	0.753	1.762	1.000	1.294	2.454	3.860	5.407	6.001	6.261	6.491	6.730
2.90	5.249	0.781	1.763	1.000	1.296	2.454	3.858	5.403	5.997	6.256	6.487	6.725
3.00	5.429	0.808	1.763	1.000	1.298	2.454	3.856	5.399	5.992	6.252	6.482	6.720
3.10	5.608	0.835	1.764	1.000	1.299	2.454	3.854	5.394	5.987	6.247	6.477	6.715
3.20	5.788	0.863	1.765	1.000	1.301	2.454	3.852	5.390	5.983	6.242	6.472	6.710
3.30	5.967	0.890	1.765	1.000	1.302	2.453	3.850	5.386	5.978	6.237	6.467	6.705
3.40	6.146	0.917	1.766	1.000	1.304	2.453	3.847	5.382	5.973	6.232	6.462	6.700
3.50	6.325	0.945	1.767	1.000	1.306	2.453	3.845	5.378	5.968	6.227	6.457	6.695
3.60	6.504	0.972	1.767	1.000	1.307	2.453	3.843	5.373	5.963	6.222	6.452	6.690
3.70	6.683	1.000	1.768	1.000	1.309	2.453	3.841	5.369	5.959	6.217	6.447	6.684
3.80	6.862	1.027	1.769	1.000	1.310	2.453	3.838	5.365	5.954	6.212	6.442	6.679
3.90	7.040	1.055	1.769	1.000	1.312	2.452	3.836	5.360	5.949	6.207	6.436	6.674
4.00	7.219	1.083	1.770	1.000	1.313	2.452	3.834	5.356	5.944	6.202	6.431	6.669
4.50	8.110	1.221	1.773	1.000	1.320	2.451	3.822	5.334	5.919	6.177	6.405	6.642
5.00	8.999	1.360	1.777	1.000	1.327	2.449	3.810	5.312	5.894	6.151	6.379	6.614
5.50	9.884	1.501	1.780	1.000	1.333	2.447	3.797	5.288	5.869	6.125	6.352	6.587
6.00	10.767	1.642	1.783	1.000	1.338	2.444	3.784	5.265	5.842	6.098	6.324	6.558
6.50	11.648	1.784	1.786	1.000	1.343	2.441	3.770	5.241	5.815	6.070	6.295	6.529
7.00	12.525	1.927	1.789	1.000	1.348	2.437	3.756	5.216	5.788	6.042	6.266	6.499
7.50	13.400	2.072	1.792	1.000	1.351	2.433	3.742	5.191	5.760	6.013	6.237	6.468
8.00	14.271	2.217	1.795	1.000	1.354	2.429	3.727	5.165	5.731	5.983	6.206	6.437

ERROR RETURN T1515 FROM 434 ARG = +5062429523

REFERENCES

- Baade, W. and Minkowski, R. 1937a, Ap. J., 86, 119.
- Baade, W. and Minkowski, R. 1937b, Ap. J., 86, 123.
- Bartkus, R. 1965, Bull. Vilnius Obs., Nr. 15, 29.
- Becklin, E. E. and Neugebauer, G. 1966, in press.
- Blaauw, A. 1963, Basic Astronomical Data, ed. by K. Aa. Strand (Chicago: University of Chicago Press) 383.
- Blaauw, A. 1964, Annual Reviews of Astronomy and Astrophysics, Vol. 2 (Palo Alto: Annual Reviews, Inc.) 213.
- Blanco, V. M. 1963, Ap. J., 137, 513.
- Blanco, V. M. and Lennon, C. J. 1961, A. J., 66, 524.
- Boggess, A. and Borgman, J. 1964, Ap. J., 140, 1636.
- Chapman, G. A. and Stockton, A. 1966, unpublished.
- Chauvenet, W. 1960, A Manual of Spherical and Practical Astronomy, Vol. II (New York: Dover Publications, Inc.) 504.
- Coyne, G. V. and Gehrels, T. 1966, A. J., 71, 355.
- Crawford, D. L. and Barnes, J. V. 1966, A. J., 71, 610.
- Danielson, R. E., Woolf, N. J. and Gaustad, J. E. 1965, Ap. J., 141, 116.
- Davis, L. Jr. and Greenstein, J. L. 1951, Ap. J., 114, 206.
- Dieter, N. H. and Goss, W. M. 1966, Rev. Mod. Physics, 38, 256.
- Divan, L. 1954, Ann. d'Ap., 17, 456.
- Donn, B. 1955, Les Particules Solid dans les Astres, Liege Symposium (4), 15, 571.
- Elvius, A. and Hall, J. S. 1966, Lowell Obs. Bull., 6, 257.

- Gehrels, T. 1960, A. J., 65, 69.
- Gehrels, T. 1966, to be published.
- Gehrels, T. and Silvester, A. B. 1965, A. J., 70, 579.
- Greenberg, J. M. 1966, Nebulae and Interstellar Matter, ed. by L. H. Aller and B. M. Middlehurst (Chicago: University of Chicago Press) in press.
- Greenberg, J. M., Lind, A., Wang, R. T., and Libelo, L. 1963, Interdisciplinary Conference on Electromagnetic Scattering (Oxford: Pergamon Press).
- Greenstein, J. L. 1951, Astrophysics, ed. by J. A. Hynek (New York: McGraw-Hill Book Company) 555.
- Hall, J. S. 1937, Ap. J., 85, 145.
- Hall, J. S. 1958, Publ. U. S. Naval Obs., 17, 275.
- Hallam, K. 1959, Unpublished Ph. D. dissertation--University of Wisconsin.
- Hardie, R. H., Heiser, A. M., and Tolbert, C. R. 1964, Ap. J., 140, 1472.
- Haro, G. 1953, Ap. J., 117, 73.
- Haro, G. and Moreno, A. 1954, Boll. Obs. Tonantzintla y Tacubaya, 2, No. 7, 15.
- Hiltner, W. A. 1954, Ap. J., 120, 367.
- Hiltner, W. A. 1956, Ap. J. Suppl., 1, Nr. 24.
- Hiltner, W. A. and Johnson, H. L. 1956, Ap. J., 124, 367.
- Hoyle, F. and Wickramasinghe, N. C. 1962, M. N., 124, 417.
- Hulst, H. C. van de 1949, Rech. Astron. Obs. Utrecht, 11, Part 2.
- Johnson, H. L. 1957, Ap. J., 126, 134.
- Johnson, H. L. 1958, Lowell Obs. Bull., 4, 37.
- Johnson, H. L. 1962, Ap. J., 136, 1135.
- Johnson, H. L. 1963, Basic Astronomical Data, ed. by K. Aa. Strand (Chicago: University of Chicago Press) 204.

- Johnson, H. L. 1965, Ap. J., 141, 923.
- Johnson, H. L. 1966a, Nebulae and Interstellar Matter, ed. by L. H. Aller and B. M. Middlehurst (Chicago: University of Chicago Press) in press.
- Johnson, H. L. 1966b, Annual Reviews of Astronomy and Astrophysics, Vol. 4 (Palo Alto: Annual Reviews, Inc.) 193.
- Johnson, H. L. 1966c, in press.
- Johnson, H. L. and Borgman, J. 1963, B. A. N., 17, 115.
- Johnson, H. L. and Mendoza V., E. E. 1964, Boll. Obs. Tonantzintla y Tacubaya, 3, 331.
- Johnson, H. L. and Mitchell, R. I. 1962, Comm. of the Lunar & Plan. Lab., 1, 73.
- Johnson, H. L. and Morgan, W. W. 1953, Ap. J., 117, 313.
- Johnson, H. L. and Morgan, W. W. 1955, Ap. J., 122, 142.
- Johnson, H. L., Mitchell, R. I., Iriarte, B., and Wisniewski, W. Z. 1966, Comm. of the Lunar and Plan. Lab., 4, 99.
- Johnson, H. M. 1961, P. A. S. P., 73, 147.
- Johnson, H. M. 1966, Trans. I. A. U., 12, 445.
- Kahn, F. D. 1952, M. N., 112, 518.
- King, I. 1952, Ap. J., 115, 580.
- Krishna Swamy, K. S. 1965, P. A. S. P., 77, 164.
- Low, F. J. 1966, private communication.
- Low, F. J. and Johnson, H. L. 1964, Ap. J., 139, 1130.
- Low, F. J. and Smith, B. J. 1966, in press.
- Mendez, M. 1965, Boll. Obs. Tonantzintla y Tacubaya, 4, 41.
- Menon, T. K. 1961, Publ. Nat. Radio Ast. Obs., 1, 1.
- Morgan, W. W. 1958, Trans. I. A. U., 10, 576.

- Münch, G. and Wilson, O. C. 1962, Z. f. Ap., 56, 127.
- O'Dell, C. R. and Hubbard, W. B. 1965, Ap. J., 142, 591.
- Oort, J. H. and Hulst, H. C. van de 1946, B. A. N., 10, 187.
- Osterbrock, D. E. and Flather, E. 1959, Ap. J., 129, 26.
- Parenago, P. P. 1954, Trudy Sternberg Astr. Inst., Vol. 25.
- Plaskett, J. S. and Pearce, J. A. 1935, Publ. Dom. Ap. Obs. Victoria, 5, 99.
- Platt, J. R. 1956, Ap. J., 123, 486.
- Reitmeyer, W. L. 1965, Ap. J., 141, 1331.
- Robinson, B. J. 1965, Sci. Am., 213, 26.
- Schalén, C. 1965, Ark. for Aston., 4, 1.
- Serkowski, K. 1963, Ap. J., 138, 1035.
- Shakhovskoi, N. M. 1965, Sov. Ast. - A. J., 8, 833.
- Sharpless, S. 1952, Ap. J., 116, 251.
- Sharpless, S. 1962, Ap. J., 136, 767.
- Sharpless, S. 1963, Basic Astronomical Data, ed. by K. Aa. Strand (Chicago: University of Chicago Press) 225.
- Stebbins, J. and Kron, G. E. 1956, Ap. J., 123, 440.
- Stebbins, J. and Whitford, A. E. 1943, Ap. J., 98, 20.
- Stebbins, J. and Whitford, A. E. 1945, Ap. J., 102, 273.
- Stebbins, J., Huffer, C. M., and Whitford, A. E. 1939, Ap. J., 90, 209.
- Stein, W. 1966, Ap. J., 145, 101.
- Straizys, V. 1963, Bull. Vilnius Obs., Nr. 7.
- Straizys, V. 1964, Bull. Vilnius Obs., Nr. 9.
- Strand, K. Aa. 1958, Ap. J., 128, 14.
- Strand, K. Aa. and Teska, T. 1958, Ann. Dearborn Obs., VII, 67.

- Trumpler, R. J. 1930, Lick Obs. Bull., 14, 154.
- Underhill, A. B. 1964, Observatory, 84, 35.
- Underhill, A. B. 1966, Trans. I. A. U., 12, 449.
- Vandervoort, P. O. 1964, Ap. J., 139, 869.
- Visvanathan, N. 1966, Ph. D. dissertation, Australian National University, Canberra.
- Wampler, E. J. 1961, Ap. J., 134, 861.
- Whiteoak, J. B. 1966, Ap. J., 144, 305.
- Whitford, A. F. 1948, Ap. J., 107, 102.
- Wickramasinghe, N. C. 1965, M. N., 131, 177.
- Wickramasinghe, N. C., Dharmawardhana, W. C., and Wild, C. 1966, in press.
- Wickramasinghe, N. C.; Donn, B. D., Stecher, T. P., and Williams, D. A. 1966, in press.
- Williams, R. E. 1966, private communication.
- Woltjer, L. 1965, Galactic Structure, ed. by A. Blaauw and M. Schmidt (Chicago: University of Chicago Press) 531.